The Influence of Film Morphology on Solution processed Organic Field-effect Transistors

Hoi Nok Tsao

The Influence of Film Morphology on Solution Processed Organic Field-effect Transistors

Hoi Nok Tsao

Dissertation
im Fachbereich Chemie
der Johannes Gutenberg Universität
Mainz

vorgelegt von
Hoi Nok Tsao
aus Macao

im Dezember 2008

Contents

Titel **iii**

Contents **v**

1 Introduction **1**

Bibliography **5**

2 Physics of OFETs **7**

2.1 Introduction 7

2.2 Operating Principle of OFETs 8

2.3 Charge Carrier Mobility μ 10

2.4 Current On/Off Ratio I_{on}/I_{off} 12

Bibliography **15**

3 Organic Semiconductors and Processing **17**

3.1 Introduction 17

3.2 Processing Techniques 18

3.2.1 Single crystal growth 19

3.2.2 Vacuum Sublimation 21

3.2.3 Solution Processing 22

3.2.4 OFET Structures 26

3.3 State of the art organic semiconductors 28

Bibliography **31**

4 P-type Polymer OFETs **35**

4.1 Introduction 35

4.2 Regioregular Thiophene Polymer OFETs 36

4.3 Liquid Crystalline Thiophene Polymer OFETs 40

4.4 Nitrogen bridged Ladder Type Polymer OFETs 42

4.5 CDT-BTZ Copolymer OFETs 50

4.6 Higher molecular weight CDT-BTZ Copolymer 60

4.6.1 Unalinged CDT-BTZ Copolymer OFETs 62

4.6.2 Alinged CDT-BTZ Copolymer OFETs 68

4.7 Summary 77

Bibliography **79**

5 N-Type Rylene Dye OFETs **83**

5.1 Introduction 83

5.2 SWPDI OFETs 87

5.3 SWTDI OFETs 95

5.3.1 Solution Processed SWTDI OFETs 95

5.3.2 Melt Processed SWTDI OFETs 99

5.4 Summary 108

Bibliography **111**

6 Ambipolar Discotic Rylene Dye OFETs **113**

6.1 Introduction 113

6.2 Ambipolar SWQDI OFETs 116

6.2.1 The Role of Charge Injection 122
6.2.2 The Role of Interface Charge Trapping 124
6.2.3 The Role of Molecular Packing 126
6.3 Summary 137

Bibliography **141**

7 Conclusion and Outlook **143**

Bibliography **147**

8 Experimental Details **149**
8.1 Transistor Probe Station 149
8.2 Bottom Contact OFET Preparation 150
8.3 Self-assembled Monolayers 152
8.3.1 Functionalization with HMDS 153
8.3.2 Functionalization with PTES 153
8.4 Dip-coating 154

Acknowledgement **155**

Publication List **157**

Chapter 1

Introduction

Transistors pervade our everyday modern life. They are basic building blocks for microelectronic integrated circuitry used in almost all parts of information technology, most notably in personal computers. Current transistors are produced from inorganic semiconductors like silicon, which is still unrivaled in transistor performance. In the light of this success story, it is justified to ask why those devices should be made of organic semiconductors as well? There are two main answers. The most imminent incentive is Moore's Law, stating that the number of transistors that can be implemented in an integrated circuit, for example in central processing units (CPUs) that drive all computers, doubles approximately every two years. This increase in transistor density leads to more powerful computers due to the fact that computation speed scales with the quantity of devices. Obviously, the smaller the transistors, the more of them can be applied in a circuit. In this aspect, inorganic semiconductors like silicon will reach their limit soon, calling for devices in molecular scale. Hereby, single molecule transistors consisting of organic semiconductors like carbon nanotubes have been realized [1]-[5].

Apart from single molecule organic devices which will not be covered in this thesis, transistors based on thin films consisting of organic semiconductors are appealing due to the following point. One significant advantage of using organic semiconduc-

tors is the possibility of processing them at low temperatures compared to state of the art inorganic silicon crystals which have to be grown on substrates at high temperatures, typically around $1000°C$. This requires hard and rigid surfaces that can withstand such heat. The low temperature manufacturing of organic transistors opens a totally new field of plastic electronics, devices that can be produced on flexible foils for example [6]. Such bendable electronic devices are among others roll-out displays (Figure 1.1a) [7]-[11] or radio frequency identification tags (RFID) (Figure 1.1b) employed for storing and transmitting information about for instance products in supermarkets or biometric data in passports. Such RFID tags based on organic transistors have been demonstrated by several groups, including logic circuits [12]-[19]. Electronic paper (Figure 1.1c) for digital newspapers or books are also appealing as well as electronic skin (Figure 1.1d) that can act as sensors for robots, for instance for detecting heat or pressure [20][21]. In addition, organic semiconducting compounds can be made soluble by proper design of the chemical structure. Introducing solubility enables the employment of cheap, fast, and large area processing techniques like ink-jet or roll printing while preserving the low temperature fabrication.

The largest prospective market for organic electronics is most probably bendable displays. Hereby, organic transistors are required as switching elements for individual pixels. Several types of displays exist. The easiest and technologically least demanding ones are electrophoretic displays. In these devices, the pixel element consists of electronic ink (E-ink) that shifts from white to black in response to an electric field. To drive these inks, transistors are typically needed with charge carrier mobilities of 0.01 to 0.1 $cm^2V^{-1}s^{-1}$ [22]. Those black and white flexible displays in A5 size have been fabricated by Plastic Logic (Figure 1.2a) and are currently planned to be commercially produced by this company. However, those displays are not colored and the images cannot be refreshed at a high rate, rendering them

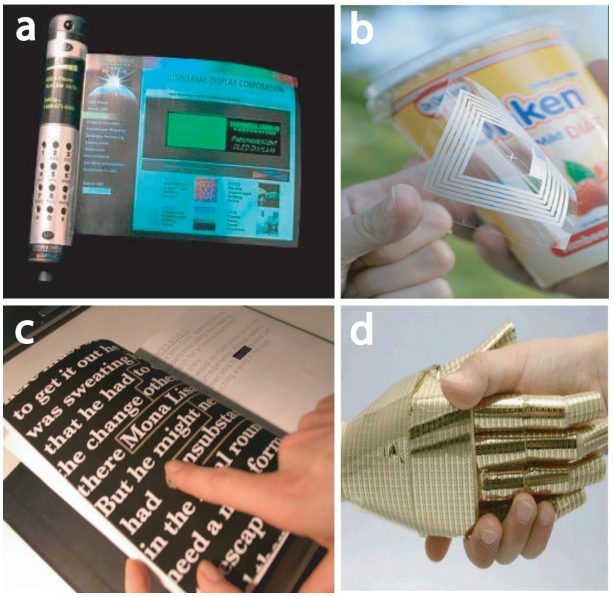

Figure 1.1: Possible applications of plastic electronics.

just attractive as electronic paper. For the larger market of colored displays functioning as television screens or computer monitors, light emitting diodes made out of organic semiconductors (OLEDs) acting as pixels are particularly appealing due to their brightness [23]-[27]. In addition, self-emitting devices like OLEDs have the advantage that their visibility is not angle dependent as is the case for the state of the art liquid crystal displays composing of a light backplane. Realization of those OLED screens is a technological challenge and poses strict and demanding requirements on organic field-effect transistors. The need for fast switching times in order to refresh every image at least every 16 ms, faster than the response time of the human eye, to create smooth moving images, typically charge carrier mobilities higher than 1 $cm^2V^{-1}s^{-1}$ are mandatory. In this aspect, Sony has just recently demonstrated their new prototype of bendable 2.5 inch full color display using OLEDs and OFETs (Figure 1.2b).

Whereas organic light emitting diodes (OLEDs) have made it to the commercial market production already, organic field-effect transistors (OFETs) are on the verge of commercialization [28]. There are still obstacles that have to be overcome towards the ultimate goal of industrially solution printing cost effective organic elec-

Figure 1.2: a.) Active-matrix black and white electrophoretic display made by Plastic Logic. b.) OLED and OFET based full color bendable active matrix display with 2.5 inch diagonal demonstrated as a prototype by Sony.

tronic devices in large scale. When using these processes, the main hurdle is device performance. Particularly, the way how molecules self-assemble to form the current carrying semiconductor film has a major impact on transistor behavior. For instance, poorly packed molecules generating a disordered or amorphous layer are generally expected to inefficiently transfer charge carriers due to insufficient overlap of the molecular orbitals containing the free charges. On the other hand, highly arranged molecules resulting in organic crystals should provide good molecular orbital overlap and maximize unhindered charge carrier transport. Therefore, the macroscopic molecular organization into specific film structures or *film morphologies* (for example amorphous, crystalline, etc.) crucially determines device performance. The occurance of a certain morphology is always an interplay between the molecules' self-organization, mostly dictated by their chemical structure, and the processing technique employed. In this aspect, the motivation of this work is to further understand the influence of film morphology on the performance of organic field-effect transistors necessary for the realization of organic electronics.

Bibliography

[1] S. J. Tans, A. R. M. Verschueren, C. Dekker, *Nature* **1998**, *393*, 49.

[2] A. Bachtold, P. Hadley, T. Nakanishi, C. Dekker, *Science* **2001**, *294*, 1317.

[3] Y. Huang, X. Duan, Y. Cui, L. J. Lauhon, K.-H. Kim, C. M. Lieber, *Science* **2001**, *294*, 1313.

[4] A. Javey, J. Guo, Q. Wang, M. Lundstrom, H. Dai, *Nature* **2003**, *424*, 654.

[5] S. Heinze, J. Tersoff, R. Martel, V. Derycke, J. Appenzeller, P. Avouris, *Phys. Rev. Lett.* **2002**, *89*, 106801.

[6] A. Dodabalapur, *Mater. Today* **2006**, *9*, 24.

[7] G. H. Gelinck, H. E. A. Huitema, E. van Veenendaal, E. Cantatore, L. Schrijnemakers, J. B. P. H. van der Putten, T. C. T. Geuns, M. Beenhakkers, J. B. Giesbers, B.-H. Huisman, E. J. Meijer, E. M. Benito, F. J. Touwslager, A. W. Marsman, B. J. E. van Rens, D. M. de Leeuw, *Nat. Mater.* **2004**, *3*, 106.

[8] J. A. Rogers, Z. Bao, *J. Polym. Sci. Part A: Polym. Chem.* **2002**, *40*, 3327.

[9] P. Mach, S. J. Rodriguez, R. Nortrup, P. Wiltzius, J. A. Rogers, *Appl. Phys. Lett.* **2001**, *78*, 3592.

[10] C. D. Sheraw, L. Zhou, J. R. Huang, D. J. Gundlach, T. N. Jackson, M. G. Kane, I. G. Hill, M. S. Hammond, J. Campi, B. K. Greening, J. Francl, J. West, *Appl. Phys. Lett.* **2002**, *80*, 1088.

[11] L. Zhou, A. Wanga, S.-C. Wu, J. Sun, S. Park, T.-N. Jackson, *Appl. Phys. Lett.* **2006**, *88*, 083502.

[12] C. J. Drury, C. M. J. Mutsaers, C. M. Hart, M. Matters, D. M. de Leeuw, *Appl. Phys. Lett.* **1998**, *73*, 108.

[13] B. Crone, A. Dodabalapur, Y.-Y. Lin, R. W. Filas, Z. Bao, A. LaDuca, R. Sarpeshkar, H. E. Katz, W. Li, *Nature* **2000**, *403*, 521.

[14] A. R. Brown, A. Pomp, C. M. Hart, D. M. de Leeuw, *Science* **1995**, *270*, 972.

[15] H. Klauk, M. Halik, U. Zschieschang, F. Eder, D. Rohde, G. Schmid, C. Dehm, *IEEE Trans. Electron Devices* **2005**, *52*, 618.

[16] J. A. Rogers, Z. Bao, A. Dodabalapur, A. Makhija, *IEEE Electron Devices Lett.* **2000**, *21*, 100.

[17] Y. Watanabe, K. Kudo, *Appl. Phys. Lett.* **2005**, *87*, 223505.

[18] Y.-Y. Noh, N. Zhao, M. Caironi, H. Sirringhaus, *Nature Nanotech.* **2007**, *2*, 784.

[19] P. F. Baude, D. A. Ender, M. A. Haase, T. W. Kelley, D. V. Muyres, S. D. Theiss, *Appl. Phys. Lett.* **2003**, *82*, 3964.

[20] T. Someya, T. Sekitani, S. Iba, Y. Kato, H. Kawaguchi, T. Sakurai, *PNAS* **2004**, *27*, 9966.

[21] T. Someya, Y. Kato, T. Sekitani, S. Iba, Y. Noguchi, Y. Murase, H. Kawaguchi, T. Sakurai, *PNAS* **2005**, *35*, 12321.

[22] H. Sirringhaus, M. Ando, *MRS Bulletin* **2008**, *33*, 676.

[23] C. W. Tang, S. A. VanSlyke, *Appl. Phys. Lett.* **1987**, *51*, 913.

[24] J. H. Burroughes, D. D. C. Bradley, A. R. Brown, R. N. Marks, K. Mackay, R. H. Friend, P. L. Burns, A. B. Holmes, *Nature* **1990**, *347*, 539.

[25] R. H. Friend, R. W. Gymer, A. B. Holmes, J. H. Burroughes, R. N. Marks, C. Taliani, D. D. C. Bradley, D. A. Dos Santos, J. L. Bredas, M. Lögdlund, W. R. Salaneck, *Nature* **1999**, *397*, 121.

[26] C. D. Müller, A. Falcou, N. Reckefuss, M. Rojahn, V. Wiederhirn, P. Rudati, H. Frohne, O. Nuyken, H. Becker, K. Meerholz, *Nature* **2003**, *421*, 829.

[27] P. E. Burrows, G. Gu, V. Bulovic, Z. Shen, S. R. Forrest, M. E. Thompson, *IEEE Trans. Electron Devices* **1997**, *44*, 1188.

[28] Y.-L. Loo, I. McCulloch, *MRS Bulletin* **2008**, *33*, 653.

Chapter 2

Physics of Organic Field-effect Transistors

2.1 Introduction

Field-effect transistors (FETs) are fundamental building blocks for modern electronics, serving as fast switches in displays or computer microprocessors. FETs come in different variations and architectures. In the case of organic transistors, the thin film transistor (TFT) is typically applied. TFTs have the advantage of easy manufacturing, simply consisting of an active semiconductor layer on top of the whole transistor configuration (Figure 2.1a). When fabricating organic TFTs, there are several architectures that one can employ. In the following when talking about FETs, the TFT structure is always implied. In this chapter, the working principles of FETs are first illustrated qualitatively to provide a simple picture of their functionality. Following this description, the physical parameters that quantify the quality of FETs will be presented.

2.2 Operating Principle of Organic Field-effect Transistors

Let us first start with the qualitative description of the operating principles of OFETs. The main task of transistors is to modulate the current. By doing this, the electric current can be switched on and off, and that is exactly what a transistor should do: acting as switches in order for example to perform binary logic for computations in microelectronics or to switch individual pixels in a display.
A field-effect transistor consists of a gate electrode covered by a dielectric layer. On top of this insulator, the semiconductor film is deposited and contacted by source and drain electrodes with a certain width and separation distance as schematically illustrated in Figure 2.1a. This distance is called the channel length since this is where the charge carriers are flowing between these two electrodes. There are two quantities instrumental for controlling the current flowing through the semiconductor from the source to the drain, namely the potential applied to these two contacts V_{SD} and the potential across the source and gate electrodes V_G (Figure 2.1a). The effect of the gate potential V_G is to accumulate charge carriers at the semiconductor-insulator interface, forming a channel, the so called *accumulation layer* filled with charge carriers connecting the source and drain electrodes (red plus signs in Figure 2.1b). This is easily understood if one keeps in mind that a transistor is akin to a capacitor. Depending on whether a positive or negative voltage is applied, either electrons or holes will be accumulated within the semiconductor layer at the dielectric surface. If, in addition, a voltage V_{SD} is applied, then a current I_{SD} will flow because the accumulated charge carriers are forced to move between the source and drain electrodes (Figure 2.1c). In this way, the current can be modified in a transistor.

Two types of measurements have to be performed in order to obtain the charac-

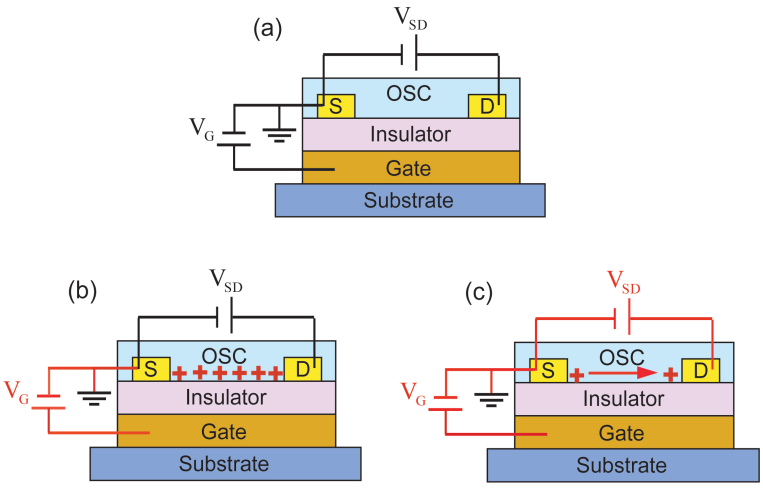

Figure 2.1: a.) Structure of an OFET (TFT). OSC stands for the organic semiconductor film. b.) Accumulation of charge carriers, in this case of holes as depicted by the red + symbols in response to an applied V_G (highlighted in red), forming the accumulation layer. c.) Current flow caused by an additional V_{SD} applied between source (S) and drain (D) electrodes.

teristics of transistors since there are two external biases that can be applied, namely V_{SD} and V_G. The first measuring possibility is to keep the gate voltage V_G constant and sweep V_{SD}, at the same time recording the current I_{SD} between the source and drain electrodes. Since V_G remains constant, the accumulated charge carrier density in the semicondutor layer at the insulator interface stays constant as well during the V_{SD} sweep. When $V_{SD} < V_G$, the current I_{SD} increases linearly, following Ohm's law (Figure 2.2a). Under these operation conditions, the transistor is said to be in the *linear regime*. When V_{SD} increases such that $V_{SD} = V_G$, all charge carriers are depleted at the drain electrode (Figure 2.2b). As V_{SD} continues to increase such that $V_{SD} > V_G$, the depletion region starts to expand from the drain into the channel. That is, all charge carriers being generated by V_G are being immediately swept from the source to the drain, and the current I_{SD} cannot change anymore with increasing V_{SD} (Figure 2.2c) [1]. The transistor in this stage is said to be in the *saturation regime*. When characterizing OFETs, most often it is convention to report transistor behavior only in saturation regime. Hence, in the following, focus will also solely be put on this saturation regime. The set of curves that are obtained by sweeping V_{SD} at various constant V_G are called *output curves*. Similarly, one

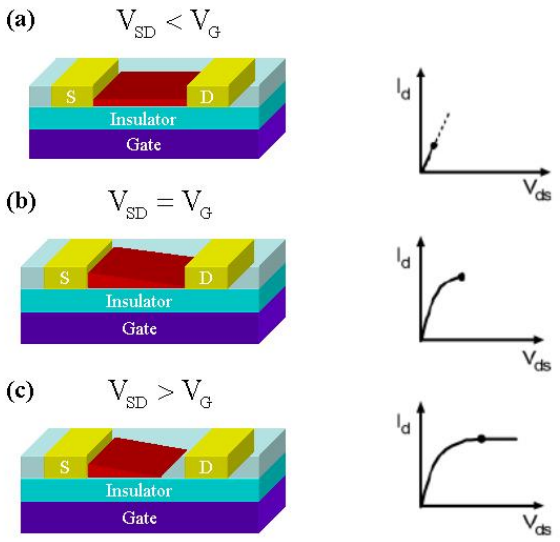

Figure 2.2: Transistor operation state as expressed by the output curve. a.) Linear increase of I_{SD} in dependence of V_{SD} when $V_{SD} < V_G$. b.) Start of charge carrier depletion at the drain electrode, leading to the onset of saturation. c.) Due to $V_{SD} > V_G$, all accumulated charge carriers are immediately swept away from the channel such that I_{SD} cannot change. The transistor is in saturation, expressed by the horizontal line in the output curve.

can keep V_{SD} constant and sweep V_G. As V_G increases, I_{SD} rises as well since more charge carriers are being accumulated with growing V_G (Figure 2.3). These set of curves are called *transfer curves*. Obtaining these two types of measurements are required for characterizing transistors [1]-[4].

2.3 Charge Carrier Mobility μ

Physical parameters are needed in order to quantify the perfromance of FETs. The most important one is the charge carrier mobility μ, expressing with what ease the charges can travel through the semiconducting layer from the source to the drain electrodes in response to an externally applied force, in this case the electric field generated by V_{SD}. The higher the charge carrier mobility, the better the transistor works, that means, the easier the charges can be moved by the applied potential. The effect is that a certain current flow can be already achieved by a low voltage bias. In nowadays large area electronic devices like flat panel displays, transistors

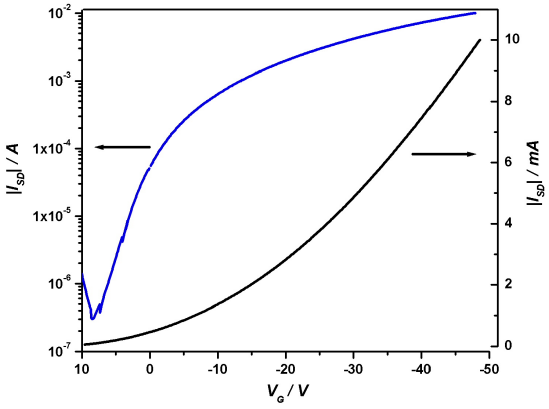

Figure 2.3: Typical FET transfer curve expressed both in linear (black curve) and logarithmic scale (blue curve).

are used that consist of amorphous silicon. Those transistors have a charge carrier mobility of typically higher than 0.1 $cm^2V^{-1}s^{-1}$. That is, organic FETs are also aimed to at least reach this value in order to be appealing for their application in everyday electronics.

The charge carrier mobility for transistors operated in saturation is given by

$$I_{SD} = \frac{W}{2L}\mu_{sat}C_i(V_G - V_T)^2 \tag{2.1}$$

where W and L are the channel width and length respectively, μ_{sat} is the charge carrier mobility in saturation, C_i the capacitance per unit area of the dielectric layer and V_T is called the *threshold voltage*. This voltage describes the gate voltage needed in order to turn the transistor on, that is, where the current starts to flow at an applied V_{SD} [5]-[7]. Most often in organic transistors where trapping sites are present due to various reasons that will be explained later, a non-zero threshold voltage has to be applied in order to get current flowing. This threshold voltage is needed to generate enough charge carriers that first fill the traps before the current carrying accumulation layer forms. Ideally, when there are no trapping sites, current should already flow at $V_G = 0V$, that is, at zero threshold voltage [8]-[12].

Taking the square root of both sides of equation 2.1, we obtain

$$\sqrt{I_{SD}} = \sqrt{\frac{W}{2L}\mu_{sat}C_i}(V_G - V_T) \tag{2.2}$$

which is a linear equation when plotting $\sqrt{I_{SD}}$ versus V_G. The slope **m** of such a plot is the coefficient of V_G in equation 2.2.

$$m = \sqrt{\frac{W}{2L}\mu_{sat}C_i} \Rightarrow m^2 = \frac{W}{2L}\mu_{sat}C_i \tag{2.3}$$

Rearranging gives

$$\mu_{sat} = \frac{m^2 2L}{WC_i} \tag{2.4}$$

That is, μ_{sat} is obtained by taking the slope **m** of the linear fit at square root of the transfer curve (Figure 2.3) and using equation 2.4.

2.4 Current On/Off Ratio I_{on}/I_{off}

Transistors are typically used as fast switches in microelectronics, for example as switches for individual pixels in flat panel displays or in computer central processing units (CPUs) for binary logic operations. Switches are considered as good switches if there is a huge difference between the off state and the on state. To quantify this feature, the current on/off ratio I_{on}/I_{off} is employed. Thus, the larger this ratio, the more easily it is to distinguish between the transistor's on and off state. Conventionally, the off current I_{off} is the I_{SD} at a specific V_{SD} with no gate voltage V_G applied. That is basically the intrinsic conductivity of the semiconductor since no additional charge carriers are being accumulated by the gate voltage. The on current I_{on} is the current I_{SD} flowing in the transistor when it is biased with $V_{SD} = V_G$ [13]. Ideally, the off current in organic semiconductors is low except for some low bandgap materials with elevated intrinsic charge carrier density contributing to the current. However, in some cases the organic semiconductor layer is doped either by

chemical impurities or oxygen and moisture. As a result, additional charge carriers are triggered even though no gate voltage is applied for generating them. These carriers lead to an off current that can be high and might not be significantly lower than the on current. Consequently, an undesirably low I_{on}/I_{off} is evoked [14]-[19]. In order to decrease the off current, a gate voltage needs to be applied that repels these charge carriers. That is, for a p-type (n-type) semiconductor, negative (positive) gate biases are required for the accumulation of holes (electrons) to form the accumulation layer for the transistor current. Therefore, applying the opposite gate bias (positive V_G for p-type and negative V_G for n-type devices) drives away those unwanted charges, in this way turning off the devices and decreasing the off current. With this method, a higher I_{on}/I_{off} can be achieved, and the off current is then not defined as the current measured at $V_G = 0V$ anymore.

Bibliography

[1] S. M. Sze, *Semiconductor Devices, Physics, and Technology*; John Wiley and Sons: New York, 1985.

[2] G. Horowitz, *Adv. Mater.* **1998**, *10*, 365.

[3] G. Horowitz, P. Delannoy, *J. Appl. Phys.* **1991**, *70*, 469.

[4] M. J. Deen, M. H. Kazemeini, Y. M. Haddara, J. Yu, G. Vamvounis, S. Holdcroft, W. Woods, *IEEE* **2004**, *51*, 1892.

[5] G. Horowitz, *J. Mater. Chem.* **1999**, *9*, 2021.

[6] G. Horowitz, *Adv. Mater.* **1996**, *8*, 177.

[7] G. Horowitz, R. Hajlaoui, R. Bourgouiga, M. Hajlaoui, *Synth. Met.* **1999**, *101*, 401.

[8] G. Horowitz, R. Hajlaoui, H. Bouchriha, R. Bourguiga, M. Hajlaoui, *Adv. Mater.* **1998**, *10*, 923.

[9] R. Schroeder, L. A. Majewski, M. Grell, *Appl. Phys. Lett.* **2003**, *83*, 3201.

[10] H. L. Gomes, P. Stallinga, F. Dinelli, M. Murgia, F. Biscarini, D. M. de Leeuw, T. Muck, J. Geurts, L. W. Molenkamp, V. Wagner, *Appl. Phys. Lett.* **2004**, *84*, 3184.

[11] E. J. Meijer, C. Tanase, P. W. M. Blom, E. van Veenendaal, B.-H. Huisman, D. M. de Leeuw, T. M. Klapwijk, *Appl. Phys. Lett.* **2002**, *80*, 3838.

[12] K. Suemori, S. Uemura, M. Yoshida, S. Hoshino, N. Takada, T. Kodzasa, T. Kamata, *Appl. Phys. Lett.* **2008**, *93*, 033308.

[13] A. R. Brown, C. P. Jarrett, D. M. de Leeuw, M. Matters, *Synth. Met.* **1997**, *88*, 37.

[14] M. S. A. Abdou, F. P. Orfino, Y. Son, S. Holdcroft, *J. Am. Chem. Soc.* **1997**, *119*, 4518.

[15] S. Hoshino, M. Yoshida, S. Uemura, T. Kodzasa, N. Takada, T. Kamata, K. Yase, *J. Appl. Phys.* **2004**, *95*, 5088.

[16] W. L. Kalb, K. Mattenberger, B. Batlogg, *Phys. Rev. B* **2008**, *78*, 035334.

[17] G. Horowitz, X. Peng, D. Fichou, F. Garnier, *J. Appl. Phys.* **1990**, *67*, 528.

[18] E. J. Meijer, C. Detcheverry, P. J. Baesjou, E. van Veenendaal, D. M. de Leeuw, T. M. Klapwijk, *J. Appl. Phys.* **2003**, *93*, 4831.

[19] T. P. I. Saragi, T. Fuhrmann-Lieker, J. Salbeck, *Synth. Met.* **2005**, *148*, 267.

Chapter 3

Organic Semiconductors and their Processing Techniques

3.1 Introduction

Organic field-effect transistors rely on a layer consisting of organic semiconductors that carries the current to be modulated. The question is then what kind of organic compounds are most suitable among the myriad of existing materials. Free charge carriers present in each molecule are required for them to be able to move through the whole film connecting the source and drain electrodes in response to an electric field. This is achieved by the alternation of single and double carbon-carbon bonds (conjugation), generating delocalized π-orbitals containing electrons as charge carriers. Hereby, the filled π bonding orbitals form the so called highest occupied molecular orbital (HOMO) whereas the empty π^* antibonding orbital represents the lowest unoccupied molecular orbital (LUMO) [1]. In the jargon of solid state physics, the HOMO would be the hole transporting valence band and the LUMO the electron carrying conduction band. Thus, conjugated systems are desired, from which almost an uncountable number can be synthesized.

The generation of free charge carriers achieved by conjugation of the organic semi-

conductor is not the only prerequisite for obtaining good transistors. Another main point is that the molecules arrange with respect to each other in a way that the delocalized molecular orbitals provide sufficient overlap over a large distance connecting source and drain electrodes such that current can flow unhindered. This macroscopic arrangement firstly depends on the tendency of the organic compound to self-assemble. What factors this self-assembly relies on will be discussed later. It is important to note that this self-orientation can be enhanced macroscopically through the proper fabrication method. In this chapter a short review of the state of the art organic semiconductors together with their processing techniques for OFETs are presented to give an idea of the existing technology. The type of organic compound dictates how they can be applied as thin films for OFETs. For example, for insoluble materials, all solution processing become void. Hence, the nature of the compound goes hand in hand with the appropriate choice of the fabrication method. At the same time, the type of film structure or morphology, that is, the way how the deposited molecules macroscopically pack, heavily depends on processing. The various resulting film morphologies in turn influence charge carrier transport and thus transistor performance. As will be illustrated, the chemical nature of the organic semiconductor, its processing and the resulting film morphology are closely related and ultimately determine OFET performance as well as the cost and simplicity of production.

3.2 Processing Techniques

A strong or weak interaction and hence self-assembly of the organic semiconductor can be imparted based on its appropriate chemical design. Further enhancement and control of the macroscopic molecular self-organization can be induced by the way how the molecules are processed. For instance, disk-shaped conjugated systems like C_{12} substituted hexa-*peri*-hexabenzocoronene ($HBC-C_{12}$) (Figure 3.2a) stands on the substrate, the so called edge-on configuration, and stack to each other into

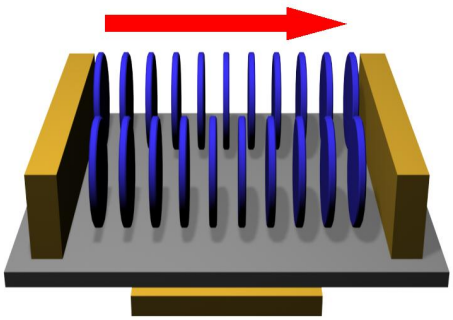

Figure 3.1: OFET based on edge-on discotic columnar structures. Red arrow indicates charge transport through the columnar stacks.

one-dimensional columns along which charge transport takes place (Figure 3.1)[2]. When no fabrication technique is applied that align this compound, randomly oriented fibers consisting of such one-dimensional columns are formed (Figure 3.2b). However, utilizing a method for directional arrangement of these ($HBC - C_{12}$) molecules results in highly ordered columns along the alignment direction (Figure 3.2c), coming along with improved OFETs [3]-[5]. Therefore, knowing which processing technique should be applied to which kind of compound is crucial. Furthermore, the ease and hence the cost of processing organic electronics depends on how the films are fabricated. In this aspect, solution deposition is favorable. However, most of the time the fabrication techniques are limited by the processability of the organic semiconductor itself. In this chapter, the most frequently employed processing methods are briefly illustrated, pointing out their individual advantages and disadvantages together with their suitability for certain groups of organic semiconductors and the resulting film morphologies.

3.2.1 Single crystal growth

In terms of the current carrying semiconducting layer, high intermolecular charge transport and hence charge carrier mobility can be achieved if the molecules pack in such a way that good π-orbital overlap between neighboring molecules is guaranteed. The most suitable structure is an organic single crystal with minimized number of

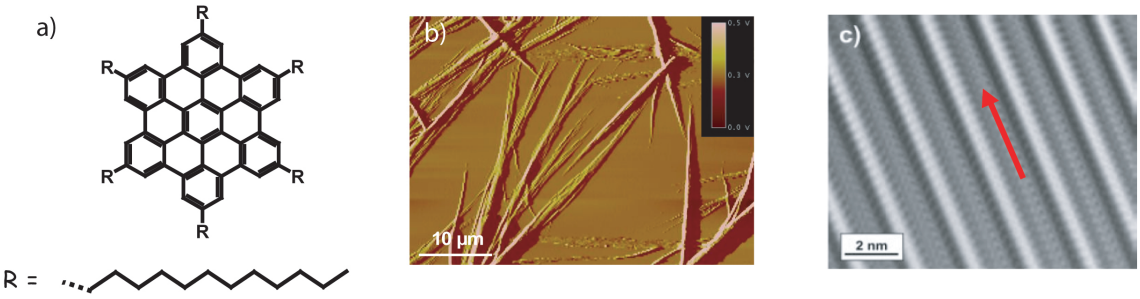

Figure 3.2: a.) Chemical structure of C_{12} substituted HBC. b.) AFM image showing self-assembly of C_{12} substituted HBC into randomly oriented fibers. c.) Aligned C_{12} substituted HBC forming highly arranged columns. Red arrow indicates direction of alignment [19].

defects. Typically organic single crystals are grown by *physical vapor transport* [6][7] which works in the following way. The organic compound is first heated to its gas phase in a tube filled with inert gas. The molecules slowly cool down on their way from the heated material source to the other end of the tube by applying a temperature gradient along the tube (Figure 3.3a). During this process, left over impurities within the material are selected out, and as it gets colder, the molecules crystallize, in this way forming single crystals (Figure 3.3b).

Based on this procedure, rubrene single crystals were for example fabricated, yielding outstanding charge carrier mobilities of 15 $cm^2V^{-1}s^{-1}$ when applied in OFETs [8]. Even though single crystals result in excellent OFETs, the method itself is not trivial and hence not appealing for cheap and simple production needed

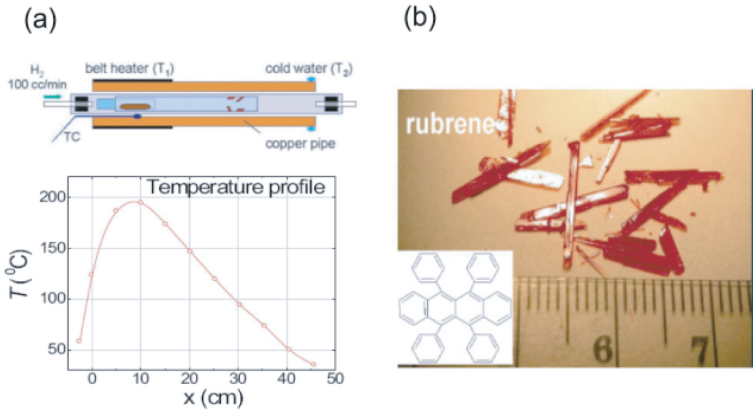

Figure 3.3: a.) Schematic presentation of Physical Vapor Transport. b.) Single rubrene crystals obtained by this method [7].

for plastic electronics. In addition, the limited size of the vapor phase transport aparatus renders the generation of large area single crystals unlikely. Typically, single crystals of at most several centimeters can be obtained, far away from for example flexible displays requiring sizes of several tens or hundreds of centimeters. Furthermore the fragility of such crystals render them questionable for their commercial use, even though large area bendable single crystal transistor arrays have been reported using a stamping technique for individual small crystals [9]. Besides, due to the fact that the organic material needs to be heated to its gas phase, one is limited in the molecular design. Only molecules with a small molecular weight can be used for forming single crystals, since higher molecular weight compounds require more heat to get them into the gas phase and are frequently disintegrated during this process.

3.2.2 Vacuum Sublimation

One possibility for circumventing the problem of delicate handling of organic single crystals is by vaccum sublimation of thin organic films. Here, the organic material is heated to its gas phase in vacuum. These molecules then adsorb on the transistor substrate (Figure 3.4a), hereby forming less fragile polycrystalline films consisting not of one single crystal but of multiple highly ordered domains as illustrated in Figure 3.4b.

In this method, the nature of the surface on which the molecules self-assemble to form the thin layer influences the packing mode and crystal domain sizes. That is why for most organic compounds, heating the substrates leads to larger crystal domains due to the changed kinetics of nucleation that precludes crystal domain formation [10]-[13]. First, islands of molecular aggregation form, building up the nucleation sites. Originating from these islands, the crystal domains grow outward where the outer boundaries meet each other, in this way creating grain boundaries as indicated by the black arrows in (Figure 3.4b). The polycrystalline thin

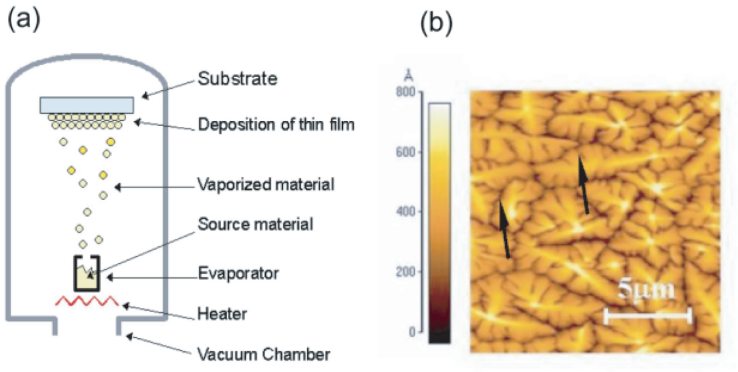

Figure 3.4: a.) Schematic presentation of Vacuum sublimation. b.) Atomic force microscope (AFM) image of sublimed polycrystalline pentacene film made out of individual highly ordered crystalline domains. The trenches between the domains represent grain boundaries as indicated by the arrows [44].

films fabricated by vacuum sublimation typically yield high transistor performances with $\mu_{sat} \geq 0.5\ cm^2V^{-1}s^{-1}$ [14] but are inferior to single crystal devices. The reason is that even though the molecular order within a single crystalline domain can be assumed to be high and comparable to single crystals, the boundaries between neighboring domains pose serious trapping sites for charge transport, in this way lowering charge carrier mobility [15][16]. Those grain boundaries are pictured as areas of poor molecular packing, thus providing insufficient connection between the ordered domains as evidenced by the trenches in Figure 3.4b. In organic single crystals, such boundaries are not present, explaining the lower performance of polycrystalline films. Most of the disadvantages of vacuum sublimation are carried over from the single crystal growth, for example the limitation to small and sublimable molecules and the lack of facile and large area processing.

3.2.3 Solution Processing

The two above mentioned processing techniques typically generate OFETs with charge carrier mobilities higher than $0.5\ cm^2V^{-1}s^{-1}$. However, both methods have several drawbacks when it comes to commercializing organic transistors, be it fragility of single crystals or lack of facile large area deposition, and particularly

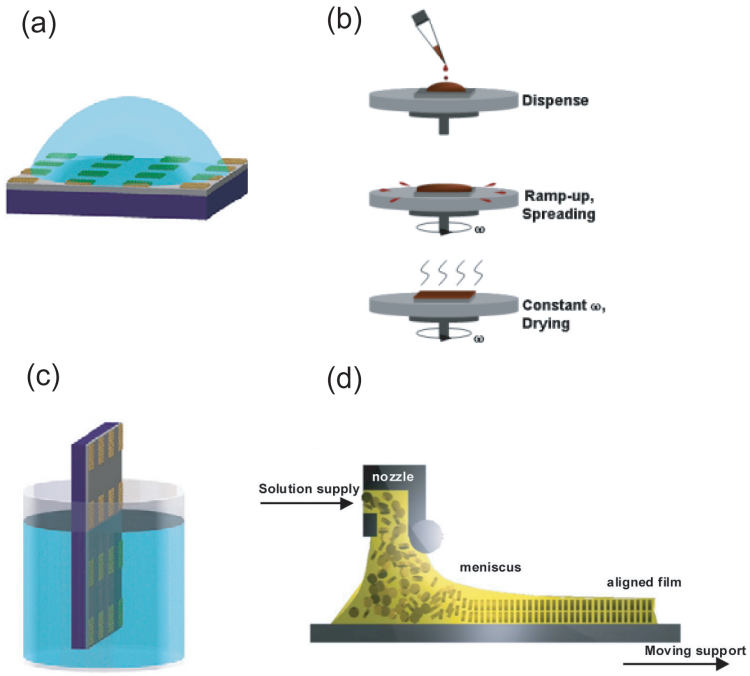

Figure 3.5: a.) Schematic presentation of drop-casting, b.) spin-coating, c.) dip-coating, and d.) zone-casting.

the limitation to low molecular weight sublimable organic materials. Solution processing is a key for circumventing these hurdles, allowing large area, easy, fast and cheap processing. In the following, the most common solution deposition methods are presented.

The simplest method is *drop-casting* (Figure 3.5a). Here, the organic semiconductor is dissolved in an organic solvent. From this solution, drops are applied on the transistor substrate. During solvent evaporation, the molecules form a thin film whose morphology depends on their tendency for self-assembly. Here, the rate of evaporation can be controlled by the type of solvent used. For example, a solvent with a high boiling point prolongs the evaporation, hence allowing more time for the molecules in the drop to self-assemble and to form a film. This is of particular interest for materials that strongly crystallizes. Larger crystallites can be obtained when giving the drop more time to evaporate, that is, when a solvent with a high boiling point is used. It is important to keep in mind that film formation is also

influenced by the surface on which deposition takes place. In some cases, especially for small molecules, no homogeneous layers are produced on hydrophobic interfaces. This drop-casting method is very simple. However, the drawback is that the self-assembly cannot be controlled to take place in a specific direction but rather occurs randomly. This also holds for *spin-coating*. Here, the solution is deposited on the substrate and spun at a specific rate and time. During the spinning, the solvent evaporates, leaving behind a thin film (Figure 3.5b). For this method, it is important to use a solvent with low boiling point such that it evaporates fast enough during the rapid spinning process. Otherwise, the whole solution is spread away from the substrate without film formation. This technique is very simple and hence particularly interesting for producing cheap and large area plastic electronics. Nevertheless, like drop-casting, spin-coating also does not allow space for controlling film formation, that is, for directional alignment of the molecules. Therefore, sometimes amorphous films are generated by this method since the molecules are not given much time to self-assemble into highly oriented structures, generating poor transistor performances.

To align the molecules in a thin film from solution, different methods exist. One simple technique is to immerse the substrate in a solution containing the dissolved compound and to take it out at a specific rate. More precisely, at the interface between the surface of the solution and the substrate, the solvent evaporates, in this way enabling self-assembly and film formation of the compound. When the substrate is additionally moved out or *dipped* of the solution, the molecules in the best case align in the direction of this dipping direction. This method is hence termed *dip-coating* (Figure 3.5c) [17][18]. Dipping rate, solution concentration, the nature of the substrate's surface and the boiling point of the solvent influence the packing of the film achieved. All these parameters have to be optimized in order to obtain a uniform, well ordered thin film for high performance OFETs. Unidirectional alignment is not always guaranteed by this method, depending again on the tendency

for self-assembly of the organic compound. A good estimate on the success of this dip-coating procedure is the investigation of the film morphology by drop-casting. If satisfactory film formation is obtained through this latter method, i.e. presence of large crystalline domains or long fiber like structures, then most likely dip-coating will further enhance these morphologies, yielding directionally oriented structures.

Based on the same principle, another alternative to dip-coating is *zone-casting* (Figure 3.5d). Here, the advantage compared to dip-coating is that the substrate and solution temperature can be additionally changed together with the rate at which the solution is supplied to the substrate [19]. These additional parameters facilitate the realization of a homogeneous ordered film. Employing this method, ($HBC-C_{12}$) was directionally aligned with the columns macroscopically connecting the source and drain electrodes (Figure 3.1, 3.2c), yielding improved transistor performance [3]-[5].

Even though the two lastly mentioned methods allow the alignment of the molecules from solution, optimization is often difficult and time consuming. For commercial use, faster methods are in need, i.e. via ink jet printing or roll printing. Ink jet printing is akin to drop-casting but in a much larger scale [20]-[22]. Multiple nozzles deposit drops on a substrate, in this way processing organic semiconductor layers for OFETs in large areas. An even faster technique is roll printing. Here, the flexible transistor substrates are printed with the liquid organic semiconductor like newspapers are printed in large rolls [23]-[27]. This is the desired fabrication method for easy, cheap, and large area plastic electronics, but at the cost of the absence of directional alignment and film morphology control. Here, organic semiconductors are suitable that give high OFET performances without the need for additional orientation. This can be achieved by compounds that self-assemble for example into highly packed typically polycrystalline layers formed after the fast printing procedure.

3.2.4 OFET Structures

So far the various techniques for depositing an organic semiconductor thin film are discussed. It is time to go on and present how a whole organic field-effect transistor is fabricated. Typical transistor structures that are employed for OFETs are depicted in (Figure 3.6) [28]. The easiest configuration is the so called bottom gate, bottom contact device (Figure 3.6a). Here, the transistors are finished by simply depositing the organic film on a device substrate that consists of source and drain electrodes patterned on top of the dielectric insulator. Even though this configuration is easy to achieve, it is sometimes not suitable for organic semiconductors that tend to form highly crystalline films. These crystallites are rigid, making it possible for them to peel off from the source and drain electrodes, providing insufficient contact and hence poor charge injection [29][30]. This leads to high contact resistances which degrade device performance. A solution would be the treatment of those contacts with soft monolayers like thiols for gold contacts that provide better adhesion of the crystals [31]-[36]. However, such a functionalization induces a different film morphology and also changes the work function of the metal than without such treatment [37]. (The theory of metal work function and charge carrier injection from the source and drain electrodes into the organic semiconductor will be discussed in chapter 4.) A possibility to circumvent this hurdle is to evaporate the source and drain electrodes on top of the thin semiconductor layer. This structure is the so called bottom gate, top contact OFET (Figure 3.6b). Since the electrodes are now situated completely on top of the active layer, there are minimal contact resistances. Nevertheless, due to the fact that the metal electrodes need to be thermally evaporated in vacuum, organic thin films that are sensible to heat might get destroyed. This is particularly fatal for systems which have phase transitions at the temperature at which the metals are deposited, leading to a totally different film morphology than initially desired.

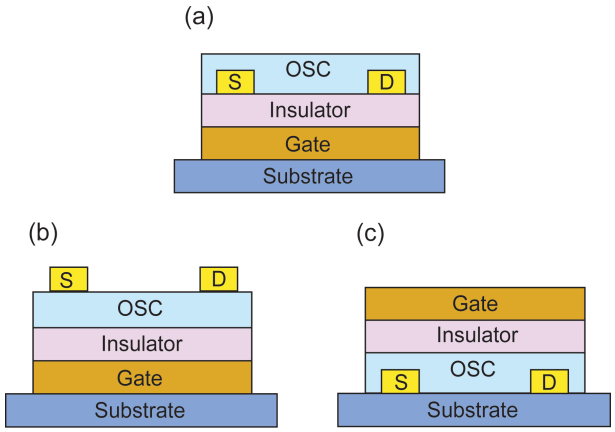

Figure 3.6: a.) Bottom contact, bottom gate, b.) top contact, bottom gate and c.) top contact, top gate OFET.

As is evident from chapter 2, the current flows in the few monolayers of the organic semiconductor film at the semiconductor-insulator interface. Since charge transport is influenced by the molecular packing at this interface, it is crucial to use an insulator surface that is very smooth and trap free in order to guarantee a well ordered film and hence excellent device performance [38]-[42]. Such a smooth surface is provided by silicon dioxide (SiO_2). Thus, silicon wafers are the first choice for the two previously discussed device structures (Figure 3.6a,b). However, for flexible plastic electronics, these rigid substrates are not suitable. In such a case, polymer dielectrics are favorable due to their mechanical flexibility and facile film formation [43][44]. In addition, most insulating polymers can be made soluble, enabling simple large area production of OFETs. Bendable OFETs can be made in a top contact, top gate configuration (Figure 3.6c), where the source and drain electrodes are first patterned on the flexible substrate and the active organic semiconductor film is deposited on top. The devices are then finished by fabricating a soluble polymer insulator, typically by spin-coating in order to achieve a thin homogenous film, followed by the deposition of the gate electrode.

3.3 State of the art organic semiconductors

There is a vast number of organic semiconductors that can be synthesized, matching desired properties like solubility, enhanced self-assembly or variations in energy bandgaps. For charge transport to take place, it is neccessary for the molecules to contain delocalized charge carriers via π-orbitals provided by conjugated systems. Thus, large conjugated organic compounds like polycyclic aromatic hydrocarbons are particularly desirable [45]. In the recent years, many such materials have been reported, leading to various degrees of transistor performances. Only the most prominent compounds, meaning the most frequently studied and the ones with the best performances will be highlighted in this section to give an idea about the current state of the art technology.

The plethora of organic semiconductors can be simplified in two main categories: The first group being the small molecules and the second one polymers. Polymers will be discussed in detail in the next chapter. Therefore, in this section, the focus will be put on small molecules. The aim here is not to be complete but instead to give a brief introduction in the area of organic semiconductors.

Small molecules have been extremely successful in OFETs because of several reasons. Owing to their low molecular weight, they can be deposited on transistor substrates via sublimation in vaccuum. This is a major advantage since no solubilizing electrically insulating substituents have to be introduced to these molecules that might hinder optimal molecular packing detrimental for high charge carrier transport and thus excellent transistor performance. Another advantage of this class of material is their ease of purification as compared to polymers where problems of polydispersity and poor solubility for high molecular weights arise. One of the first class of low molecular weight organic semiconductor showing a charge carrier mobility higher than 0.1 $cm^2V^{-1}s^{-1}$ was the family of acenes, among them most notably pentacene (Figure 3.7a) [46]-[49]. As mentioned before, pentacene forms polycrystalline films. The crystalline domains consist of pentacene molecules

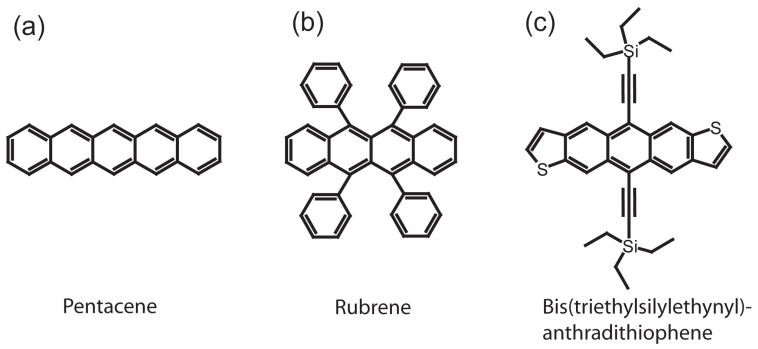

Figure 3.7: a.) Chemical structure of pentacene b.) rubrene and c.) bis(triethylsilylethynyl)-anthradithiophene.

packed in a herringbone structure as illustrated in (Figure 3.8c) [50]-[52], where the partial overlap of neighboring sites along the a-axis provides fast charge carrier transport, resulting in high mobilities. However, the polycrystallinity containing numerous grain boundaries limit more superior transistor behavior. Due to its high performance and commercial availability, many groups have devoted and are still devoting extensively to the study of pentacene based OFETs. Hence, for many years, pentacene has become the benchmark organic semiconductor. However, the main problem with pentacene is that it cannot be dissolved in organic solvents, making it unsuitable for commercialization in everyday electronic devices. One of the major selling points of organic semiconductors is that they can be used in easy, cheap and large area fabrication of electronic products. In order to realize this goal, solution processing is crucial. In an effort to solve this problem, soluble pentacene precursors have been synthesized. Once deposited from solution into a thin film, additional heat treatment turns these precursors into pentacene, resulting in high mobilities of up to 0.98 $cm^2V^{-1}s^{-1}$ [53]-[55].

Another successful strategy for solubilizing small molecules is the introduction of triethylsilylethynyl substituents to thiophene-anthracene fused rod-like molecules. Bis(triethylsilylethynyl)-anthradithiophene (Figure 3.7c) has been produced in such a way, yielding drop-cast OFETs with mobilities of 1 $cm^2V^{-1}s^{-1}$ [56]. In single crys-

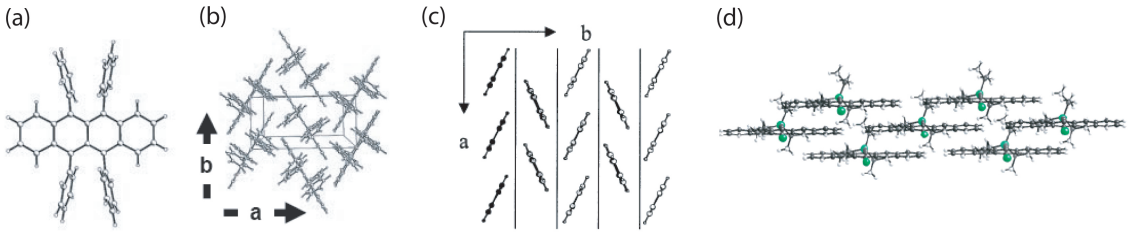

Figure 3.8: a.) 3-dimensional chemical structure of rubrene and b.) orthorhombic packing of single crystal rubrene [8]. c.) Herringbone crystal packing of pentacene [50]. d.) Brick-like crystal structure of bis(triethylsilylethynyl)-anthradithiophene [56].

tals, this compound packs in a brick-like fashion as schematically presented in (Figure 3.8d). Partial overlap of neighboring molecules is present, in this way providing efficient intermolecular charge transport necessary for high mobilities. Subsequent work following similar chemical structures with different acene building blocks have been reported [57][58]. Nevertheless, the material with one of the highest mobility up to date is an organic single crystal OFET made out of rubrene (Figure 3.7b) exhibiting an orthorhombic structure as highlighted in (Figure 3.8b). A mobility of 15 $cm^2V^{-1}s^{-1}$ was measured along the b-axis where molecular orbital overlap is more pronounced that along the a-axis. Charge carrier mobility deduced from OFET characterization along this direction was only 4 $cm^2V^{-1}s^{-1}$ [8]. Rubrene, which is soluble due to the four phenyl rings attached to the anthracene backbone, has also been solution processed, yielding mobilities of 0.78 $cm^2V^{-1}s^{-1}$ [59]. In this case, no single crystal was formed but rather a polycrystalline film.

Bibliography

[1] G. Malliaras, R. Friend, *Physics Today* **2005**, *58*, 53.

[2] S. Sergeyev, W. Pisula, Y. H. Geerts, *Chem. Soc. Rev.* **2007**, *36*, 1902.

[3] J. Piris, M. G. Debije, N. Stutzmann, B. W. Laursen, W. Pisula, M. D. Watson, T. Bjornholm, K. Müllen, J. M. Warman, *Adv. Funct. Mater.* **2004**, *14*, 1053.

[4] A. Tracz, J. K. Jeszka, M. D. Watson, W. Pisula, K. Müllen, T. Pakula, *J. Am. Chem. Soc.* **2003**, *125*, 1682.

[5] W. Pisula, Z. Tomovic, M. Stepputat, U. Kolb, T. Pakula, K. Müllen, *Chem. Mater.* **2005**, *17*, 2641.

[6] C. Reese, Z. Bao, *materialstoday* **2007**, *10*, 20.

[7] R. W. I. de Boer, M. E. Gershenson, A. F. Morpurgo, V. Podzorov, *phys. stat. sol. (a)* **2004**, *201*, 1302.

[8] V. C. Sundar, J. Zaumseil, V. Podzorov, E. Menard, R. L. Willett, T. Someya, M. E. Gershenson, J. A. Rogers, *Science* **2004**, *303*, 1644.

[9] A. L. Briseno, S. C. B. Mannsfeld, M. M. Ling, S. Liu, R. J. Tseng, C. Reese, M. E. Roberts, Y. Yang, F. Wudl, Z. Bao, *Nature* **2006**, *444*, 913.

[10] R. Ruiz, D. Choudhary, B. Nickel, T. Toccoli, K.-C. Chang, A. C. Mayer, P. Clancy, J. M. Blakely, R. L. Headrick, S. Iannotta, G. G. Malliaras, *Chem. Mater.* **2004**, *16*, 4497.

[11] C. D. Dimitrakopoulos, D. J. Mascaro, *IBM J. RES. and DEV.* **2001**, *45*, 11.

[12] S. E. Fritz, S. M. Martin, C. D. Frisbie, M. D. Ward, M. F. Toney, *J. Am. Chem. Soc.* **2004**, *126*, 4084.

[13] R. A. Laudise, C. Kloc, P. G. Simpkins, T. Siegrist, *Journal of Crystal Growth* **1998**, *187*, 449.

[14] C. D. Dimitrakopoulos, P. R. L. Malenfant, *Adv. Mater.* **2002**, *14*, 99.

[15] A. B. Chwang, C. D. Frisbie, *J. Appl. Phys.* **2001**, *90*, 1342.

[16] A. Bolognesi, M. Berliocchi, M. Manenti, A. Di Carlo, P. Lugli, K. Lmimouni, C. Dufour, *IEEE* **2004**, *51*, 1997.

[17] M. Kastler, W. Pisula, D. Wasserfallen, T. Pakula, K. Müllen, *J. Am. Chem. Soc.* **2005**, *127*, 4286.

[18] B. N. Pal, P. Trottman, J. Sun, H. E. Katz, *Adv. Funct. Mater.* **2008**, *18*, 1832.

[19] W. Pisula, A. Menon, M. Stepputat, I. Lieberwirth, U. Kolb, A. Tracz, H. Sirringhaus, T. Pakula, K. Müllen, *Adv. Mater.* **2005**, *17*, 684.

[20] H. Sirringhaus, T. Kawase, R. H. Friend, T. Shimoda, M. Inbasekaran, W. Wu, E. P. Woo, *Science* **2000**, *290*, 2123.

[21] R. A. Street, W. S. Wong, S. E. Ready, M. L. Chabinyc, A. C. Arias, S. Limb, A. Salleo, R. Lujan, *Mater. Today* **2006**, *9*, 32.

[22] H. Sirringhaus, T. Kawase, R. H. Friend, *MRS Bulletin* **2001**, 539.

[23] S. R. Forrest, *Nature* **2004**, *428*, 911.

[24] M. Berggren, D. Nilsson, N. D. Robinson, *Nat. Mater.* **2007**, *6*, 3.

[25] D. Zielke, A. C. Hübler, U. Hahn, N. Brandt, M. Bartzsch, U. Fügmann, T. Fischer, J. Veres, S. Ogier, *Appl. Phys. Lett.* **2005**, *87*, 123508.

[26] B. D. Gates, Q. Xu, M. Stewart, D. Ryan, C. Grant Willson, G. M. Whitesides, *Chem. Rev.* **2005**, *105*, 1171.

[27] H. E. Katz, *Chem. Mater.* **2004**, *16*, 4748.

[28] T. B. Singh, N. S. Sariciftci, *Annu. Rev. Mater. Res.* **2006**, *36*, 199.

[29] E. Menard, V. Podzorov, S.-H. Hur, A. Gaur, M. E. Gershenson, J. A. Rogers, *Adv. Mater.* **2004**, *16*, 23.

[30] C. Goldmann, S. Haas, C. Krellner, K. P. Pernstich, D. J. Gundlach, B. Batlogg, *J. Appl. Phys.* **2004**, *96*, 2080.

[31] W. Wang, T. Lee, M. A. Reed *Phys. Rev. B* **2003**, *68*, 035416.

[32] R. W. Zehner, B. F. Parsons, R. P. Hsung, L. R. Sita, *Langmuir* **1999**, *15*, 1121.

[33] H. E. Katz, J. Johnson, A. J. Lovinger, *J. Am. Chem. Soc.* **2000**, *122*, 7787.

[34] D. J. Gundlach, L. L. Jia, T. N. Jackson, *Electr. Dev. Lett.* **2001**, *22*, 571.

[35] I. H. Campell, J. D. Kress, R. L. Martin, D. L. Smith, N. N. Barashkov, J. P. Ferraris, *Appl. Phys. Lett.* **1997**, *71*, 3528.

[36] S. Subramanian, S. Park, S. R. Parkin, V. Podzorov, T. N. Jackson, J. E. Anthony, *Chem. Rev.* **2008**, *130*, 2706.

[37] B. de Boer, A. Hadipour, M. M. Mandoc, T. v. Woudenbergh, P. W. M. Blom, *Adv. Mater.* **2005**, *17*, 621.

[38] J. Veres, S. Ogier, G. Lloyd, *Chem. Mater.* **2004**, *16*, 4543.

[39] S. Kobayashi, T. Nishikawa, T. Takenobu, S. Mori, T. Shimoda, T. Mitani, H. Shimotani, N. Yoshimoto, S. Ogawa, Y. Iwasa, *Nat. Mater.* **2004**, *3*, 317.

[40] M.-H. Yoon, A. Facchetti, T. J. Marks, *PNAS* **2005**, *102*, 4678.

[41] A. Facchetti, M.-H. Yoon, T. J. Marks, *Adv. Mater.* **2005**, *17*, 1705.

[42] M.-H. Yoon, C. Kim, A. Facchetti, T. J. Marks, *J. Am. Chem. Soc.* **2006**, *128*, 12851.

[43] R. Parashkov, E. Becker, G. Ginev, T. Riedl, H.-H. Johannes, W. Kowalsky, *J. Appl. Phys.* **2004**, *95*, 1594.

[44] H. Klauk, M. Halik, U. Zschieschang, G. Schmid, W. Radlik, W. Weber, *J. Appl. Phys.* **2002**, *92*, 5259.

[45] J. Wu, W. Pisula, K. Müllen, *Chem. Rev.* **2007**, *107*, 718.

[46] S. F. Nelson, Y.-Y. Lin, D. J. Gundlach, T. N. Jackson, *Appl. Phys. Lett.* **1998**, *72*, 1854.

[47] Y.-Y. Lin, D. J. Gundlach, S. F. Nelson, T. N. Jackson, *IEEE* **1997**, *18*, 0741.

[48] V. Y. Butko, X. Chi, D. V. Lang, A. P. Ramirez, *Appl. Phys. Lett.* **2003**, *83*, 4773.

[49] H.-S. Seo, Y.-S. Jang, Y. Zhang, P. S. Abthagir, J.-H. Choi, *Org. Electron.* **2008**, *9*, 432.

[50] C. C. Mattheus, A. B. Dros, J. Baas, G. T. Oostergetel, A. Meetsma, J. L. de Boer, T. T. M. Palstra, *Synth. Met.* **2003**, *138*, 475.

[51] C. C. Mattheus, G. A. de Wijs, R. A. de Groot, T. T. M. Palstra, *J. Am. Chem. Soc.* **2003**, *125*, 6323.

[52] S. Schiefer, M. Huth, A. Dobrinevski, B. Nickel, *J. Am. Chem. Soc.* **2007**, *129*, 10316.

[53] A. R. Brown, A. Pomp, C. M. Hart, D. M. de Leeuw, *Science* **1995**, *270*, 972.

[54] P. T. Herwig, K. Müllen, *Adv. Mater.* **1999**, *11*, 480.

[55] A. Afzali, C. D. Dimitrakopoulos, T. L. Breen, *J. Am. Chem. Soc.* **2002**, *124*, 8812.

[56] M. M. Payne, S. R. Parkin, J. E. Anthony, C.-C. Kuo, T. N. Jackson, *J. Am. Chem. Soc.* **2005**, *127*, 4986.

[57] M. L. Tang, A. D. Reichardt, T. Okamoto, N. Miyaki, Z. Bao, *Adv. Funct. Mater.* **2008**, *18*, 1579.

[58] M. L. Tang, A. D. Reichardt, N. Miyaki, R. M. Stoltenberg, Z. Bao, *J. Am. Chem. Soc.* **2008**, *130*, 6064.

[59] N. Stingelin-Stutzmann, E. Smits, H. Wondergem, C. Tanase, P. Blom, P. Smith, D. de Leeuw, *Nat. Mater.* **2005**, *4*, 601.

Chapter 4

P-type Polymer OFETs

4.1 Introduction

Polymer organic semiconductors are due to their mechanical flexibility particularly interesting for application in bendable electronic devices. In addition, compared to small molecules, polymers in general readily form thin films when solution deposited, making this material group extremely suitable for fast processing techniques like roll to roll printing of plastic circuits. However, polymer OFETs have been hampered by too low charge carrier mobilities, often less than 0.01 $cm^2V^{-1}s^{-1}$ [1]-[4]. Unlike small molecules which frequently tend to form crystalline structures, such high long range molecular order is difficult to achieve for polymers. Whereas small molecules can be simply sublimed into highly ordered crystalline films in vacuum enabled by their low molecular weight, polymers on the other hand cannot be processed in this way owing to their much higher mass. Hence, the only method applicable for polymers is by solution processing. To guarantee solubility, solubilizing groups have to be introduced to the conjugated polymer backbone. Such groups can be for example alkyl chains which are indeed most often employed. However, those alkyl chains can potentially have a tremendous impact on the self-assembly and therefore on the charge transport between the polymer chains. This point will

be highlighted in this chapter. Despite the generally low tendency of polymers to form highly ordered layers akin to most small molecules, in the past few years, significant progress has been made in terms of increasing charge mobility in polymer OFETs surpassing 0.1 $cm^2V^{-1}s^{-1}$ [5], a value qualifying their commercial use. In this chapter, the different approaches towards this device performance are briefly illustrated. In essence, enhancement of molecular self-assembly into highly packed superstructures and linked to this maximization of charge carrier transport was reached by appropriate chemical structure design of the polymers. Furthermore, it is highlighted how molecular weight and the proper solution processing potentially dictate film morphology and thus transistor behavior, ultimately resulting in an excellent hole mobility of up to 1.4 $cm^2V^{-1}s^{-1}$.

4.2 Regioregular Thiophene Polymer OFETs

The first method to achieve high performance transistors with mobilities larger than 0.1 $cm^2V^{-1}s^{-1}$ was the introduction of regioregular alkyl chains in polythiophenes. Application of regioregular head-to-tail poly(3-hexylthiophene) (HT-P3HT) (Figure 4.1a) showed that the regioregularity induces lamellar $\pi - \pi$ stacks of the polymer chains which in addition adopted an edge-on orientation on the surface (Figure 4.2). In comparison to regiorandom polyalkylthiophenes which did not exhibit any ordering when deposited as a thin film, the HT-P3HT with their hexyl alkyl chains arranged from head to tail as schematically depicted in Figure 4.3a triggers the formation of polycrystalline layers. That is, solution processed HT-P3HT films resulted in crystalline domains consisting of lamellar stacked polymer chains induced by the head-to-tail regioregularity. Such ordered, edge on lamellar packing yielded hole mobilities of up to 0.1 $cm^2V^{-1}s^{-1}$ [6]. The degree of regioregularity was found to play a significant role in determing whether the HT-P3HT polymers adopt an edge on or face on configuration which in turn influence transistor performance. For the face on case, the plane of the polymer backbone is placed on the substrate

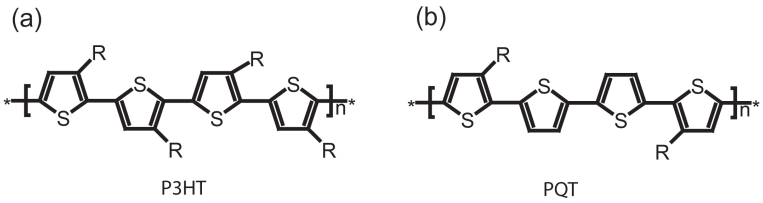

Figure 4.1: a.) Chemical structure of regioregular head-to-tail poly(3-hexylthiophene) (HT-P3HT, R is hexyl) and b.) regioregular poly(3,3‴-dialkyl-quaterthiophene) (PQT) with R = C_{12} .

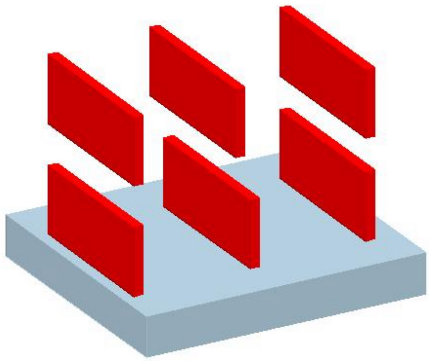

Figure 4.2: Schematic presentation of lamellar packing with edge-on arrangement. Red rectangles represent polymer chains.

and not perpendicularly to it as in the edge on arrangement depicted in Figure 4.2. The face on configuration was found to exhibit three orders of magnitude lower charge carrier mobilities than for the edge on packing due to weaker intermolecular $\pi - \pi$ overlap caused by the insulating alkyl chains separating neighboring polymer chains. The face on configuration was observed for a regioregularity of around 80 percent whereas a regioregularity larger than 95 percent is required for an edge on adoption.

The film morphology of the high performance spin-coated HT-P3HT films was investigated by several groups in order to understand the origin for the high mobility in more detail. Hereby, it was found that film morphology critically depends on the molecular weight of the HT-P3HT polymers. Low molecular weight polymers generated randomly oriented nanorod like films when spin-coated (Figure 4.4a) whereas high molecular weight polymers deposited in the same way

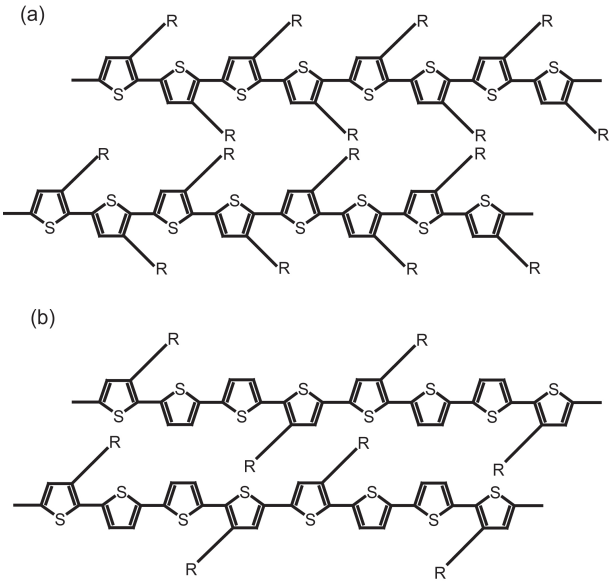

Figure 4.3: a.) Schematic representation of intermolecular head-to-tail side chain packing in HT-P3HT and b.) interdigitated intermolecular side chain lamellar packing in PQT.

resulted in nodule like structures (Figure 4.4b) [7]. In particular, the nanorods were clearly distinguishable and more crystalline than the higher molecular weight nodule like films that contain less distinctly separated domains. Nevertheless, lamellar stacking of the polymers was present in both low and high molecular weight layers. It is argued that the nanorod morphology for low molecular weight polymers is more ordered due to the lower viscosity than for the higher molecular weight compounds. The chains in the latter group are kinetically less mobile, in this way being less able to form highly packed crystallites, resulting in less arranged nodule like morphologies. Surprisingly, the more crystalline nanorod shaped layers showed lower charge carrier mobilities than for the less well packed higher molecular weight polymers. In fact, a difference of three orders of magnitude in mobility was measured between low and high molecular weight polymers. This phenomenon is attributed to the various degrees of connectivity of the individual ordered domains in which efficient charge carrier transport is expected. Those ordered domains for low molecular weight HT-P3HT polymers are the nanorods. Scanning tunneling microscope (STM) measurements on spin coated films on

highly oriented pyrolytic graphite (HOPG) revealed polycrystallinity with domains consisting of packed nanorods embedded in an amorphous matrix [8][9]. This means that those domains are separated by disordered regions through which charge transport is severely impeded. Effectively, when charges travel from one to another highly ordered region on their way from the source to the drain electrode, they have to pass through such amorphous areas which slow down charge transport. As a consequence, charge carrier mobility is low. However, care has to be taken here. Those polycrystalline films were cast on HOPG but OFETs were measured employing layers formed on SiO_2. Even though lamellar packing was present on both surfaces, film morphologies might vary depending on the nature of the surface on which the polymers are deposited. The more enhanced charge carrier mobility in the higher molecular weight case is attributed to the better connectivity between ordered domains. It was postulated that the higher the molecular weight, the longer the polymer chains and thus the better the connectivity between ordered regions enabling elevated mobilities. Those longer chains more frequently extend from one well arranged domain to the other, in this way minimizing charge trapping sites and thus leading to higher mobilities. This point is further strenghtened by Verilhac and coworkers who studied HT-P3HT via dip-coating [10]. Hereby, the film crystallinity and morphology did not change with molecular weight. Nevertheless, charge carrier mobility was still more pronounced for higher molecular weight polymer layers, underlining the importance of connectivity [10]. One has to keep in mind that those reported studies did not include the influence of polydispersity which might trigger different film morphologies and transistor behavior as well. Unfortunately, up to date, no systematic work concerning this aspect has been reported yet.

As was evident from the results of HT-P3HT, the proper placement of the alkyl chains in thiophene polymer backbones influences molecular packing and linked to this transistor performance. The head-to-tail alignment of the regioregular alkyl

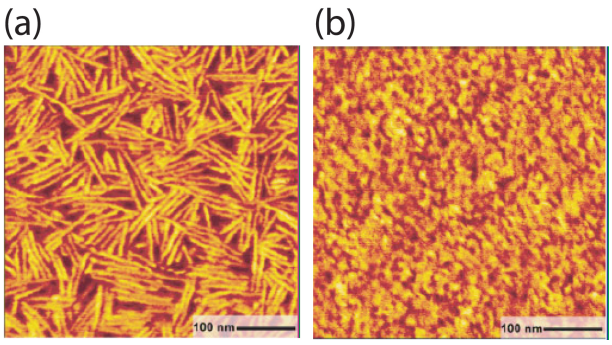

Figure 4.4: a.) AFM image of low molecular weight HT-P3HT showing nanofiber like morphology and b.) AFM image of ten times higher molecular weight HT-P3HT film with nodule like structures [7].

chains significantly contributes to the lamellar stacking of the polymer chains. However, this head-to-tail arrangement is not the optimized structure yet. As was demonstrated by Ong and coworkers, interdigitated intermolecular side chains trigger more effective lamellar organization than in the head-to-tail case (Figure 4.3b), leading to expected longer range ordering and higher mobility. This interdigitation was achieved by the larger separation between the alkyl chains in the regioregular thiophene polymer monomer, as is true for regioregular poly(3,3$'''$-dialkyl-quaterthiophene) (PQT) with C_{12} alkyl chains (Figure 4.1b). This polymer exhibited mobilities of 0.25 $cm^2V^{-1}s^{-1}$ for spin-coated, top contact OFETs, higher than for HT-P3HT [5][21][11], stressing the impact of alkyl chain placement in such polythiophene systems on film morphology and transistor behavior.

4.3 Liquid Crystalline Thiophene Polymer OFETs

Another approach to further enhance charge carrier mobility is to increase supramolecular organization, in addition to the lamellar order induced by the regioregular polythiophenes guaranteeing sufficent molecular orbital overlap for efficient charge transport. Such macromolecular alignment can be for example obtained through a better intermolecular packing or/and phase transitions. In this sense, I.

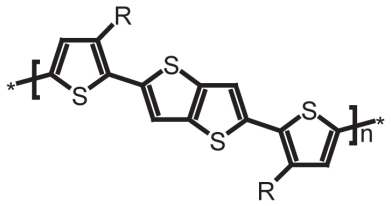

PBTTT

Figure 4.5: Chemical structure of poly(2,5-bis(3-alkylthiophen-2-yl)thieno[3,2-b]thiophene) (PBTTT) with R = C_{14}.

McCulloch and coworkers have developed a regioregular polythiophene similar to PQT for which more pronounced long range order was achieved than for HT-P3HT. However, the middle two thiophene units are replaced by the linearly conjugated comonomer thieno[3,2-b]thiophene (Figure 4.5) which is rotationally invariant as compared to the two thiophene monomers in PQT. This more rigid thieno[3,2-b]thiophene comonomer is expected to promote the formation of ordered crystalline domains. Indeed, as X-ray diffraction measurements of spin-coated PBTTT polymer (Figure 4.5) films clearly demonstrated, lamellar packing was present [12].

Furthermore, the polymer PBTTT posess a liquid crystalline state. That is, when heated to this condition, the polymer chains gain enough energy to reassemble in a more favorable arrangement. Hereby, the initial structure is not destroyed as would be the case for the isotropic phase where the material turns or melts from its solid state to the liquid phase. After having reached the liquid crystalline state, controlled cooling of the material's film results in the achieved better molecular order. Due to this phenomenon, some materials can self-heal, that it, small defects within the structure can be cured in this way [13]. Following this idea, the spin-coated PBTTT film was heated to the liquid crystalline state and cooled down to room temperature. Hereby, hole mobilities reached up to 0.6 $cm^2V^{-1}s^{-1}$ [12]. The liquid crystalline mediated films showed X-ray diffraction peaks with higher intensities than the layers prior to this phase transition, suggesting better molecular packing. Both types of films contain lamellar structures, hence the more pronounced ordering was attributed to a growth of the more ordered domain sizes.

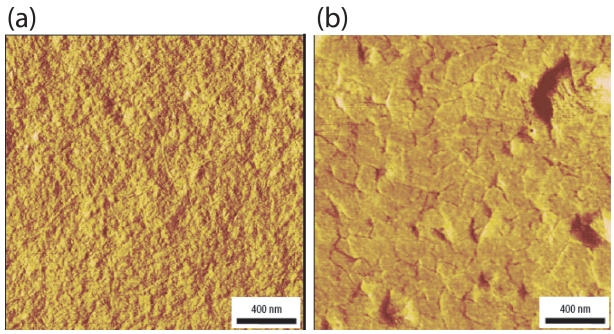

Figure 4.6: a.) AFM image of PBTTT film prior to and b.) after crystallization from the liquid crystalline phase [12].

This point was underlined by AFM images where larger domain sizes were observed for the liquid crystalline films (Figure 4.6b) compared to the morphology prior to this treatment (Figure 4.6a). The authors hypothesized that the polymer films were polycrystalline akin to HT-P3HT containing ordered regions separated by disordered or amorphous space. The higher mobility films formed from the liquid crystalline most probably resulted from the overall growth of ordered domains and better connectivity of those domains by the better aligned disordered regions.

4.4 Nitrogen bridged Ladder Type Polymer OFETs

For the three high performance polymers reviewed so far, molecular packing was forced by regioregularly placed alkyl chains in the polythiophene backbones. Hereby, self-assembly in huge parts relied on the interaction between those alkyl chains. Another decisive factor influencing molecular self assembly is the interaction between the delocalized π-orbitals of the conjugated polymer backbones. Such π-π intermolecular interaction has proven to play a crucial role particularly for systems with large extended π-orbitals like polycyclic aromatic hydrocarbons (PAHs). For instance, HBCs form one columnar stacks mostly driven by such π-π interaction. Of

course, the self-assembly is not only evoked by this π-stacking but is more or less an interplay with the kinetics of the alkyl chains [14]-[17]. Taking into consideration the influence of π-π interaction, it is appealing to apply polymers with a large extended delocalized π-orbital in OFETs. Such a system is expected to exhibit strong π-stacking, in this way potentially generating highly ordered structures like lamellar packing found in HT-P3HT or PBTTT. Based on these ideas, long, rod-like conjugated polymers are expecially attractive candidates. Furthermore, a rigid backbone with rotational invariance would not inhibit charge transport along the conjugation plane of the individual polymer chains. Since it has been shown that charge transport along the conjugation plane of the individual polymer chains is fastest, this lack of twisting is crucial in avoiding charge scattering and hence lowering of charge carrier mobility. Sirringhaus and coworkes have demonstrated that directionally aligned HT-P3HT films where charge carrier mobility measured along the conjugation plane was four orders of magnitudes higher than measured along the intermolecular π-π-stacking transport [18]. This phenomenon was explained by the longer charge diffusion along the polymer backbone (black arrow in Figure 4.7b) till the charge encounters another polymer chain to which charges continue their path via a slower hopping mechanism (green and red arrows in Figure 4.7b). Loosely spoken, this thermally activated hopping takes place when charge carriers have to overcome a discontinuity in molecular orbital as is for example the case when travelling from one chain to the other or when overcoming deeper trapping sites like in a highly disordered film [19][20]. In the π-π-stacking transport on the other hand, that is charge transfer perpendicular to the polymer backbone plane (red arrow in Figure 4.7b), mainly hopping takes place, leading to lower charge carrier mobilities. Based on these findings, it is advantageous to apply long, rigid rod like polymers in OFETs. Also, in this light, short polymer chains most probably lead to an overall shortening of the fast intramolecular charge transport (black arrow in Figure 4.7a) prior to the occurance of intermolecular hopping (green and red arrows in Figure 4.7a). Based

Figure 4.7: a.) Charge transport in short polymer chain assembly. Blue rectangles represent polymer chains. Black arrow illustrates fast charge diffusion along the individual polymer chain. Green and red arrows depict slow intermolecular hopping processes from one chain end to the other and along the π-π stacking respectively. b.) Same charge transport phenomena in an assembly of longer polymer chains. Charges can travel over a longer distance via the fast charge diffusion along the polymer chains (black arrow) before intermolecular hopping process takes place (green and red arrows).

on these findings, it is advantageous to apply long, rigid rod like polymers in OFETs with highly extended π-molecular orbitals to minimize hopping events.

Theoretical predictions indicated charge carrier mobilities up to 1000 $cm^2V^{-1}s^{-1}$ along a perfectly ordered polymer chain, while time-resolved microwave conductivity experiments have proven 600 $cm^2V^{-1}s^{-1}$ for isolated ladder-type poly(paraphenylene)chains in dilute solutions [24].

Two examples of intrinsic properties of organic materials that limit the charge carrier mobility are interchain transport and charge transport over grain boundary junctions between different relatively ordered domains within the sample. Both processes are expected to be significantly slower than intrachain transport and depend strongly on the material morphology on a supramolecular scale [25][28]. Furthermore, the intrachain charge carrier mobility can be limited by disorder along

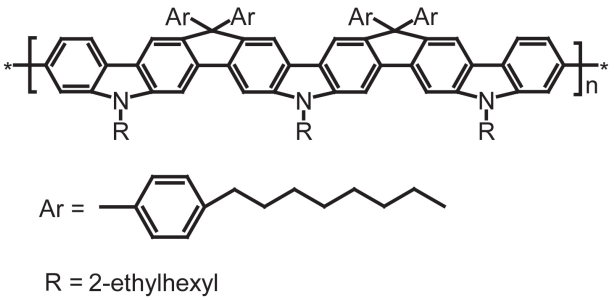

Figure 4.8: Chemical structure of nitrogen bridged ladder type polymer.

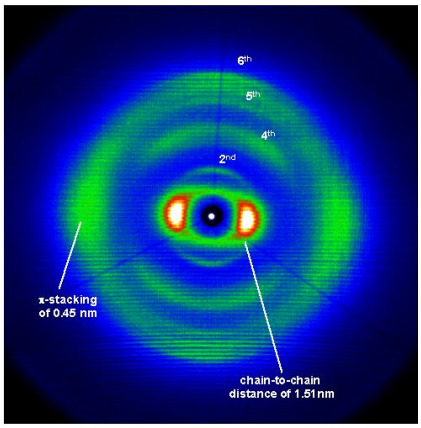

Figure 4.9: 2D-WAXS of extruded nitrogen bridged ladder type polymer.

the polymer chains. Effects that cause such intrachain disorder include torsion of the polymer backbone and the presence of chemical defects that can act as barriers for charge transport [29][30]. The nitrogen bridged ladder-type polymer (Figure 4.8) with a number average molecular weight M_n of 2.3 $\times 10^4 g\ mol^{-1}$ is structurally well defined with no torsional disorder, since it is restricted to a planar geometry by abridging carbon atom. Such a structure is optimal for charge transport because the electronic coupling between neighboring units is maximal for a planar structure [31]. Also, this is a long rod-like polymer delivering the desired extended delocalized π-orbital for expected better packing and charge transport. However, such a large rigid system is not soluble and solubility has to be achieved by introducing alkly chains for instance. The attachment of 2-ethylhexyl chains to the nitrogen atoms in the carbazole together with additional aryl groups as shown in Figure 4.8 solves the solubility problem of this ladder-type polymer.

This polymer was synthesized by Dr. Ashok K. Mishra and investigated by Dr. Wojciech Pisula (both at the Max-Planck Institute for Polymer Research in Mainz) by X-ray scattering to relate its macromolecular architectures with its supramolecular organizations. Differential scanning calorimetry (DSC) measurements did not reveal any phase transitions for the investigated polymer within a temperature range

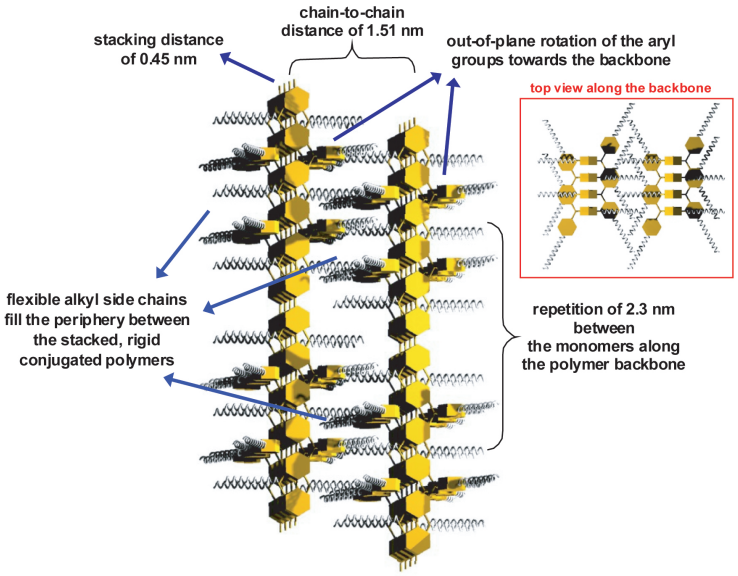

Figure 4.10: Self-assembly of extruded nitrogen bridged ladder type polymer.

of −100°C to 220°C. For the structural investigation, the polymer was extruded under the same conditions to ensure a proper comparison of the supramolecular assembly between the different compounds [32]. The sample preparation was carried out using a home-built mini-extruder at a temperature of 200°C at which the materials showed only limited plasticity. The two-dimensional wide-angle X-ray scattering (2D-WAXS) experiments were performed at room temperature. The organization of the polymer did not change at higher temperatures or after annealing. The extruded filaments were positioned vertically towards the 2D-WAXS detector. The distribution of the reflections over the scattering pattern allows elucidation of the relative arrangement of the building units within the supramolecular organization. Figure 4.9 shows a typical 2D-WAXS pattern of the extruded polymer. The high intensity and distinct reflections point toward a pronounced organization of the polymer in the extruded sample. The sharp equatorial small-angle reflections in Figure 4.9, indicating the alignment of the macromolecules along the shearing direction and thus along the filament axis, correspond to a distance of 1.51 nm. This value was related to the chain-to-chain distance of the conjugated polymer chains [33]. On the other hand, the equatorial wide-angle reflections at a correlation distance of 0.45 nm sig-

nified the π-stacking spacing between the polymer units. The meridional reflections correspond to the repeating distance between monomers along the polymer backbone. The theoretical distance between single units of 2.3 nm could not be derived in a straightforward way, since this reflection position was superimposed by the equatorial scattering intensity corresponding to 1.51 nm. However, multiple higher order reflections, which correlated with the distance between monomer units, appeared in the pattern. For instance, the second higher order reflection in the meridional was related to 1.15 nm, which was the half value of 2.3 nm. Reflections up to the sixth order were obvious, confirming the high order of the polymer chains towards each other. This was in good accordance with the strong π-stacking reflection, which suggests a pronounced interaction between the single building blocks. The organization of the conjugated polymer is illustrated schematically in Figure 4.10. All essential periodicities are pointed out in the drawing. Due to simplifications, the alkyl side chains are shown as stiff. But in reality, the alkyl substituents are flexible and rather disordered, filling the periphery of the rigid conjugated macromolecules stacked on top of each other. The aryl groups play an important role not only in the solubility of the compound, but also influence the packing. Since these groups posess a rather high steric demand due to their out-of-plane position towards the polymer backbone, one can assume a flipping of the conjugated chain during self-assembly, leading to the most favorable arrangement as highlighted in the inset in Figure 4.10. A poor amorphous halo was also observed for the polymer which is typical for the disordered alkyl side chains filling the periphery of the conjugated polymers.

To relate the polymer architecture to device operation the performance of the ladder type polymer in field-effect transistors was investigated. Polymer films were obtained by spin-coating at 3000 rpm (rotations per minute) for 40 seconds from 20 mg/ml toluene solution on the hexamethyldisilazane (HMDS) treated device substrates with bottom-contact and bottom-gate geometry. The channel length and width are 10 μm and 5 mm respectively. The samples were annealed at 120°C

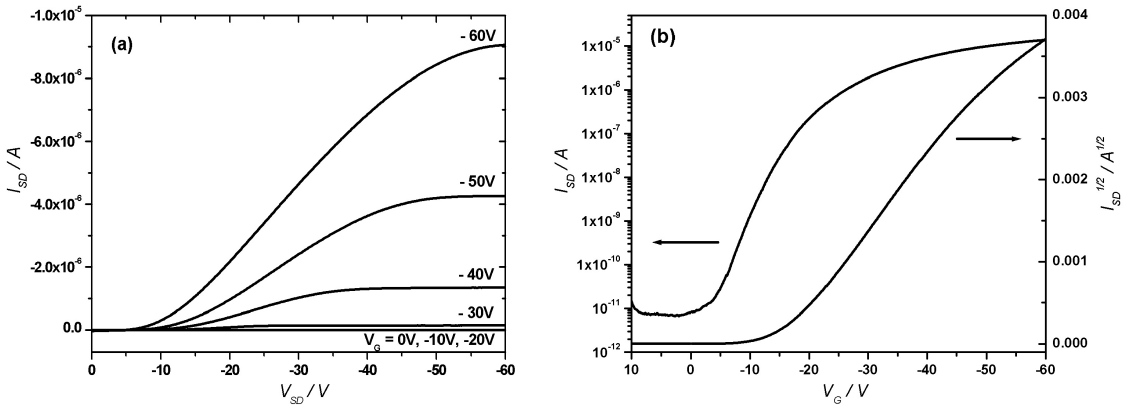

Figure 4.11: a.) Output curves for various gate biases V_G and b.) transfer characteristics at V_{SD} = -60V of nitrogen bridged ladder type polymer OFETs.

for 12 hours to remove residual solvent that might be trapped in the film. As a representative example, the resulting FET behavior of the polymer is illustrated in Figure 4.11, revealing a characteristic p-type performance as manifested in the transfer and output curves. The polymer provided consistent OFET operation following the conventional transistor models in both the linear and saturated regimes. The output curves displayed clear saturation, with the extracted mobility from the saturated regimes being up to $\mu_{sat} = 5\times10^{-4} cm^2V^{-1}s^{-1}$ with a typical on/off ratio of 10^5. The mobility after annealing was $\mu_{sat} = 5\times10^{-3} cm^2V^{-1}s^{-1}$, one order of magnitude higher than that of the devices before annealing. This moderate increase suggests that thermal treatment rather removes residual solvent and trapped oxygen than improves the semiconductor ordering within the thin layer.

This nitrogen bridged ladder type polymer exhibited low charge carrier mobility even though long range order was observed by 2D-WAXS in the extruded fibers. This macromolecular lamellar organization should lead to rapid charge transport along the polymer chains and good interchain π-molecular overlap that facilitate intermolecular charge hopping. Both aspects are expected to yield high mobilities. However, as in the case of HT-P3HT, PQT, and PBTTT, film morphology might play a decisive role in limiting transistor operation. In this aspect, an AFM image

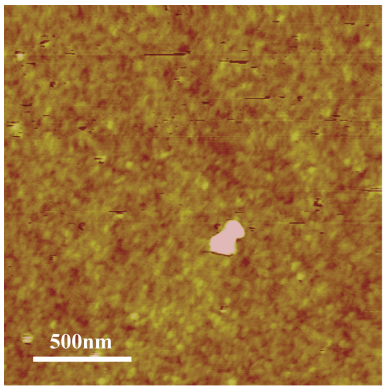

Figure 4.12: AFM image of spin-coated ladder-type polymer film on HMDS treated SiO_2.

of a spin-coated ladder-type polymer film on HMDS treated SiO_2 as used for OFET measurements was taken as depicted in Figure 4.12b. A polycrystalline morphology was present, akin to the high molecular weight P3HT film structure (Figure 4.4). This similar morphology allows the reasonable assumption that the lamellar packed domains of the ladder-type polymers are connected to a certain extend, leading to smoothed out grain boundaries as reported for HT-P3HT. Particularly, no distinct structure boundary like the nanorod morphology for low molecular weight HT-P3HT films (Figure 4.12a) were present that might trap charge carriers. Based on these observations, grain boundaries do not seem to effectively degrade transistor performance.

The measured low mobility can rather be attributed to the large π-stacking distance of 0.45 nm between the polymer backbones, in this way making interchain charge transfer difficult. In order to make this long rigid rod like polymer soluble, aryl groups and long alkyl chains had to be introduced to the polymer backbone. These substituents result in high steric hindrance of the polymer chains, leading to this large π-stacking distance and thus unfavorable charge transport from one chain to the other, in this way yielding poor transistor behavior. HT-P3HT on the other hand, exhibiting the same lamellar packing and comparable morphology, has a closer π-stacking distance of 0.38 nm [34], in this way providing better intermolecular

π-orbital overlap and thus potentially facilitating charge transport. It is obvious from this ladder-type polymer system that it is a formidable task to find the right balance between solubility, good molecular self-assembly and linked to this high device performance.

4.5 Donor Acceptor Cyclopentadithiophene - Benzothiadiazole (CDT-BTZ) Copolymer OFETs

For the nitrogen bridged ladder type polymer, lamellar packing was stimulated by the π-π interaction of the long, rigid rod like polymer backbones. However, charge carrier mobility was two orders of magnitude lower than for regioregular HT-P3HT and PQT as well as for the liquid crystalline PBTTT. One reason potentially responsible for this inferior transistor performance might be the larger intermolecular π-stacking distance in the nitrogen bridged ladder type polymer. Also, the presence of ordered lamellar arrangement even without regioregularity of the alkly chains in this system provides the freedom for designing other polymers with planar rod like backbones. In particular, in order to minimize the intermolecular π-stacking distance, one possibility would be to reduce the number or length of the alkyl chains for example in the ladder type polymer. However, the price that has to be paid is the insolubility of this compound, rendering film processing impossible. A different concept might be the employment of a rigid, rod like donor-acceptor copolymer backbone. It has been shown that in such a donor-acceptor system, the donor can pack with an acceptor and vice versa, leading to lamellar ordered self-assembly. In the polymer reported, a close intermolecular π-stacking distance of 0.37nm was obtained [37]. However, charge carrier mobility was low, in the order of $10^{-3} cm^2 V^{-1} s^{-1}$, even though lamellar order similar to the other known high performance polymers like HT-P3HT or PBTTT was present. Unfortunately, the authors did not mention film

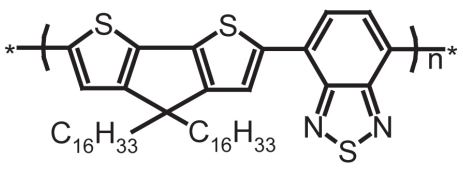

Figure 4.13: C_{16} substituted CDT-BTZ donor acceptor copolymer.

morphology and the effect of grain boundaries on charge carrier mobility that might have been responsible for the inferior transistor behavior.

In fact, all the high performance polymers discussed so far showed lamellar packing and intermolecular π-stacking distance smaller than 0.4 nm [6][12]. Surely, film morphology plays a crucial role as well in terms of grain boundaries and connectivity of the ordered domains for a minimization of charge trapping sites. This aspect was particularly evident for PBTTT where through the liquid crystalline phase larger domain sizes could be achieved, leading to one of the highest charge carrier mobilities up to now for polymeric systems. For the nitrogen bridged ladder-type polymer, nodule like films were present, indicating the minimization of grain boundaries and thus stressing the main contribution of a large intermolecular π-stacking distance to the degradation of transistor performance. Keeping this in mind, a cyclopentadithiophene (CDT) and benzothiadiazole (BTZ) copolymer (Figure 4.13) was synthesized by Dr. Ming Zhang at the Max-Planck Institute for Polymer Research in Mainz. BTZ is a well known strong acceptor frequently applied in low bandgap organic donor-acceptor semiconductor polymers for organic photovoltaics (OPVs) like solar cells [35][36]. Motivated by the success of polyalkylthiophene polymers, a CDT donor was used substituted with C_{16} for solubility purposes. With this copolymer architecture, we keep in mind that the donor part of the copolymer monomer is expected to pack with the acceptor part of a neighboring copolymer monomer and vice versa (acceptor packs with donor), in this way driving forward long-range and close intermolecular self-assembly [37].

Gel-permeation chromatography (GPC) analysis with polystyrene standard exhibited a number-average molecular weight M_n of 12K g mol^{-1}. In low boiling

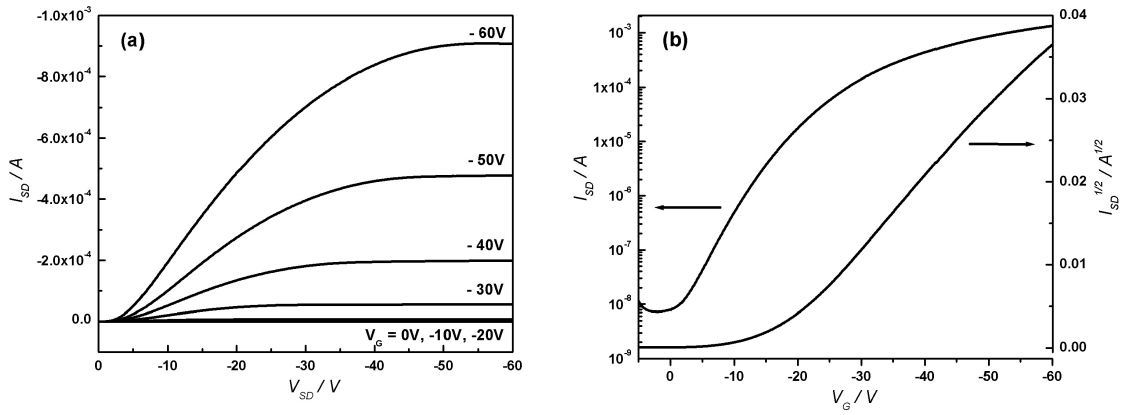

Figure 4.14: a.) Output curves for various gate biases V_G and b.) transfer characteristics at V_{SD} = -60V of drop-cast CDT-BTZ copolymer OFETs.

solvents like chloroform or THF, the copolymer cannot be completely dissolved at a concentration of 1 mg ml^{-1}. Instead, a solution with this concentration was obtained using the high boiling solvent 1,2,4-trichlorobenzene via heating at 150°C. Bottom contact FETs were fabricated by drop-casting on highly n-doped silicon wafer with a 150 nm thermally grown and HMDS treated silicon dioxide layer. The transistor substrate was held at 100°C during solvent evaporation and film formation. Prior to annealing, the transistors showed a mobility of $\mu_{sat} = 4{\times}10^{-4} cm^2V^{-1}s^{-1}$ together with a low on/off ratio of 10^2. Annealing the devices at 200°C for 2 hours led to improved charge carrier mobilites of up to $\mu_{sat} = 0.11\ cm^2V^{-1}s^{-1}$ as extracted from the slope of the transistor curve illustrated in Figure 4.14 and utilizing equation 2.4 with channel length L = 10 μm and width W = 5 mm. The on/off ratio increased to 10^5 as well, owing to the higher on current. The devices saturated as can be clearly seen in the output characteristics (Figure 4.14a) and exhibited typical transistor behavior.

When drop-casting from a ten times more concentrated solution followed by the same annealing step as mentioned above, we observed an elevated saturated mobility of $\mu_{sat} = 0.17\ cm^2V^{-1}s^{-1}$ and an on/off ratio of 10^5 (Figure 4.15). We assume that this higher μ_{sat} arose from the increased number of charge carriers induced in the saturation regime due to the larger amount of material deposited. The thicker the

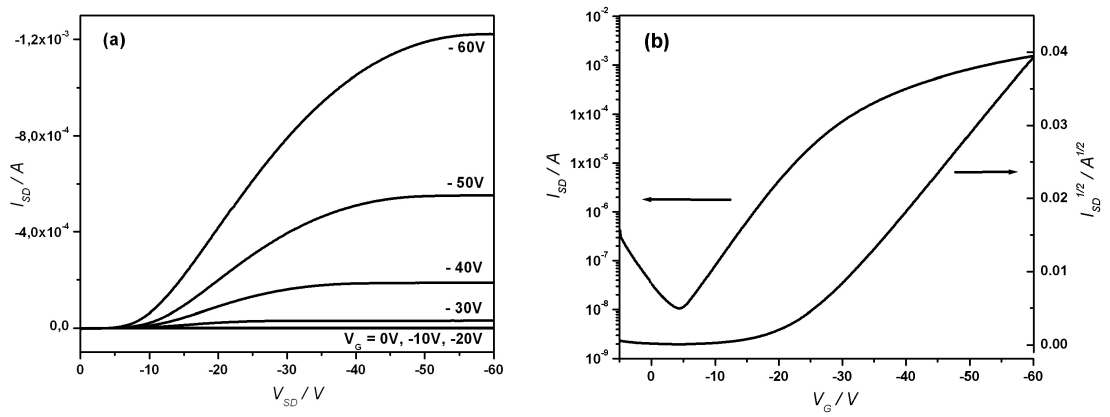

Figure 4.15: a.) Output curves for various gate biases V_G and b.) transfer characteristics at V_{SD} = -60V of drop-cast 10 mg ml^{-1} CDT-BTZ copolymer OFETs.

deposited film, the more charge carriers can be accumulated from the bulk in the saturated regime at higher gate voltages. Compared to the lower concentration case, a more distinct non-linear behavior of the output curves at low source-drain voltages (Figure 4.15a) is evident, indicating the presence of contact resistance. This is generally caused by the higher molecular disorder at the electrodes possibly due to the hydrophobic HMDS treated SiO_2 on which drop-casting was conducted. That is, the higher the concentration, the more polymers are driven away from the hydrophobic transistor channel towards the gold source and drain contacts on which the molecules can randomly adsorb. This point is strengthened by the fact that when spin-coating this polymer on the hydrophobic surface without gold electrodes, no film was formed. Without the repelling nature of the interface, the parts of the polymers might contribute to bulk formation within the channel rather than enhancing the disorder at the gold contacts.

The increase of charge carrier mobility after heating the semiconductor layer might have resulted in the improvement of molecular packing. This can be first caused by inducing a phase transition of the material, for example a liquid crystalline state or even a totally isotropic state (unordered state) that enables the molecules to be mobile and upon cooling down to reorganize into a more ordered arrangement. The isotropic state which can be reached upon melting the film

very apparently did not take place in this polymer system since no melting of the polymer layer was observed after heating the samples to 250°C. Another possibility can arise from the liquid crystallline phase or the glass transistion state. In both phases, the molecules get mobile within their localized positions, giving them the possibility to reassemble in a more highly packed (or less packed) configuration. Upon cooling down, this improved structure may yield more favorable charge transport. To study whether a thermally induced higher molecular order was indeed achieved, large-area X-ray diffraction (XRD) in reflection mode was carried out. Therefore, the films were prepared in the same way as for the device and deposited on a HMDS modified glass substrate. The experiments were performed on films before and after annealing. Surprisingly, no scattering intensities were observed, indicating considerable macroscopic disorder and thus an amorphous structure in both thin layers (Figure 4.16). Consequently, we assign the significant mobility increase by annealing to the elimination of the residual solvent molecules which act as trapping sites. Since differential scanning calorimetry (DSC) did not display any phase transition up to 250°C (thermal stability up to 450°C, Figure 4.17) and additionally the thin films did not show any birefringence under the polarized optical microscope, the lack of reorganization after annealing indicated by the X-ray study was in good agreement. XRD of the 10 mg ml^{-1} drop-cast polymer film lead to the same result that no diffraction peaks were observed.

That a highly disordered system exhibits high mobilities is rather counterintuitive. Such disordered structures are expected to contain numerous trapping sites due to poor intermolecular π-orbital overlap. Thus, severe hole trapping should occur, leading to lowering of charge carrier mobility and not to the observed high performance. The reason for this phenomenon is still unclear. Nevertheless, the morphology related transistor behavior studies of HT-P3HT as discussed previously is partly similar to this CDT-BTZ copolymer system. To recall, low molecular

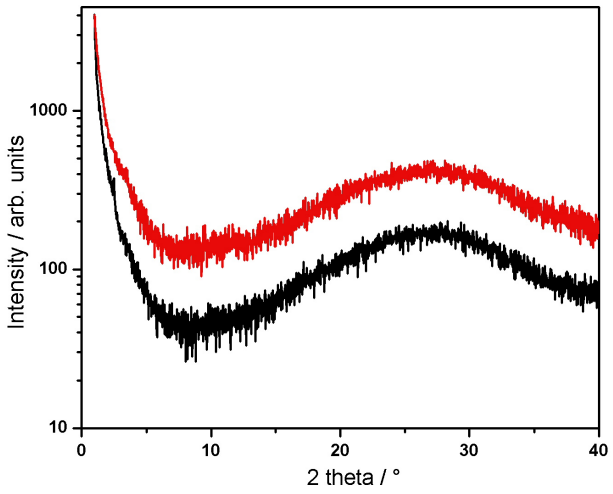

Figure 4.16: X-ray diffraction of drop-cast CDT-BTZ copolymer film. The black curve indicates diffraction from the as cast film, whereas the red curve stands for the same film annealed at 200°C for 2h.

weight HT-P3HT films showed highly ordered lamellar nanorod like domains separated by amorphous regions that provide poor connectivity between the ordered spaces, resulting in overall inferior mobility. Higher molecular weight HT-P3HT on the other hand also contained lamellar arrangement but less crystalline nodule like areas with higher connectivity, therefore yielding better transistor performance. That is, apparently higher crystalline order does not necessarily imply better charge transport in polymer layers but also severely depends on the connectivity between the regions containing some degree of order. Also, the crystallite grains in HT-P3HT are not perfectly arranged because of torsional rotations of the thiophene rings within each polymer chain and furthermore possibly due to chain defects and impurities [38]. This might be an additional reason for the inferior device behavior of crystalline low molecular weight HT-P3HT OFETs. For the CDT-BTZ donor-acceptor copolymer case, the situation is more extreme, since no ordered domains were present in the drop-cast films. It is probable that disordered polymer networks are more favorable for charge transport than polycrystalline films with poorly connected ordered domains as in the case of low molecular weight HT-P3HT for reasons

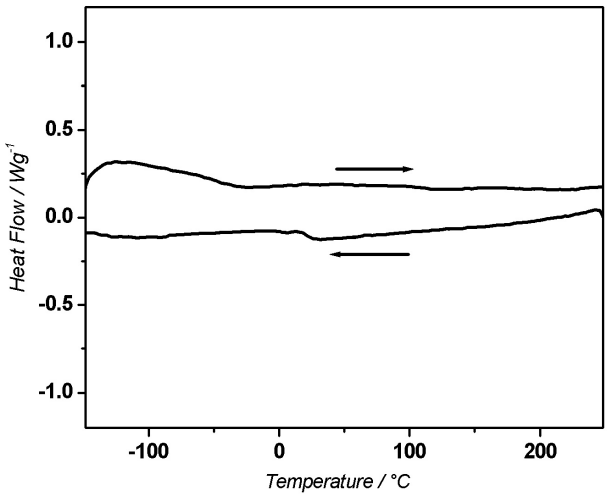

Figure 4.17: Differential scanning calorimetry of CDT-BTZ copolymer, showing no phase transition.

that are not yet understood. Theoretically, disorder implies the presence of traps that hinder charge transport, therefore lowering device performance. However, as illustrated in this donor-acceptor copolymer system, obviously it cannot be generalized that amorphous films lead to low charge carrier mobilities. The importance of grain boundaries in the form of domain connectivity in polymeric films is further underlined by the PBTTT layers generated from the liquid crystalline phase. In this system, one of the highest mobilities up to date was achieved by expanding the crystalline domains and thus by reducing the grain boundaries. Still, this CDT-BTZ donor-acceptor copolymer is the first highly disordered polymer up to date with a hole mobility exceeding 0.1 $cm^2V^{-1}s^{-1}$.

Another amorphous polymer showing mobilities up to $10^{-2}cm^2V^{-1}s^{-1}$ is polytriarylamine (PTAA). This performance was achieved using low-k polymer dielectrics instead of SiO_2. The authors explained this performance not with morphology considerations but with energetic disorder at the semiconductor-insulator interface. By energetic disorder it is refered to the localization of charge carriers at this interface due to the presence of dipoles that energetically trap the charge carriers, rendering them immobile (Figure 4.18b). The emergence of these dipole states are caused by

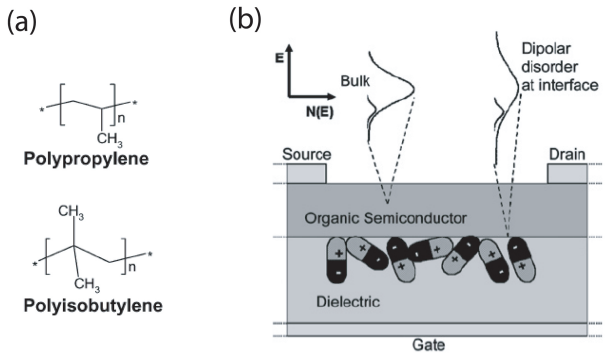

Figure 4.18: a.) Low-k dielectrics used for amorphous PTAA OFETs. b.) Schematic representation of random dipole formation at the surface of the dielectric, leading to local charge trapping at the semiconductor/insulator interface [40].

the polarization of the insulator in response to an applied gate electric field [39][40]. Conventionally, low-k dielectrics are all insulators with a dielectric constant lower than that of SiO_2, namely 3.9. Low-k dielectrics used for amorphous PTAA were for example polypropylene or polyisobutylene (Figure 4.18a) with dielectric constants of 2.1 and 2.2 respectively. Polytriarylamine polymer OFETs exhibited just one order of magnitude lower mobilities than the CDT-BTZ donor-acceptor copolymer even though both films were amorphous. The reason was the minimization of dipolar disorder and hence energetic charge carrier localization at the semiconductor-insulator interface by using a low-k dielectric which is generally not easily polarizable in response to the applied gate electric field. For HMDS treated SiO_2, PTAA showed low mobilities in the range of 10^{-3} to $10^{-4} cm^2 V^{-1} s^{-1}$ [39][40]. Since the measured mobility of the CDT-BTZ copolymer was two to three orders of magnitude higher on this same dielectric surface, it can be excluded that energetic disorder due to interface polarization played a major role in these copolymer OFETs.

As an additional approach to probe whether structural order of the copolymer can be induced by mechanical force, two-dimensional wide-angle X-ray scattering (2D-WAXS) was performed on filament extruded samples of the copolymer to reveal its supramolecular arrangement. Indeed, reflections appeared in the pattern, which are characteristic for organization (Figure 4.19). However, relatively diffuse reflections and the lack of higher order ones imply pronounced disorder. The equa-

torial scattering intensities at small angles describe the orientation of the polymer chains along the shearing direction. The position of the reflections is related to the lateral distance of 2.66 nm between the polymer chains. They are arranged in a lamella structure consisting of the aromatic rigid backbone separated by disordered aliphatic side chains filling the periphery. More crucially, the wide-angle located also in the equatorial of the pattern was attributed to the exceptionally small π-stacking distance of 0.37 nm between macromolecules in comparison to the nitrogen bridged ladder type polymer (Figure 4.8) where the π-spacing is 0.45 nm. This short distance coincided with similar values reported for conjugated polymers like HT-P3HT, PQT and PBTTT that reveal also a high performance in a device [6][11][12][23]. Temperature-dependent measurements of the extruded sample also did not show any annealing effect on the position and intensity of the reflections. Since the macroscopic order of the film was extremely poor in the presented case, only the small π-stacking distance is believed to have a major contribution to the pronounced FET mobility. It is difficult to transfer this small π-stacking distance result to the packing in thin films since XRD revealed disorder. A close π-stacking makes sense if some order, for example lamellar structures, are present. In the copolymer case however it is rather pictured that the polymer chains are macroscopically randomly distributed based on the lack of diffraction peaks in thin film XRD (Figure 4.20a). Nevertheless, the 2D-WAXS illustrated lamellar packing, suggesting that the copolymer has a tendency for this packing mode in the bulk. The question is to what degree lamellar arrangement can also possibly be found in the thin film. The existence of such packed regions would make the measured high mobility more reasonable. One possible picture is that the rigid copolymer chains form ordered randomly distributed lamella probably just in the nanoscopic scale consisting of a few chains (Figure 4.20b) and thus not observable by XRD. A combination of this nanoscopic arrangement with close π-stacking distance connected by randomly oriented polymer chains might be a possible film morphology. In general, in

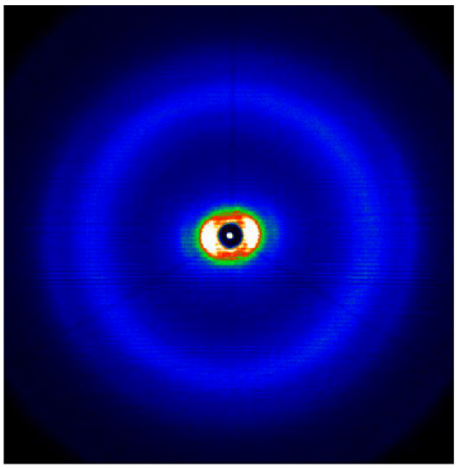

Figure 4.19: 2D-WAXS of extruded CDT-BTZ copolymer.

amorphous polymers charge transport is mainly along the polymer chain and therefore locally confined to one dimension. The presence of order, for instance lamellar packing, provides an additional charge transfer path along the π-stacking direction, in this way reducing trapping sites due to molecular disorder in an amorphous layer and therefore improving charge carrier transport and potentially mobility if grain boundaries do not play a dominant role in reducing this mobility. Therefore, such a nanoscopically closely π-stacked lamellar film morphology exhibiting good connectivity in a disordered matrix seems to be a reasonable explanation for the observed high performance copolymer OFET.

This directly highlights the great importance to control and thus increase the

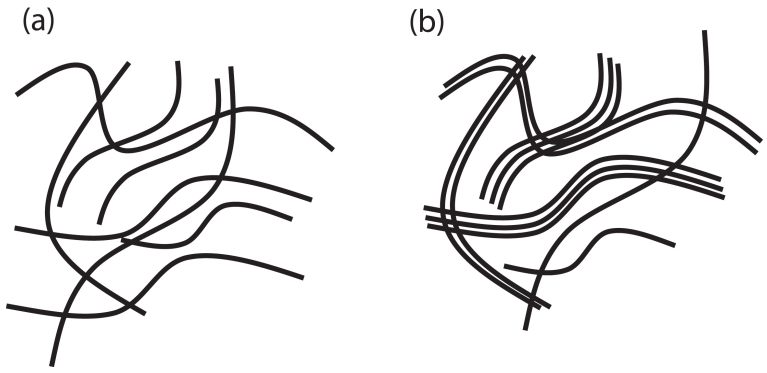

Figure 4.20: a.) Generally pictured highly disordered polymer film. b.) Pictured possible CDT-BTZ copolymer film as suggested by 2D-WAXS and XRD containing randomly oriented lamellar packing of only a few polymer chains.

intermolecular interaction by the variation of the chemical design and to decrease the gap between building blocks. Furthermore, in many other cases, it was necessary to post-treat the thin layers in the FET geometry after solution deposition in a controlled way to achieve remarkable mobilities [41][42]. Since the amorphous film structure of this CDT-BTZ copolymer does not require any controlled and complex processing, this behavior makes this material an attractive candidate for low-cost electronics. With this donor-acceptor copolymer we succeeded in designing a compound that self-assembles with close π-stacking distances even though no long-range order could be observed. Nevertheless, a high mobility was achieved, highlighting that the presence of trapping sites induced by the high disorder can be overcome by close intermolecular packing and that macroscopic order is not a necessity. This is the first system where such a phenomenon could be observed and is a direct support for the findings gained from the nitrogen bridged ladder type polymer investigated in the previous section.

4.6 Higher molecular weight CDT-BTZ Copolymer

In our study so far, the nitrogen bridged ladder type polymer showed long range order but large π-stacking distance between neighboring molecules, leading to low charge carrier mobilities. On the other hand, the donor-acceptor CDT-BTZ copolymer exhibited close intermolecular packing but was macroscopically disordered. Nevertheless, high mobilities were achieved, alluding to the importance of close π-stacking. To draw a conclusion from these two polymer systems, the best architecture would be a donor-acceptor copolymer giving also long range order. One possibility to induce macromolecular arrangement might be through the variation of molecular weight. For instance, in the case of HT-P3HT, it has been shown that charge carrier mobility depends on the molecular weight of the polymer [43].

Particularly, the mobility increases with molecular weight [44]. The lower molecular weights resulted in more crystalline films than the higher molecular weight polymers. The authors explain this phenomenon with their observation that even though the higher molecular weight polymer films were not as crystalline and hence contained less ordered domains, the longer polymer chains helped connecting the domains and in this way facilitating charge transport between the grain boundaries [7]. That is, some polymer chains extent to other domains and thus smear out the grain boundaries. This leads to higher charge carrier mobility. For HT-P3HT, both low and high molecular weights lead to the preservation of molecular order in form of lamellar packing. For the CDT-BTZ copolymer, it is not predictable whether a lower or higher molecular weight than the one exhibiting disorder would trigger macroscopic packing or whether a variation of molecular weight will change film morphology at all. However, following the trend of HT-P3HT where charge carrier mobility increased with molecular weight, focus was put on synthesizing rather a higher molecular weight. Another consideration prompted us to follow this path as well. As was already mentioned, one advantage of using polymer semiconductors is the fast charge transport along the conjugation plane of the polymer chains as long as no strong torsion is present that disrupt a continuous delocalized π molecular orbital over the entire polymer chain, in this way potentially inhibit charge transfer. Because of this intrachain charge diffusion, a longer polymer chain would even enhance charge transport along the chain over a larger distance (Figure 4.21b) than for shorter chains (Figure 4.21a) before encountering a discontinuous site that leads to the slower charge hopping mechanism. Such a site can be for instance the interconnect between two polymer chains along the conjugation plane, as schematically presented as red circles in Figures 4.21a,b. Obviously, the longer the chain, the less trapping sites and thus hopping events occur. This is particularly true for ordered polymer films in which the curling and winding of polymer chains are not serious to the extent of negating the effect of longer unhindered charge transport along the

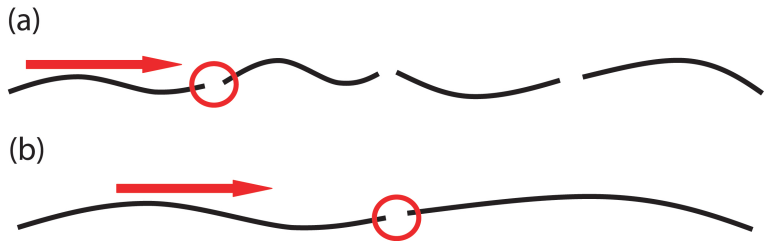

Figure 4.21: a.) Charge transport along the conjugation plane of a polymer chain (red arrow) for low molecular weights and thus shorter chains. Red circles indicate trapping site caused by the end to start chain connection that forces charge carriers into the slower charge hopping mechanism compared to fast intrachain transfer. b.) Charge transport along the conjugation plane of higher molecular weight and thus longer polymer chains (red arrow). Less end to start chain connections are encountered, prolonging the fast intrachain charge transport and hence potentially leading to a higher mobility.

conjugation plane of the polymer chain. For an ordered layer, for example a lamellar arrangement in which the chains are pictured as rigid rod like, longer chains are expected to lead to higher charge carrier mobility due to the reasons mentioned.

Thus following the initial synthesis of our previously reported CDT-BTZ copolymer, an increase of its molecular weight was accomplished by multiple recrystallizations of the BTZ unit and by passing the CDT monomer through a recycling HPLC/GPC just before polymerization (those experiments were done by Don Cho at the Max-Planck Institute for Polymer Research in Mainz). The obtained number average molecular weight M_n was 50K g mol^{-1} as measured by gel permeation chromatography (GPC) against polystyrene standards.

4.6.1 OFET based on Unalinged CDT-BTZ Copolymer

This higher molecular weight copolymer is applied in OFETs by spin-coating in air from a 5 mg ml^{-1} chlorobenzene solution on SiO_2 substrates modified by phenyltriethoxysilane (PTES) to reduce interface charge trapping and to guarantee that the spin-coated solution will stay on the surface since PTES makes it hydrophilic compared to HMDS which was used for the drop-casting of the lower molecular weight copolymer. The highly n++ doped Si wafers covered by PTES

functionalized 150 nm thick SiO_2 dielectric served as the gate electrode, and 60 nm thick gold source and drain contacts were evaporated in vacuum through a shadow mask onto the polymer film to finish these top-contact transistors. The channel width and length were 290 μm and 25 μm respectively. Here, top contact devices were employed in order to reduce contact resistance that has shown to inhibit charge carrier mobility for the lower molecular weight OFETs. Indeed, improved saturated hole mobilities of up to 0.67 $cm^2V^{-1}s^{-1}$ and a current on/off ratio I_{on}/I_{off} of 2×10^4 as determined under glove box conditions after annealing the samples at 200° for 1h in nitrogen atmosphere were achieved. This on/off ratio was calculated by taking the off current at a gate bias of $V_G = +10$V as compared to the lower molecular weight devices where the off current was used at zero gate voltage. The reason for applying a positive gate bias in these high molecular weight OFETs is driven by the high off current of 10^{-6}A (Figure 4.22b) when no gate voltage is present as opposed to the two order of magnitude lower off current for the lower molecular weight devices (Figure 4.14b). Pronounced off currents are generally caused by doping of the semiconductor by chemical impurities or by oxygen and moisture [45]-[47]. Chemical impurities for instance by conductive residual metallic catalysts seem unlikely to be the cause for the high off current due to the fact that no Ohmic behavior was observed when sweeping V_{SD} at zero V_G, that is, when measuring the intrinsic conductivity of the film. Instead, saturation as is typical for a pure semiconductor emerged [48][49]. Furthermore, a positive gate bias in a hole conducting semiconductor leads to depletion of the transistor channel (holes are repelled from the current carrying channel such that no holes are accumulated), in this way minimizing the off current. This phenomenon exactly took place, the off current dropped down one order of magnitude (Figure 4.22b). Any metallic species would trigger no decrease in current. As far as oxygen or moisture is concerned, it is reasonable to assume that they might have been trapped within the polymer film since processing was conducted in ambient conditions. However, annealing

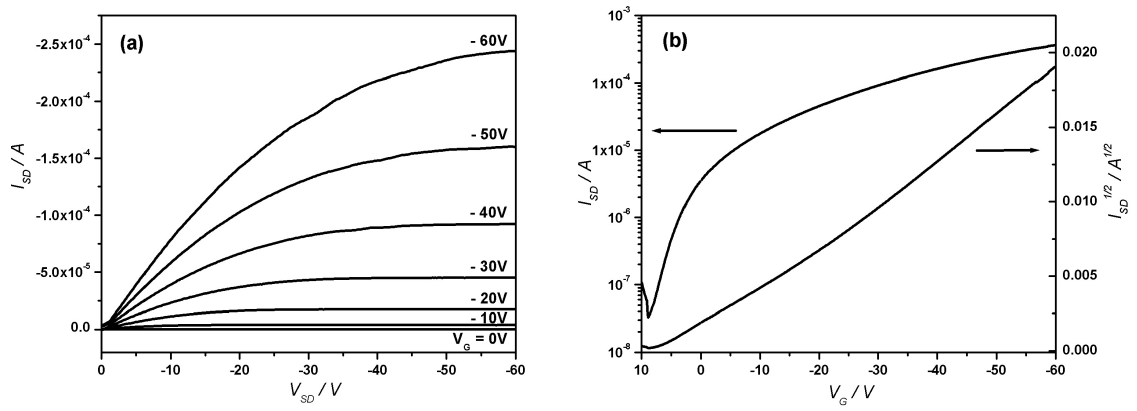

Figure 4.22: a.) Output curves for various gate biases V_G and b.) transfer characteristics at V_{SD} = -60V of spin-coated top contact CDT-BTZ C_{16} copolymer OFETs.

the layer afterwards at 200°C for 1h in nitrogen atmosphere is sufficient enough to dry the film, at least within the couple monolayers at the semiconductor/insulator interface transporting the transistor current. Instead, the high off state is probably due to an increased charge carrier density within the film promoted by an improved molecular order. That is, for the lower molecular weight film, disorder was present, in this way decreasing the intrinsic charge density since some holes are trapped, leading to minimal off current. For the higher molecular layer on the other hand macroscopic arrangement occurred, enhancing charge carrier density due to lesser trapping sites, causing an elevated off state. The transistor characteristics are depicted in Figure 4.22, showing the typical saturation and hence clean transistor performance. Furthermore, there is no non-linear rise of the current I_{SD} at low V_{SD}, alluding to the minimization of contact resistance. This mobility of 0.67 $cm^2V^{-1}s^{-1}$ is amongst the highest reported for polymer systems so far, surpassing the state of the art polymers like HT-P3HT, PQT, and PBTTT. The fact that these transistors can be fabricated in air and not only in nitrogen atmosphere gives the possibility for a large number of other processing methods like printing which is particularly attractive for commercial fabrication of plastic electronics.

In order to study whether a change in film morphology is responsible for the

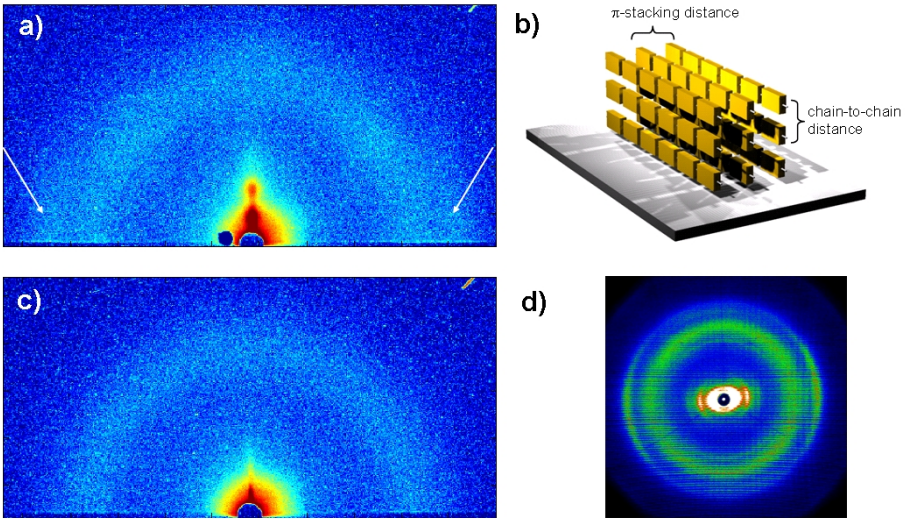

Figure 4.23: GIWAXS of spin-coated a) higher (M_n = 50K g mol^{-1}) and c) lower (M_n = 12K g mol^{-1}) molecular weight CDT-BTZ copolymer films (white arrow in a) corresponds to the π-stacking), b) schematic illustration of the higher molecular weight CDT-BTZ arrangement on the surface, d) 2D-WAXS of the higher molecular weight CDT-BTZ extruded filament.

increased device performance for the higher molecular weight copolymer, grazing incidence wide angle x-ray scattering (GIWAXS) (conducted by Dr. Jens Wenzel Andreasen and Prof. Dr. Dag W. Breiby in Denmark) was performed to gain an insight into macromolecular organization of this high performance spin-coated polymer film. This X-ray scattering method is chosen since we aimed for the elucidation of not only the out of plane packing of the polymers but also of the in-plane arrangement, that is, how the polymers self-assemble on the plane of the surface. As the diffraction pattern in Figure 4.23a suggests, the polymer chains are ordered in a typical lamellar-like fashion as observed for other high mobility conjugated polymers like HT-P3HT, PQT, or PBTTT as described in the previous sections in this chapter. Apparently, this packing structure seems to be favorable for high performance OFETs. The derived arrangement of the polymers is schematically presented in Figure 4.23b, illustrating an edge-on orientation of the backbone on the surface with the π-stacking directed in-plane. From the position of the scattering intensities a chain-to-chain spacing of 2.66 nm with the π-stacking distance of 0.39 nm was determined. The diffraction signal from the

thin film is closely similar to that obtained from 2D-WAXS extruded polymer bulk measurements, indicating that the supramolecular arrangments in bulk and thin films are comparable (Figure 4.23d). For the spin-coated lower molecular weight polymer film on the other hand, no crystalline order was present as depicted in Figure 4.23c by the absence of diffraction peaks. This absence of order is expected since XRD from the drop-cast film already showed no supramolecular organization (Figure 4.16). In that case, the high mobility was attributed only to the close π-stacking distance of 0.37 nm as derived from the bulk using 2D-WAXS. As mentioned above, a comparable π-stacking distance was observed as well for the higher molecular weight copolymer. However, in addition, crystalline packing was present, leading to supramolecular ordering and thus increased mobility. This result stresses the importance of both close π-stacking distance and long-range order for achieving high mobilities. To further investigate the macromolecular organization, atomic force microscopy (AFM) of the spin-coated polymer layers used in the actual OFET measurements was employed. As depicted in Figure 4.25a, the as spun polymers form a film with spot-like features of an approximately 50 nm diameter average size. Interestingly, these small domains consist of rings as indicated by the red arrows in Figure 4.25a, suggesting that the polymer chains self-assemble into circular structures when spin-coated (see illustration Figure 4.25a). Such donut-shaped nanostructures lie next to each other, in this way establishing a polymer network that seems to provide efficient charge carrier transport with a high mobility of $\mu_{sat} = 0.67\ cm^2V^{-1}s^{-1}$ provided that this AFM topographic analysis reflects the same morphology at the polymer film/insulator interface. It is the first time that this film morphology is shown to exhibit such high charge carrier mobility. It is not absolutely clear how the polymers are packed within such a donut structure. Based on the high molecular weight and thus the numerous repeating units of the monomers, it seems reasonable to conclude that the polymer chains do not form circles by chain folding like in the case of HT-P3HT where the chains

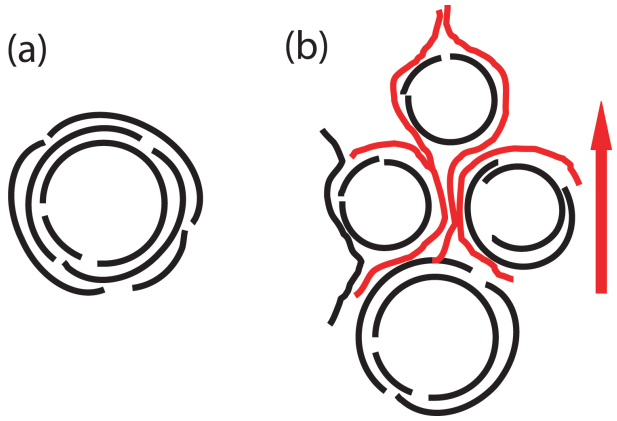

Figure 4.24: a.) Lamellar packing of spin-coated higher M_n CDT-BTZ copolymer with the whole lamellar structure bent into a ring shaped domain. b.) Interdomain connectivity as highlighted by the red copolymer chains. In this way, fast intrachain charge transport within the transistor channel (red arrow) is facilitated, leading to the observed high mobility.

fold to create the typical fibers [43][50][51] Instead, the copolymer chains pack in a lamellar structure as indicated by GIWAXS, with this whole lamellar domain being bent into the observed supramolecular circular architecture as schematically illustrated in Figure 4.24a.

These results clearly show that by changing the molecular weight, polymer self-assembly and film morphology was altered. Compared to the lower molecular weight case for which disorder was present, this higher molecular weight copolymer forms lamellar order packed into circular domains. For HT-P3HT, PQT, or PBTTT, lamellar fiber like regions combined with good connectivity lead to high mobilities. Intuitively, however, the circular domains should yield shorter charge transport pathways than the fibrous morphology when considering only fast intrachain transfer along the polymer conjugation plane. Thus, it is surprising that the donut-shaped structure shows comparable charge carrier mobility as the other above mentioned fibrous polymer systems. From the AFM images, it seems that the circular domains are not strictly separated from each other as was for instance the case of low molecular weight crystalline nanofiber domains in HT-P3HT. Rather, the rings seem to be partially fused with each other, in this way guaranteeing the interdomain con-

nectivity. That is, the most realistic picture is one where parts of the copolymer chains making up one ring domain extend into the neighboring circular region (red polymer chains in Figure 4.24b) such that fast interdomain charge transfer along the conjugation plane of the polymer chains takes place, leading to the observed high mobility. Hereby, the charges are not confined to move around the individual circular structures without being able to move forward from source to drain, in this way potentially resulting in low device performance.

4.6.2 OFET based on Alinged CDT-BTZ Copolymer

It is evident that supramolecular order is crucial for obtaining high performance OFETs. For the spin-coated film, long range order was observed. However, the polymers are not aligned in one direction. Hence, there is still room for enhancing supramolecular organization of this copolymer. In this aspect, further increase of charge carrier mobility should be achieved. One method for unidirectionally aligning molecules from solution is by dip-coating. This is a simple technique where the transistor substrate is immersed in the polymer solution and slowly taken out, in this way potentially forming a well aligned film. This dip-coating is easy and does not consume as much material as for example zone-casting. Following this idea, the high molecular weight polymer was dip-coated on PTES modified 150 nm thick SiO_2 wafers at a rate of 1 μm per second from a 1 mg ml^{-1} chlorobenzene solution in air to form the semiconducting layer. This processing method is known to induce directional long-range alignment of the molecules (Figure 4.27) which is particularly interesting for rigid rod like polymers not only in terms of increasing charge carrier mobility but also to probe the anisotropy of charge transport. This direction dependent mobility was first observed in the case of HT-P3HT where charge transport along the π-stacking of the polymer backbones (Figure 4.26 z-axis) was reported to be faster than along the plane of the insulating alkyl chains (Figure 4.26 y-axis) [6]. That is, charge mobility is higher for the polymers standing on the surface as

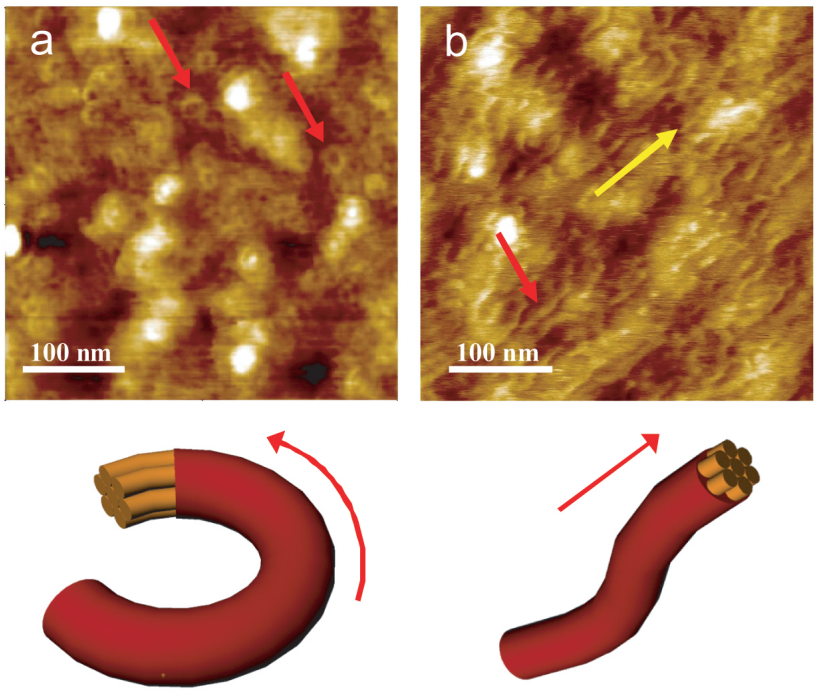

Figure 4.25: AFM image of a) spin-coated and b) dip-coated CDT-BTZ copolymer. Yellow arrow indicates the dipping direction. Schematic drawings illustrate the structure formation into the donut-like structures in a) and aligned fibers in b).

schematically illustrated in Figure 4.26 than when they are lying face down.

However, till now it has not been shown whether charge transport along the conjugation plane of the polymers (x-axis direction in Figure 4.26) is even faster than along the π-stacking. It has been proposed by Salleo that fast charge transport is indeed expected in the conjugation direction [50]. Apart from dip-coating of regioregular HT-P3HT that did not lead to higher charge carrier mobilities than from the non-aligned techniques like drop-casting or spin-coating [10], this is the first time that a polymer is solution aligned for OFET applications yielding better device performance. The dip-coated, top-contact OFETs were fabricated by evaporating 60 nm gold source and drain contacts in vacuum through a shadow mask with channel lengths of 25 μm and widths of 290 μm on top of the polymer layer. Figure 4.28 highlights the resulting transistor operation when measured along the dip-coating direction after annealing the sample at 200°C for 1h in nitrogen atmosphere. As evidenced by the output curves in Figure 4.28a, the

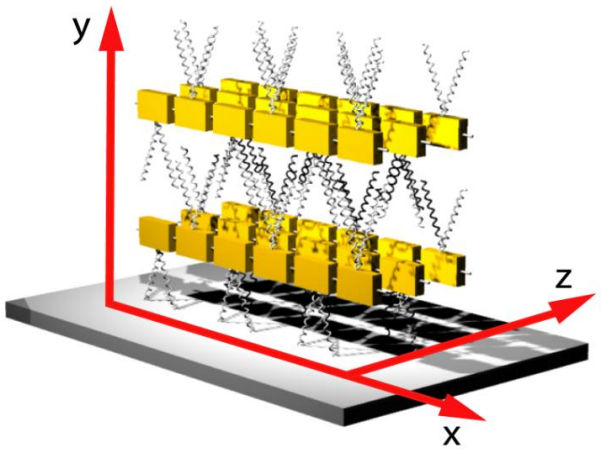

Figure 4.26: Charge transport along the polymer conjugation (x-axis), along the alkyl chains (y-axis) and along the π-stacking (z-axis).

devices saturated and showed clean transistor performance. Hole mobilities in the range of μ_{sat} = 1 - 1.4 $cm^2V^{-1}s^{-1}$ and current on/off ratios I_{on}/I_{off} of $10^4 - 10^5$ were extracted from the transfer characteristic (Figure 4.28b). This is among the highest mobilities reported so far for polymer based OFETs. Remarkably yet, compared to the polymer with the best performance up to date, namely PBTTT (Figure 4.5) exhibiting μ_{sat} = 0.7 $cm^2V^{-1}s^{-1}$, this was only achieved by employing a short transistor channel of 5 μm. The advantage of utilizing a short distance between the source and drain electrodes is to minimize the trapping sites within the film that inhibit charge transport. In our aligned copolymer system however, a five times longer channel was employed, in this way increasing the number of potential trapping sites. Nevertheless, charge carrier mobility was still excellent, indicating the high quality of this directionally oriented system. The mobility is about twice as high as in the spin-coated samples. Measurements perpendicular to the dip-coating direction revealed a lower mobility of μ_{sat} = 0.5 - 0.9 $cm^2V^{-1}s^{-1}$ with I_{on}/I_{off} of 10^3 after the same annealing step (Figure 4.29).

In order to examine whether the dip-coated film indeed reached higher molecular order than the spin-coated layer as the elevated OFET mobilities suggest, GIWAXS was again applied as illustrated in Figure 4.30. Evidenced by the diffraction

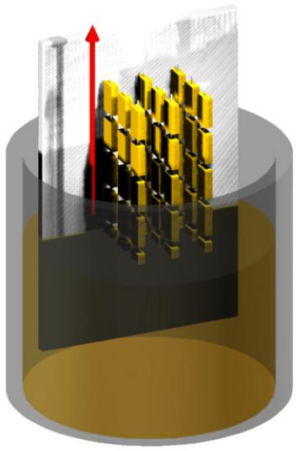

Figure 4.27: Schematic representation of dip-coating.

pattern, the lamellar packing, which was already observed for the spin-coated case, stays intact. However, the long range order has improved after dip-coating, leading to more pronounced diffraction features in the pattern (Figure 4.30a) and to the measured two fold increase in charge carrier mobility. Perpendicular and parallel GIWAXS measurements with respect to the dip-coating direction revealed the structural in-plane anisotropy in the thin film. The measurement parallel to the dip-coating direction (Figure 4.30b) showed well defined in-plane peaks corresponding to a real-space periodicity of 0.35 nm which was in good agreement with the π-stack peak identified from the bulk 2D-WAXS measurement (Figure 4.23d). With the dip-coating direction oriented perpendicular to the incident X-ray beam (Schematic in Figure 4.30a), we observed weaker and less well defined in-plane peaks corresponding to periodicities of 0.60 nm and 0.39 nm, which presumably originated from the backbone repeat. With the lamellar stack oriented along the surface normal, these observations agree with a biaxial texture having the conjugated backbone oriented parallel with the dip-coating direction and with the π-stack oriented edge-on with respect to the substrate. The narrow azimuthal distribution of the reflections from the lamellar stack when probed perpendicular to the dip-coating direction indicates that the molecules are highly oriented with respect to their long axis (the backbone) relative to the substrate surface (Figure

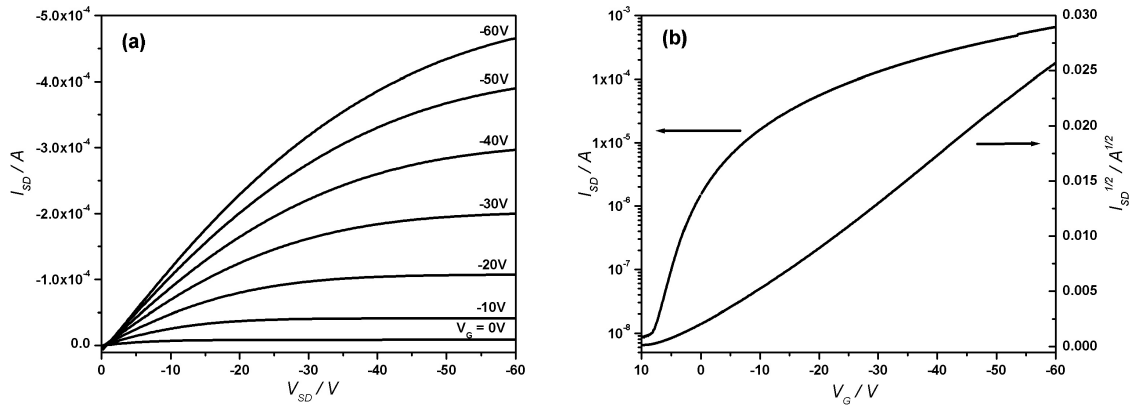

Figure 4.28: a.) Output curves for various gate biases V_G and b.) transfer characteristics at V_{SD} = -60V of dip-coated top contact CDT-BTZ C_{16} copolymer OFETs measured along the dip-coating direction.

4.30a). The orientation distribution of molecules around the axis of the conjugated backbone is broader as evidenced by the azimuthal smearing of the reflections from the lamellar stack when probed parallel with the dip-coating direction, indicating some freedom to rotate around the long axis.

In the case of the not directionally aligned, spin-coated copolymer film, lamellar packing was observed via GIWAXS but morphology studies with the help of AFM revealed a circular macromolecular organization. In order to gain an insight into the morphology of the dip-coated layer, AFM was applied. For the dip-coated polymers, a film containing a fibrous morphology (Figure 4.25b) was present instead of the circular assembly for the spin-coated devices. The observation of fibers leads to the conclusion that the polymers were aligned by the dip-coating. In fact, a significant number of the fibers were oriented parallel to the dip-coating direction illustrated by the yellow arrow in Figure 4.25b, suggesting that the plane of conjugation of the polymers lies parallel to this direction as well. It seems that the circular fibers from the spin-coated films were being stretched when dip-coating was applied. Based on the assumption that the polymers pack in a lamellar fashion with the conjugation plane directed along the fiber, the

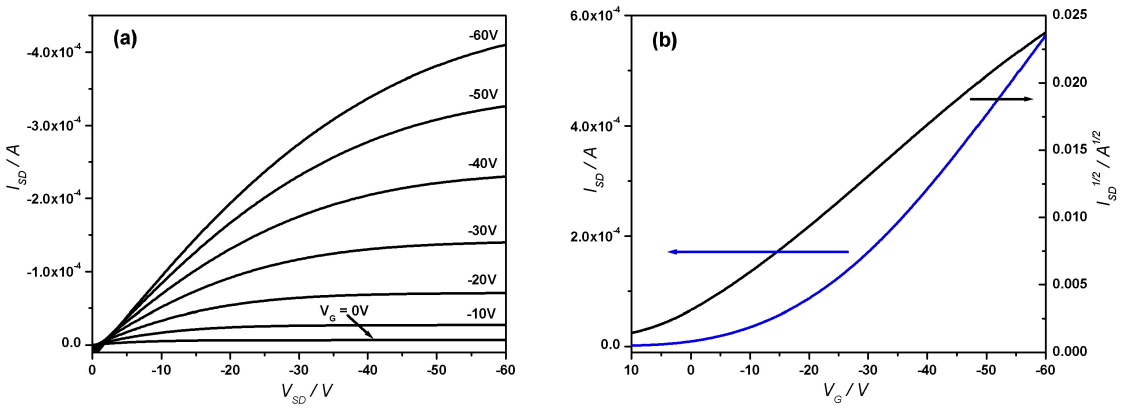

Figure 4.29: a.) Output curves for various gate biases V_G and b.) transfer characteristics at V_{SD} = -60V of dip-coated top contact CDT-BTZ C_{16} copolymer OFETs measured perpendicular to the dip-coating direction.

previous OFET measurements along the dip-coated direction must reflect charge transport through the plane of conjugation, whereas measurements perpendicular to the casting direction correspond to charge transport along the π-stacking of the polymer backbones within a single fiber. As mentioned, an anisotropy of the charge mobility was observed when measuring OFETs along those two directions: the mobility along the conjugation is about twice as high as along the π-stacking polymer planes. Based on this finding, one might be tempted to deduce that charge transport along the conjugation plane is indeed faster than along the π-stacking. However, one has to keep in mind that the dip-coated polymer film consists of multiple fiber domains. When charges travel from one fiber to the other, the boundaries between those domains have to be overcome. Those domain boundaries pose trapping sites for the charge carriers, in this way limiting their transport [52][53], prohibiting a more distinct anisotropy of the mobility. In fact, when talking about charge transport along the polymer chain and perpendicular to it, one has also to consider in more detail the possibilities of how the fiber domains might be connected to each other. Taking into account the length of the fibers (see Figure 4.25b), the domain boundary between two neighbouring fibers might be thought to be larger than when the fibers are connected end to end, since the

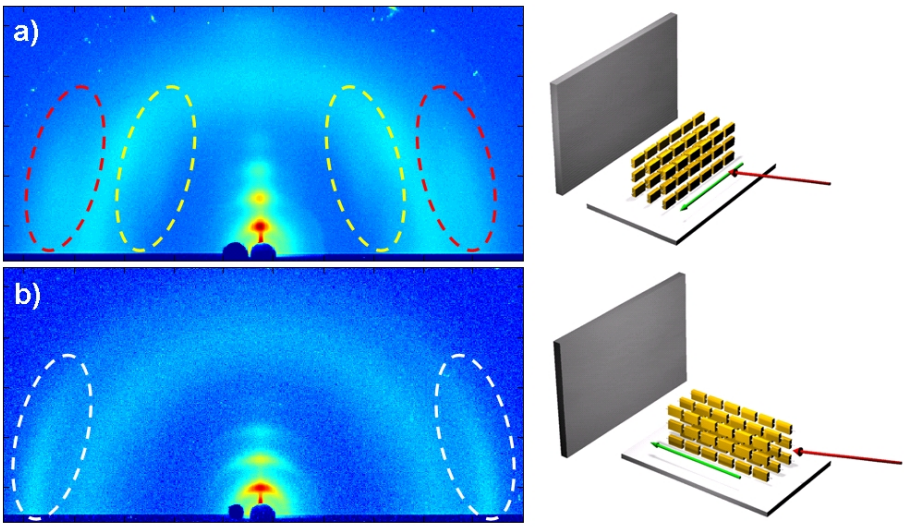

Figure 4.30: GIWAXS of dip-coated higher molecular weight CDT-BTZ films after annealing. The patterns have been recorded a) perpendicular to (red and yellow dashed lines suggest the scattering related to the repeat units along the polymer backbone) and b) parallel with the dipping direction (white dashed lines point towards the scattering from the in-plane π-stacking). The green arrow in the schematic drawings indicates the dipping and alignment direction, while red corresponds to the incident X-ray beam.

diameter of the fibers are much smaller than their lengths. Hence, it is reasonable to believe that charge transport along the π-stacking is even more hindered by the larger fiber boundary acting as trapping site. But one has to be careful here. No information is present disclosing the transition from one fiber to the other, that is, whether there is disorder of the polymers at the boundary between two fibers or whether the boundary is more or less smoothed out. In the latter case, the domain boundary would not pose such a strict trapping site and charge hopping might be relatively easy. It has been shown for HT-P3HT that such fiber boundaries can be bridged by polymer chains extending to the other domain, in this way enabling charge transport between individual fibers [43][50]. Therefore, if one assumes that all fibers are uniformly aligned in one direction with them being connected from end to end and if the boundaries are strict, then no clear conclusion can be drawn whether charge transport along the polymer conjugation plane is faster than along the π-stacking since the domain boundary is larger in this latter direction. The

reason for the two times lower mobility can then simply result from this heavier trapping site. However, if the boundaries are considered to be smoother, those trapping sites do not have such a strong influence on charge transport and mobility along the conjugation plane is indeed higher than along the π-stacking.
This relatively low ratio between both directions is additionally strengthened by the lack of uniform and unidirectional orientation of the fibers as illustrated in Figure 4.25b. Instead, some branching and interruptions of the fibers were present, in this way enforcing the number of trapping sites which hinder charge transport. The same reasoning holds for the difference in device performance after spin-coating. Compared to the ring-shaped structures that occurred in the spin-coated films, this "linear" fibrous morphology results in a more distinct long-range order as also supported by the discussed GIWAXS experiments of dip-coated films, leading to higher charge carrier mobilities. However, the branching and disruptions in the fiber structures limit an increase of mobility of more than a factor of two. What happens in the spin-coated case is that in the circular morphology, charge transport cannot be simply boiled down to either along the conjugation plane or the π-stacking. Instead, charge transport takes place as a combination of both directions, more or less two-dimensional charge transport, leading to a not so distinct mobility compared to the dip-coated transistors measured along the π-stacking direction. However, the mobility along the dip-coating direction and hence along the conjugation plane is still about two times higher than in the spin-coated devices, suggesting that charge transport along the conjugation plane is indeed faster for this copolymer system.

The dip-coated polymer transistors exhibited excellent performance when prepared in air and measured in dry nitrogen amtmosphere. For organic OFETs to be attractive for commercial use, not only outstanding performance but also device stability in air is of great importance. Hence, the dip-coated OFETs were tested in

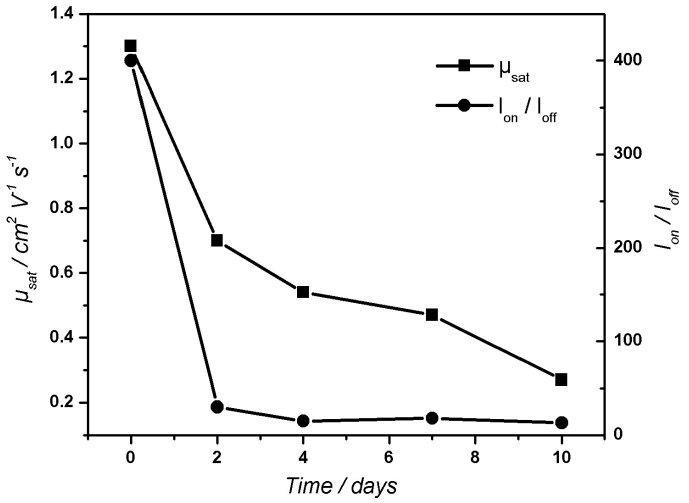

Figure 4.31: CDT-BTZ copolymer FET long term performance in ambient conditions.

ambient atmosphere, where Figure 4.31 shows the changes in mobility and I_{on}/I_{off} ratio over time. When the devices were first measured in air they exhibited a mobility of $\mu_{sat} = 1.3\ cm^2V^{-1}s^{-1}$ which was nearly the same value as obtained in dry nitrogen atmosphere. However, the I_{on}/I_{off} decreased to 4×10^2, almost three orders of magnitude lower than the performance in nitrogen. This low ratio was caused by the increasing off current in air probably due to doping of the polymer film through oxidation [54]. After storing the OFETs for two days in ambient conditions, the mobility dropped down to half its initial value and the I_{on}/I_{off} ratio decreased by one order of magnitude. The transistors degraded in mobility with longer air storage time, whereas the I_{on}/I_{off} ratio did not decrease significantly anymore. Nethertheless, even after ten days in ambient conditions the devices still showed a relatively high mobility of $\mu_{sat} = 0.27\ cm^2V^{-1}s^{-1}$, making these polymer devices attractive for organic electronics in conjunction with proper encapsulation to circumvent the ease of doping and thus the low I_{on}/I_{off} ratio. Such an encapsulation can for example simply be achieved by the top gate configuration (Figure 3.6c) where the active organic semiconductor film is sandwiched between the substrate and the insulator and thus protected from oxygen and moisture when exposed to ambient conditions. This

concept has been demonstrated for HT-P3HT, leading to shelf lifes of the devices in air of several months [55]-[57].

4.7 Summary

In this chapter it was shown that in the case of ladder type polymers, long range order was present. However, the charge carrier mobility was still low despite this ordering. The reason is the large π-stacking distance which is on the other hand small in the donor acceptor copolymer. For this CDT-BTZ copolymer, no long range packing was observed, indicating that a close π-stacking distance between the rigid polymer chains has a deeper impact on better charge transport than long range order. Achieving a higher molecular weight copolymer of M_n = 50K g mol^{-1} lead to the improvement of OFET performance by the occurrence of macromolecular arrangement which was not observed in the lower molecular weight case. These devices were further improved by directionally aligning the polymers via dip-coating, in this way inducing a tendency of long-range molecular orientation. It is apparent that for the fabrication of high performance FETs, control of organization of the organic compound plays a crucial role. As a consequence, a mobility of up to μ_{sat} = 1.4 $cm^2V^{-1}s^{-1}$ was achieved, one of the highest values reported so far for polymer based transistors. This donor-acceptor copolymer is unique in the sense of the change of polymer chain self assembly with respect to molecular weight. For the other high performance polymer systems like HT-P3HT, PQT, or PBTTT, lamellar structure is preserved independent of molecular weight which just has an impact on film morphology and thus on device performance. For the CDT-BTZ copolymer on the other hand, a higher molecular weight turns a disordered film into an ordered lamellar structure. The mechanism causing this phenomenon is not clear yet and also not reported in literature. Whereas for the above mentioned state of the art high performance polymers lamellar arrangement is induced mainly by alkly chains and to a lesser extend by intermolecular π-stacking interaction as deduced from disordered

regiorandom P3HT, it is an open question whether the increased number of alkyl chains or the more extended CDT-BTZ copolymer backbone of the higher molecular weight contribute to which parts to the emergence of lamellar packing. To find an answer to this question, a detailed study about the variation in self-assembly, film morphology and transistor performance in relation to additional various molecular weights is in need.

Bibliography

[1] H. Usta, G. Lu, A. Facchetti, T. J. Marks, *J. Am. Chem. Soc.* **2006**, *128*, 9034.

[2] L. A. Majewski, R. Schroeder, M. Grell, *Adv. Funct. Mater.* **2005**, *15*, 1017.

[3] Y. Li, T.-H. Kim, Q. Zhao, E.-K. Kim, S.-H. Han, Y.-H. Kim, J. Jang, S.-K. Kwon, *J. Polym. Sci. Part A: Polym. Chem.* **2008**, *46*, 5115.

[4] Y. Wang, L. Hou, K. Yang, J. Chen, F. Wang, Y. Cao, *Macromol. Chem. Phys.* **2005**, *206*, 2190.

[5] B. S. Ong, Y. Wu, Y. Li, P. Liu, H. Pan, *Chem. Eur. J.* **2008**, *14*, 4766.

[6] H. Sirringhaus, P. J. Brown, R. H. Friend, M. M. Nielsen, K. Bechgaard, B. M. W. Langeveld-Voss, A. J. H. Spiering, R. A. J. Janssen, E. W. Meijer, P. Herwig, D. M. de Leeuw, *Nature* **1999**, *401*, 685.

[7] R. J. Kline, M. D. McGehee, E. N. Kadnikova, J. Liu, J. M. J. Frechet, *Adv. Mater.* **2003**, *15*, 1519.

[8] S. Hugger, R. Thomann, T. Heinzel, T. Thurn-Albrecht, *Colloid Polym. Sci.* **2004**, *282*, 932.

[9] E. Mena-Osteritz, *Adv. Mater.* **2002**, *14*, 609.

[10] J.-M. Verilhac, G. LeBlevennec, D. Djurado, F. Rieutord, M. Chouiki, J.-P. Travers, A. Pron, *Synth. Met.* **2006**, *156*, 815.

[11] B. S. Ong, Y. Wu, P. Liu, S. Gardner, *Adv. Mater.* **2005**, *17*, 1141.

[12] I. McCulloch, M. Heeney, C. Bailey, K. Genevicius, I. MacDonald, M. Shkunov, D. Sparrowe, S. Tierney, R. Wagner, W. Zhang, M. L. Chabinyc, R. J. Kline, M. D. McGehee, M. F. Toney, *Nat. Mater.* **2006**, *5*, 328.

[13] S. Sergeyev, W. Pisula, Y. H. Geerts, *Chem. Soc. Rev.* **2007**, *36*, 1902.

[14] M. Kastler, W. Pisula, D. Wasserfallen, T. Pakula, K. Müllen, *J. Am. Chem. Soc.* **2005**, *127*, 4286.

[15] W. Pisula, M. Kastler, D. Wasserfallen, T. Pakula, K. Müllen, *J. Am. Chem. Soc.* **2004**, *126*, 8074.

[16] W. Pisula, Z. Tomovic, C. Simpson, M. Kastler, T. Pakula, K. Müllen, *Chem. Mater.* **2005**, *17*, 4296.

[17] W. Pisula, M. Kastler, D. Wasserfallen, M. Mondeshki, J. Piris, I. Schnell, K. Müllen, *Chem. Mater.* **2006**, *18*, 3634.

[18] Y. Y. Deng, H. Sirringhaus, *Phys. Rev. B* **2005**, *72*, 045207.

[19] M. C. J. M. Vissenberg, M. Matters, *Phys. Rev. B* **1998**, *57*, 12964.

[20] N. Karl, *Synth. Met.* **2003**, *133*, 649.

[21] B. S. Ong, Y. Wu, P. Liu, S. Gardner, *J. Am. Chem. Soc.* **2004**, *126*, 3378.

[22] Y. Li, Y. Wu, P. Liu, M. Birau, H. Pan, B. S. Ong, *Adv. Mater.* **2006**, *18*, 3029.

[23] I. Osaka, G. Sauv, R. Zhang, T. Kowalewski, R. D. McCullough, *Adv. Mater.* **2007**, *19*, 4160.

[24] H. Wang, F. P. Uckert, S. Kim, *US Patent* **2004**, 20040826.

[25] R. J. Kline, M. D. McGehee, M. F. Toney, *Nature Mater.* **2006**, *5*, 222.

[26] H. Yang, T. J. Shin, L. Yang, K. Cho, C. Y. Ryu, Z. Bao, *Adv. Funct. Mater.* **2005**, *15*, 671.

[27] T. Hassenkam, D. R. Greve, T. Bjornholm, *Adv. Mater.* **2001**, *13*, 631.

[28] J.-F. Chang, B. Sun, D. W. Breiby, M. M. Nielsen, T. I. Sölling, M. Giles, I. McCulloch, H. Sirringhaus, *Chem. Mater.* **2004**, *16*, 4772.

[29] S. A. Patil, U. Scherf, A. Kadashchuk, *Adv. Funct. Mater.* **2003**, *13*, 609.

[30] F. Laquai, A. K. Mishra, K. Müllen, R. H. Friend, *Adv. Funct. Mater.* submitted.

[31] A. K. Mishra, M. Graf, F. Grasse, J. Jacob, E. J. W. List, K. Müllen, *Chem. Mater.* **2006**, *18*, 2879.

[32] W. Pisula, Z. Tomovic, C. Simpson, M. Kastler, T. Pakula, K. Müllen, *Chem. Mater.* **2005**, *17*, 4296.

[33] M. Zhang, C. Yang, A. K. Mishra, W. Pisula, G. Zhou, B. Schmaltz, M. Baumgarten, K. Müllen, *Chem. Commun.* **2007**, *17*, 1704.

[34] H. Sirringhaus, P. J. Brown, R. H. Friend, M. M. Nielsen, K. Bechgaard, B. M. W. Langeveld-Voss, A. J. H. Spiering, R. A. J. Janssen, E. W. Meijer, *Synth. Met.* **2000**, *111*, 129.

[35] J. Y. Kim, K. Lee, N. E. Coates, D. Moses, T.-Q. Nguyen, M. Dante, A. J. Heeger, *Science* **2007**, *317*, 222.

[36] C. J. Brabec, C. Winder, N. S. Sariciftci, J. C. Hummelen, A. Dhanabalan, P. A. van Hal, R. A. J. Janssen, *Adv. Funct. Mater.* **2002**, *12*, 709.

[37] T. Yamamoto, H. Kokubo, M. Kobashi, Y. Sakai, *Chem. Mater.* **2004**, *16*, 4616.

[38] R. A. Street, J. E. Northrup, A. Salleo, *Phys. Rev. B* **2005**, *71*, 165202.

[39] J. Veres, S. D. Ogier, S. W. Leeming, D. C. Cupertino, S. M. Khaffaf, *Adv. Funct. Mater.* **2003**, *13*, 199.

[40] J. Veres, S. Ogier, G. Lloyd, D. de Leeuw, *Chem. Mater.* **2004**, *16*, 4543.

[41] H. Sirringhaus, R. J. Wilson, R. H. Friend, M. Inbasekaran, W. Wu, E. P. Woo, M. Grell, D. D. C. Bradley, *Appl. Phys. Lett* **2000**, *77*, 406.

[42] G. Xu, Z. Bao, J. T. Groves, *Langmuir* **2000**, *16*, 1834.

[43] J.-F. Chang, J. Clark, N. Zhao, H. Sirringhaus, D. W. Breiby, J. W. Andreasen, M. M. Nielsen, M. Giles, M. Heeney, I. McCulloch, *Phys. Rev. B* **2006**, *74*, 115318.

[44] A. Zen, J. Pflaum, S. Hirschmann, W. Zhuang, F. Jaiser, U. Asawapirom, J. P. Rabe, U. Scherf, D. Neher, *Adv. Funct. Mater.* **2004**, *14*, 757.

[45] M. S. A. Abdou, F. Orfino, Y. Son, S. Holdcroft, *J. Am. Chem. Soc.* **1997**, *119*, 4518.

[46] C.-K. Lu, H.-F. Meng, *Phys. Rev. B* **2007**, *75*, 235206.

[47] E. J. Meijer, C. Detcheverry, P. J. Baesjou, E. van Veenendaal, D. M. de Leeuw, T. M. Klapwijk, *J. Appl. Phys.* **2003**, *93*, 4831.

[48] G. Horowitz, *Adv. Mater.* **1996**, *8*, 177.

[49] M. S. A. Abdou, X. Lu, Z. W. Xie, F. Orfino, M. J. Deen, S. Holdcroft, *Chem. Mater.* **1995**, *7*, 631.

[50] A. Salleo, *materialstoday* **2007**, *10*, 38.

[51] B. Grevin, P. Rannou, R. Payerne, A. Pron, J.-P. Travers, *Adv. Mater.* **2003**, *15*, 881.

[52] R. A. Street, D. Knipp, A. R. Völkel, *Appl. Phys. Lett.* **2002**, *80*, 1q.

[53] J. Chen, C. K. Tee, M. Shtein, J. Anthony, D. C. Martin, *J. Appl. Phys.* **2008**, *103*, 114513.

[54] D. M. de Leeuw, M. M. J. Simenon, A. R. Brown, R. E. F. Einerhand, *Synth. Met.* **1997**, *87*, 53.

[55] W. Fix, A. Ullmann, J. Ficker, W. Clemens, *Appl. Phys. Lett.* **2002**, *81*, 1735.

[56] J. Ficker, A. Ullmann, W. Fix, H. Rost, W. Clemens, *Proc. SPIE* **2001**, *4466*, 95.

[57] H. Rost, J. Ficker, J. S. Alonso, L. Leenders, I. McCulloch, *Synth. Met.* **2004**, *145*, 83.

Chapter 5

N-Type Rylene Dye OFETs

5.1 Introduction

For useful electronic devices, not only hole transporting transistors (p-type transistors) that has been studied and discussed till now are required. Current electronic technology like processors (CPU's) in computers are all based on complementary metal oxide semiconductor (CMOS) units that allow the operation of binary logic, the basic calculation language for computers. CMOS requires both hole and electron transporting transistors. Hence, organic semiconductors where electron currents flow (n-type semiconductors) are in need [1]. Compared to p-type organic semiconductors, n-type semiconductors are still rare. In fact, it has been found that intrinsically, all organic semiconductors should be transporting both holes and electrons [2].

The reasons why most of them do not are twofold. First, when fabricating OFETs, gold is most often used as source and drain electrodes since it is enviromentally stable and does not easily oxidize when handling it in air or organic solvents. The downturn however is that the work function (the energy required to free an electron from the metal) of gold is so high (typically 4.8 to 5.1 eV) [3][4] that injection of electrons into the lowest unoccupied molecular orbital (LUMO) energy level (typically lower than 4.0 eV in value) that is responsible for electron

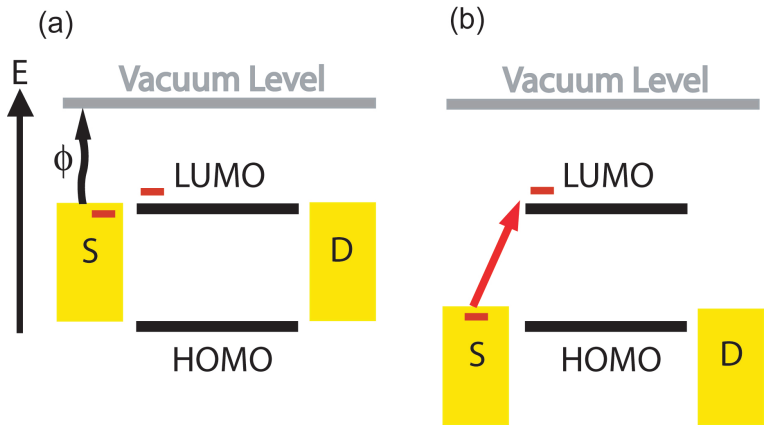

Figure 5.1: a.) Idealized electron injection from the source (S) electrode into the LUMO energy level of the organic semiconductor and b.) injection barrier for electrons from the source to the LUMO. ϕ depicts the work function of the source and drain electrodes and HOMO the highest occupied molecular orbital.

transport within the organic semiconductor is energetically difficult (Figure 5.1) [5]. Therefore, in order to achieve electron operation, electrodes with a low work function like aluminum or calcium have to be employed. Following this factor, n-type pentacene OFETs have beed demonstrated which, when used in combination with gold source and drain electrodes, yield hole transport only. However, the disadvantage of those metals is their sensitivity to oxygen and moisture. Exposed under these conditions, these materials form a thin oxidation layer on their surfaces, in this way inhibiting effective electron injection into the LUMO of the organic semiconductor. Hence, these low work function metals have to be carefully handled in exclusion of air, rendering them unattractive for easy and large area organic electronics processing that require work in ambient conditions due to space demands of large printing machines for example.

The second reason is that the SiO_2 dielectric surface that is also most often employed for OFETs contains polar silanol groups that trap electrons flowing through the organic semiconductor, leading to the observation of hole transport only [6]. Proper extinction of these trapping sites by modifications of the SiO_2 with self-assembled monolayers like HMDS or PTES as has been applied in our previous experiments or with various polymer dielectrics are beneficial for n-type

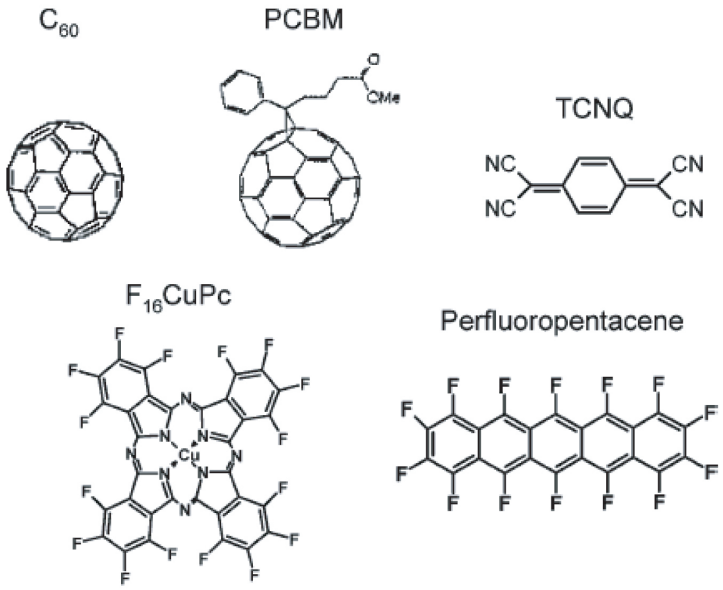

Figure 5.2: Organic semiconductors exhibiting n-type behavior.

OFETs. Conclusively, from the device fabrication point of view, the use of low work function electrodes that facilitate electron injection into the LUMO energy level of the organic semiconductor in combination with the proper insulator surface modifications that minimize electron trapping will theoretically yield n-type OFETs for all organic semiconductors.

Owing to these challenges, research in n-type organic semiconductors lagged behind p-type OFETs. Whereas hole transporting transistors with mobilities higher than 1 $cm^2V^{-1}s^{-1}$ can be readily achieved nowadays, particularly by single crystals or vacuum sublimation of small molecules, but also from solution processing, electron

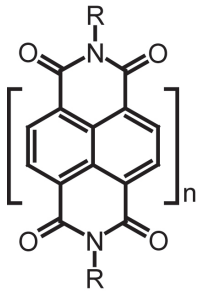

Figure 5.3: General chemical structure of rylene dyes. n=1 is Naphthalene tetracarboxdiimide, n=2 is Perylene tetracarboxdiimide.

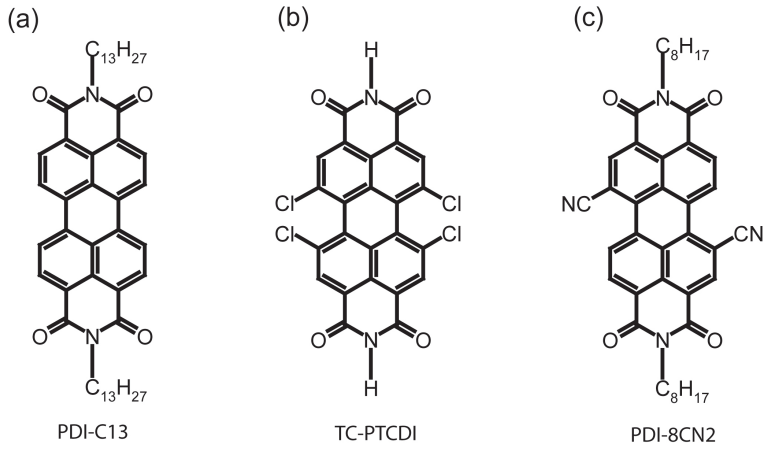

Figure 5.4: a.) Chemical structure of N,N'-ditridecyl-3,4,9,10-perylenetetracarboxylic diimide (PDI-C13), b.) tetrachloroperylene tetracarboxyldiimide (TC-PTCDI) and c.) N,N'-bis(n-octyl)-dicyanoperylene-3,4:9,10-bis(dicarboximide).

mobilities exceeding 0.1 $cm^2V^{-1}s^{-1}$ are already considered outstanding. In terms of molecular design, the incorporation of electron withdrawing groups like cyano or fluoro groups lower the LUMO energy level of the organic semiconductor, in this way enabling efficient electron injection from high work function and air stable metals like gold [7]-[10]. In this way, fluoro groups were attached to pentacene (Figure 5.2), with this perfluoropentacene yielding instead of the typical p-type behavior in pentacene, n-type performance when using gold electrodes as electron injectors [8]. Other material groups leading to n-type OFETs are C_{60}, PCBM, fluorinated copper phtalocyanine or TCNQ (Figure 5.2). The most prominent and studied n-type organic semiconductors are tetracarboxdiimide rylene dyes whose general chemical structure is illustrated in Figure 5.3. The first one of this family was C_8H_{17} substituted naphtalene tetracarboxdiimide (Figure 5.3 with n=1 and R=C_8H_{17}) which was first introduced as solution processed electron transporting layer for OFETs, resulting in high electron mobilities of up to 0.16 $cm^2V^{-1}s^{-1}$ [11]. Later, various derivatives of perylene tetracarboxdiimide (PDI) followed (Figure 5.4).

Among those, PDI-C13 (Figure 5.4a) gave the highest electron mobility up to

date, namely 2.1 $cm^2V^{-1}s^{-1}$ [12]. Later, more electron withdrawing groups like cyano were introduced to the PDI core, for example dicyano (Figure 5.4c) or tetrachloro substituted PDI's (Figure 5.4b), yielding OFETs with mobilities around 0.1 $cm^2V^{-1}s^{-1}$ [13][14]. In addition, a combination of core cyanted PDI with fluorine containing alkyl chains were used in OFETs, resulting in air stable n-type transistors with mobilities up to 0.1 $cm^2V^{-1}s^{-1}$ [15]. Rylene dyes with tetracarboxdiimides are particularly appealing since the tetracarboxdiimides are strong electron withdrawing groups, favoring electron transport in OFETs. Despite the powerful results, the downturn of those PDI derivatives are their insolubility. All compounds were deposited by vacuum sublimation. For the more appealing solution processing, PDI derivatives have to be made soluble. With this in mind, soluble rylene dyes from PDI to Terrylene tetracarboxdiimide (Figure 5.3 with n=3) were synthesized and applied in OFETs.

5.2 Swallow-tailed Perylene tetracarboxdiimide OFETs

With the aim to produce solution processable n-type OFETs, perylene tetracarboxdiimide with swallow-tailed alkyl substituents $C_{8,7}$ (SWPDI) (Figure 5.5) was synthesized by Fabian Nolde and Dr. Zhihong Liu at the Max-Planck Institute for Polymer Research in Mainz. The swallow-tailed substituents make this material nicely soluble in most common organic solvents, enabling solution deposition. Particularly, the conjugated extended PDI core has a high tendency for intermolecular $\pi-$stacking, possibly generating high molecular order beneficial for good transistor performance. In this aspect, this SWPDI was dissolved in toluene with the concentration of 10 mg ml^{-1} and drop-cast in nitrogen atmosphere on HMDS treated 300 nm thick SiO_2 bottom contact transistor substrates. The gate electrode consisted of highly p++ doped silicon and 40 nm gold source and drain contacts were evapo-

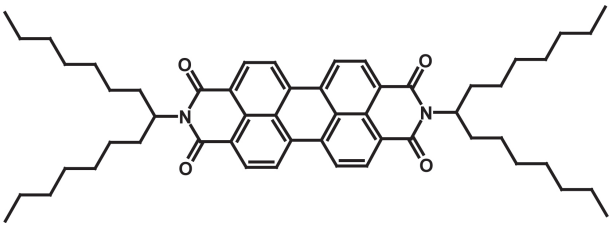

Figure 5.5: Chemical structure of SWPDI.

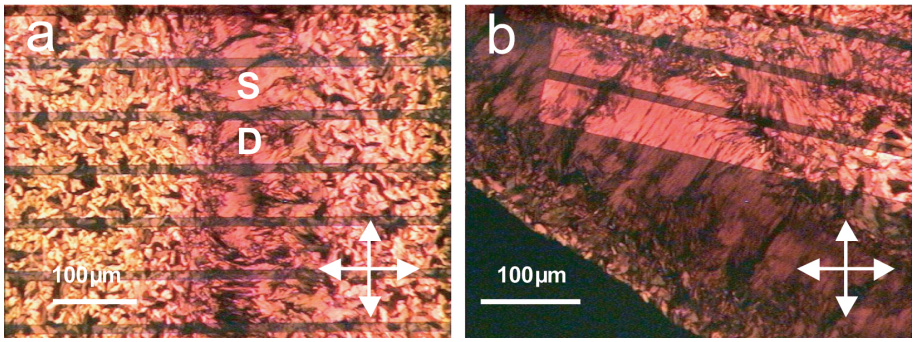

Figure 5.6: a.) POM of drop-cast SWPDI film on transistor substrates b.) at a different film position.

rated in vacuum to form transistors with channel lengths and widths of 10 μm and 5 mm respectively. Gold was chosen in place of the lower work function metals aluminum or calcium because of its enviromental stability. The resulting film is shown in Figure 5.6 taken with a polarized optical microscope (POM).

The rectangular stripes are the source and drain electrodes on which the film was deposited, labeled in Figure 5.6a by S and D. It is evident that a polycrystalline layer is formed with various crystalline domain sizes, with the largest ones extending over several hundreds of micrometers (Figure 5.6b). The transistor characteristics obtained from this film is illustrated in Figure 5.7, yielding only moderate electron mobilities of up to $\mu_{sat} = 1 \times 10^{-4} cm^2 V^{-1} s^{-1}$ and I_{on}/I_{off} ratios of 10^5 as extracted from the transfer characteristics (Figure 5.7b).

Compared to the vacuum sublimed PDI's shown in Figure 5.4, this mobility is quite low. Solely based on the chemical structure, SWPDI is more similar to PDI-C13 (Figure 5.4a) with the only difference in alkyl chain and not in the introduction of additional electron withdrawing groups at the perylene core as is

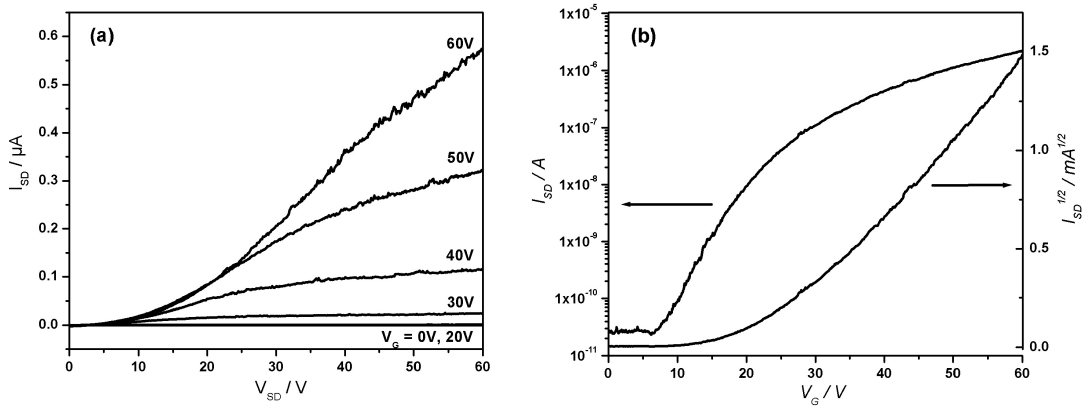

Figure 5.7: a.) Output curves for various gate biases V_G and b.) transfer characteristics at $V_{SD} = 60$V of drop-cast SWPDI OFETs.

the case of TC-PTCDI and PDI-8CN2 (Figure 5.4b and c respectively). However, the SWPDI is four orders of magnitude lower in mobility than the C_{13} substituted PDI even though the difference in chemical structure only lies in different alkyl chains used. One effect alkyl chains might have is the generation of different packing structures. In the case of vacuum sublimed PDI-C13, the resulting films are crystalline with a triclinic unit cell [12]. SWPDI on the other hand self-assemble into one dimensional columns in which each SWPDI molecule is rotated by 45 degrees from the next molecule, in this way forming a helical structure as evidenced by 2D-WAXS of extruded fibers. This arrangement is most probably triggered by the bulky swallow tail alkyl chains which have a great space demand, forcing the SWPDI molecules into this columnar helical packing [24]. However, these columns provide only a one-dimensional charge transport, in this way reducing multiple possible charge transfer paths advantageous for achieving high mobilities. Worse yet, any disor-der in a column will act as trapping site and thus further hinder charge carrier transport. The helical structure present in SWPDI also implies that the columns do not form by cofacial stacking of the perylene cores as for example in the case of HBC, but rather only parts of the perylene core form $\pi - \pi$ overlap with its neighboring molecule due to the 45 degree rotation. This incomplete molecular overlap might also play a role in lowering charge carrier transfer within

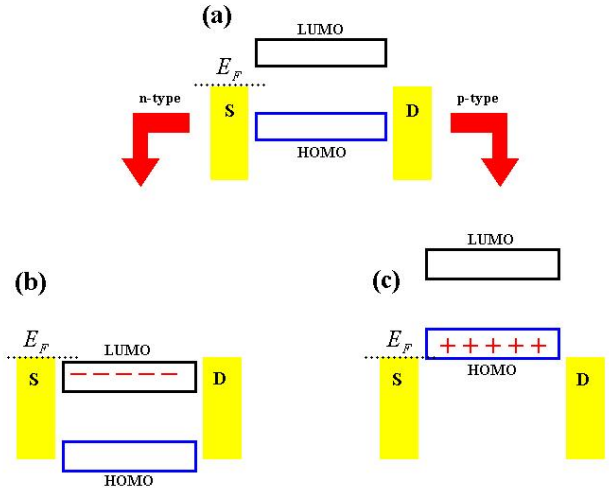

Figure 5.8: a.) Charge carrier injection barriers from the source (S) electrode into the LUMO or HOMO energy levels of the organic semiconductor at zero gate bias $V_G = 0$. b.) Accumulation of electrons in the LUMO caused by an applied $V_G > 0$, ideally triggering energy level matching with the Fermi level E_F of the electrodes. Injection barrier for electrons from the source to the LUMO can be overcome. c.) Accumulation of holes in the HOMO caused by an applied $V_G < 0$, ideally triggering energy level matching with the Fermi level of the electrodes. Injection barrier for holes from the source to the HOMO can be overcome.

each column. Thus, in the light of self-assembly, this one-dimensional helical arrangement potentially explains the observed inferior charge carrier mobility in SWPDI OFETs as compared to a three-dimensional triclinic crystalline film of PDI-C13. Furthermore, intercolumnar charge hopping is a solution to the one-dimensional columnar charge transport restriction. However, the space demanding swallow tail alkyl chains in SWPDI establish an insulating cylindrical shell around the columnar structure, rendering intercolumnar charge transport difficult.

Another explanation for the drastically different device performance between SWPDI and PDI-C13 might be a variation in film morphology. PDI-C13 based transistors exhibiting the excellent electron mobility of 2.1 $cm^2V^{-1}s^{-1}$ emerged from the vacuum sublimed, polycrystalline film containing micrometer sized tilelike grains obtained by keeping the transistor substrate at 140°C during sublimation as evidenced by AFM (Figure 5.10a) [12]. Based on this image, several grains are needed to

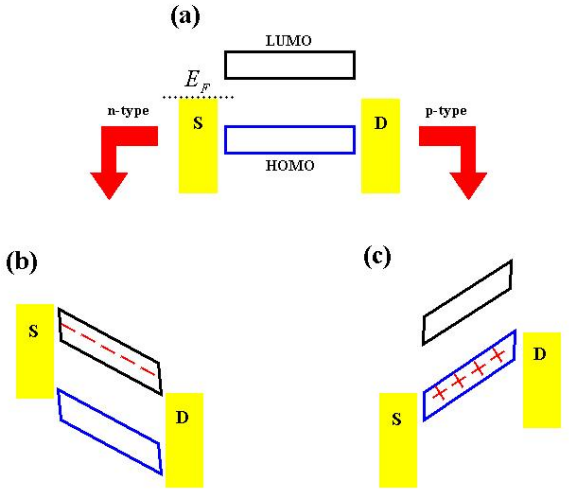

Figure 5.9: a.) Charge carrier injection barriers from the source (S) electrode into the LUMO or HOMO energy levels of the organic semiconductor at zero source-drain bias $V_{SD} = 0$. b.) Fermi level shift of the electrodes caused by an applied $V_{SD} > 0$, ideally triggering energy level matching with the LUMO of the organic semiconductor. Injection barrier for electrons from the source to the LUMO can be overcome and current flow I_{SD} is established. c.) Similarly, Fermi level shift of the electrodes caused by an applied $V_{SD} < 0$, ideally triggering energy level matching with the HOMO of the organic semiconductor. Injection barrier for holes from the source to the HOMO can be overcome and current flow I_{SD} is established.

establish the transistor channel of 10 μm as was used for the SWPDI OFETs. For SWPDI on the other hand, POM images of drop-cast films show that on average two crystalline domains were present in the channel (Figure 5.6a), in this way reducing the number of grain boundaries that might inhibit charge carrier transport [16]-[19]. That is, the crystalline domains in SWPDI films were on average larger and therefore, in terms of morphology only, charge transport in these films should be more elevated as in PDI-C13 layers. However, care has to be taken here. PDI-C13 films with larger crystal grains comparable to those obtained for SWPDI were also achieved by vacuum sublimation on transistor substrates heated at 200°C (Figure 5.10b) without a change in crystal structure. Surprisingly, electron mobilities of up to 0.54 $cm^2V^{-1}s^{-1}$ were obtained, about four times lower than for the film containing smaller grains. The authors explained this result by the presence of deeper cracks within the large grains, in this way posing more severe trapping sites and hence resulting in lower charge carrier mobility. To which extend grain boundaries

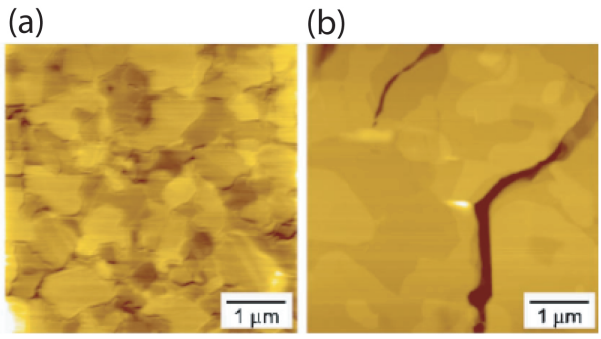

Figure 5.10: a.) AFM images of tilelike morphology of PDI-C13 vacuum sublimed film at 140°C substrate temperature and b.) few micrometers large crystalline PDI-C13 grains evaporated at 200°C substrate temperature [12].

in SWPDI films are responsible for the significantly inferior transistor performance compared to PDI-C13 layers cannot be exactly quantified since other factors such as different molecular packing cannot be neglected. Nevertheless, since a morphology alteration in PDI-C13 yield not orders of magnitude but just four times lower mobilities, it is reasonable to suggest that variation in crystal packing (triclinic crystal for PDI-C13 compared to one-dimensional columns for SWPDI) has a deeper impact on device performance than film morphology.

Another factor that is known to hinder charge carrier transport is contact resistance which is caused by an energetic barrier for charge injection from the source and drain contacts into the organic semiconductor film. As is evident from the output curves in Figure 5.7a, there is a non-linear increase in I_{SD} at low V_{SD} and a lack of saturation. This is an indication for large contact resistances, either caused by bad molecular odering at the source and drain electrodes [20] or by a high Schottky barrier, that is by a huge energy difference in LUMO and the work function of the gold electrodes that were used. This Schottky barrier limits injection of electrons from the electrodes into the LUMO energy level of the organic semiconductor (Figure 5.1b) [21]. The LUMO energy levels of PDI is around 3.7 eV [22], indicating an injection barrier of larger than 1 eV, assuming the work function of gold to be at least 4.8 eV. Despite this high energy barrier, obviously electron injection was nevertheless enabled since n-type behavior was detected. This can be readily explained

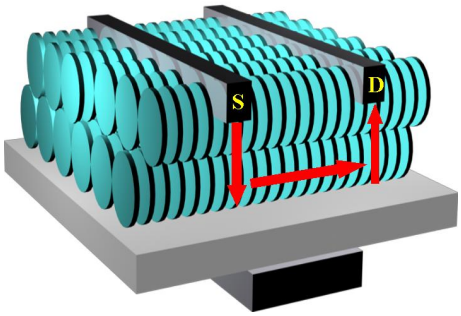

Figure 5.11: Schematic representation of charge carrier transport (red arrows) in top-contact OFETs comprised of discotic columnar structures.

by the operation principle of OFETs. When electrons are accumulated in the organic semiconductor as a response to the gate bias V_G, the LUMO moves closer to the Fermi level of the gold electrodes, in this way partially overcoming the Schottky barrier (Figure 5.8b). Additional V_{SD} bias shifts the gold Fermi level even closer to the LUMO, further bridging the injection gap (Figure 5.9b). Based on these processes, sufficient electron injection was guaranteed to achieve n-type OFETs. Still, due to the observed contact resistance, the Schottky barrier was apparently not completely avoided. However, owing to the crystallinity of the SWPDI film, it is also possible that the rigidity of the crystalline domains at the electrodes enhanced the high contact resistance. This problem was not encountered for PDI-C13 since gold top contact OFETs were fabricated.

With the aim to minimize those contact resistances, top contact devices were fabricated with the drop-cast SWPDI films. 80 nm gold electrodes with channel lengths and widths of 290 μm and 25 μm respectively were thermally evaporated on top of the SWPDI layer which was processed in the same way as described for the bottom contact case. Unfortunately, no transistor operation could be observed. The same was true for top contact devices fabricated with calcium electrodes. This is surprising since both the top contact structure should avoid the contact problem with the rigid crystalline film and calcium (work function about 3 eV) is supposed to better match the LUMO of SWPDI, leading to improved electron injection. One

explanation might be the grain boundaries. Whereas for the bottom contact devices there were only few crystalline domains distributed along the 10 μm channel length, for the top-contact configuration the channel length increased to 25 μm, containing more grain boundaries. Consequently, charge transport was severely hindered. This phenomenon is further enhanced by the one-dimensional columnar arrangement of the SWPDI molecules as revealed by 2D-WAXS experiments on extruded SWPDI fibers [24]. Electron transfer is confined to take place only along the SWPDI core that are stacked together to form this one-dimensional columnar structure. Intercolumnar charge hopping is limited by the insulating alkyl chains filling the column periphery. This aspect holds for both bottom and top contact OFETs where for the latter case, this intercolumnar charge transport might play an even more crucial role. In contrast to bottom contact devices, the current has to first flow from the source electrode through the entire thickness of the organic layer to the insulator surface where the whole channel is passed. Then, the electrons flow from the insulator surface through the entire film thickness again to reach the drain electrode, in this way establishing the transistor current I_{SD} as schematically illustrated in Figure 5.11 [23]. During their way through the film thickness, charge transport is entirely of the intercolumnar type which, owing to the insulating alkyl chains, is strongly hindered. Combined with the increased number of grain boundaries most probably explains the absence of transistor performance for the top-contact geometry even though contact resistance has been lowered, facilitating electron injection.

Based on these results, it is evident what effect different alkly chains might have on molecular self-assembly and thus on transistor behavior. Motivated by the excellent mobility of vacuum sublimed PDI-C13, our aim was to achieve comparable device performance but with a soluble compound. This was achieved by introducing swallow tail alkyl chains to the PDI instead of C_{13}. However, helical one-dimensional columns emerged for this SWPDI system, in this way most probably significantly limiting charge carrier mobility. A possible way out of this dilemma is the replace-

ment of the swallow tail alkyl chain with a longer linear alkyl substituent to induce solubility. As revealed by PDI-C13, linear alkyl chains seems to be the proper choice for avoiding one-dimensional columnar structures and hence might lead to high performance solution processable n-type OFETs.

5.3 Swallow-tailed Terrylene tetracarboxdiimide OFETs

5.3.1 Solution Processed SWTDI OFETs

The OFETs based on SWPDI did not show high electron mobility. In an attempt to solubilize the PDI with space demanding swallow tailed alkyl chains $C_{8,7}$, one dimensional columnar structures were induced that restrict charge carrier transport. Despite the possibility of introducing longer linear alkyl chains to potentially avoid columnar packing, it is questionable whether a linear alkyl chain or a less branched one like for example $C_{8,2}$ will indeed provide enough solubility and also not form columnar arrangements. Instead, we follow the approach of extending the PDI core by one more naphtalene unit with the aim of enhancing intermolecular packing due to the larger conjugated core. This approach might increase the crystalline domains as compared to SWPDI, therefore limiting grain boundaries that in part degrade charge carrier mobility. At the same time, the swallow tail alkyl chains $C_{8,7}$ were added like in the case of SWPDI in order to induce enough solubility even though with this procedure the problem of columnar self-assembly might stay intact. However, by following this approach of unchanged swallow tail alkyl chains, information can be gained about the role of extended rylene cores in influencing molecular self-assembly, film morphology and ultimately transistor performance. In this aspect, swallow tailed terrylene tetracarboxdiimide (SWTDI) dyes were synthesized (synthesis was performaned by Fabian Nolde and Dr. Zhihong Liu at the Max-Planck Institute for

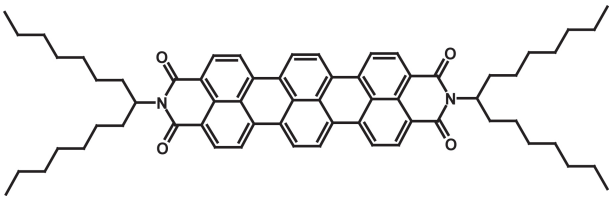

Figure 5.12: Chemical structure of SWTDI.

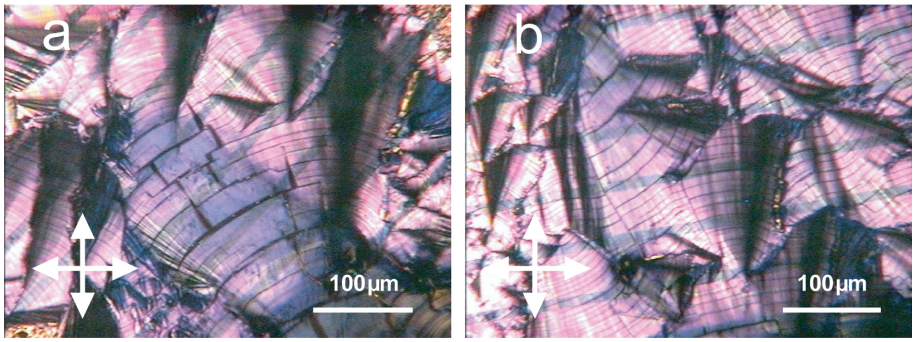

Figure 5.13: a.) POM of drop-cast SWTDI film on transistor substrates b.) at a different film position.

Polymer Research in Mainz) whose chemical structure is illustrated in Figure 5.12. This SWTDI was applied in OFETs by drop-casting from a 10 mg ml^{-1} toluene solution on HMDS treated 300 nm thick SiO_2 bottom contact transistor substrates akin to the SWPDI devices. The resulting thin film is illustrated in Figure 5.13, revealing a highly crystalline morphology. It is evident from these images that the crystalline domains grow outwards from a nucleation site, that is, from a certain point on, the structures become larger and larger, building cone shapes. This film morphology resulted in electron mobilities of up to $10^{-3}cm^2V^{-1}s^{-1}$ as measured from ten devices and deduced from the typical transistor characteristics shown in Figure 5.14. The mobility was one order of magnitude higher than for the SWPDI case. As 2D-WAXS measurements on extruded SWTDI fibers suggest, the compound self-assembles into columnar stacks (Figure 5.15a) where in each column the molecules are helically packed (Figure 5.15b) akin to the case of SWPDI [24].

Based on this similar order, one reason for this elevated mobility might not be a different molecular packing between those two dyes but rather the larger crystal domain sizes of SWTDI. As is evident in Figure 5.13, the cone shaped domains

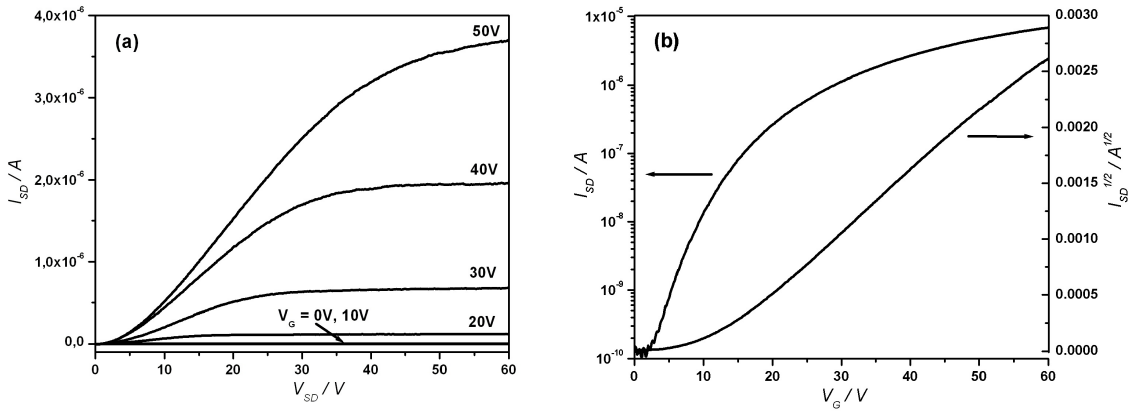

Figure 5.14: a.) Output curves for various gate biases V_G and b.) transfer characteristics at $V_{SD} = 50$V of drop-cast SWTDI OFETs.

range from several tens to hundreds of micrometers in size and are therefore several times larger than the SWPDI crystalline grains. Owing to these extended crystallites, the SWTDI transistor channel lengths were almost completely covered by a single domain, in this way decreasing the number of grain boundaries and hence the number of trapping sites. Apparently, the extended conjugated core of SWTDI compared to SWPDI are beneficial in impinging longer range supramolecular order, possibly due to stronger $\pi - \pi$ interaction of the larger $\pi-$molecular orbital of the TDI core. In addition, in terms of contact resistance that was present in SWPDI devices and that was a possible factor for the reduction of charge carrier

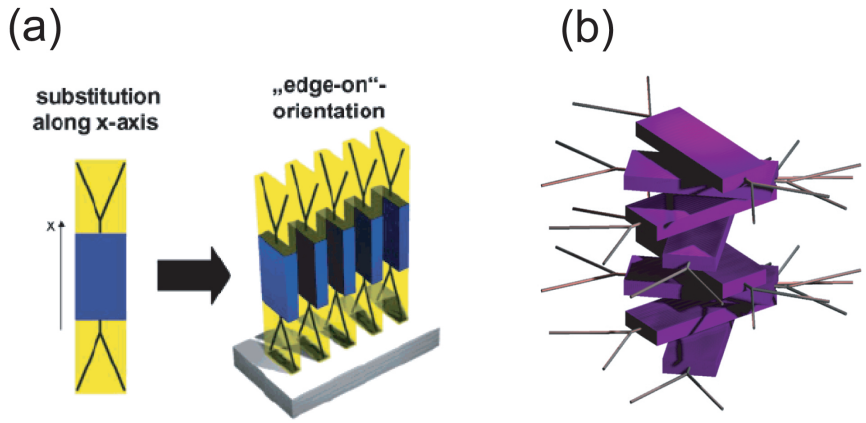

Figure 5.15: a.) Edge on assembly of SWTDI into one dimensional columns [24]. b.) Schematic presentation of helical twist of SWTDI molecules within one column.

mobility, contact resistance in SWTDI OFETs existed as well, however to a lesser extend. This point can be readily understood by comparing the output curves of both OFETs. For SWPDI, the nonlinear increase in source drain current I_{SD} prevailed from $V_{SD} = 0V$ to about $V_{SD} = 10V$ (Figure 5.7a) higher than in the case of SWTDI where linear rise of I_{SD} started at considerably lower V_{SD} (around $V_{SD} = 5V$, Figure 5.14a). Therefore, this lower contact resistance might have lead to a higher charge carrier mobility. The reduction of contact resistance in SWTDI is unlikely evoked by an increased Schottky barrier compared to SWPDI. In fact, the LUMO energy levels of both compounds are comparable [22], ruling out contact resistance caused by electron injection barriers. One possible reason for the reduced contact resistance in SWTDI might be a better molecular arrangement of the molecules at the gold source and drain electrodes, in this way guaranteeing improved electron injection from the contacts into the SWTDI layer. Maybe the stronger $\pi - \pi$ interaction promotes this smoother transition in supramolecular film formation at the source and drain contact/SWTDI layer [25][26].

Furthermore, the threshold voltage of SWPDI devices was $V_T = 20V$ whereas $V_T = 10V$ for SWTDI, half the value of SWPDI. This lower threshold voltage of SWTDI is an indication of less trapping sites than in SWPDI films. These trapping sites can arise from disorder at the semiconductor/insulator interface or within the film itself. Since for both compounds the same interface treatment was used (both HMDS) and identical columnar structures were formed, the decreased trapping site most probably arose from less disorder within the SWTDI bulk layer. This point is in good accordance with the more extended crystal domains in SWTDI films, thus effectively limiting traps within the channel. Hence, a combination of both improved contact resistance and reduced macromolecular disorder in the SWTDI film most apparently triggered the ten times higher mobility as compared to SWPDI. Despite the large crystal domains, the electron mobility of SWTDI films were still not high. This phenomenon is attributed

to the one dimensional columnar packing of the SWTDI molecules evoked by the swallow tail alkyl chains attached to the TDI. This one dimensional charge transport is prone to structural defects within a single column. Such defects act as trapping sites and hinder charge transport. Nevertheless, keeping in mind that, via zone-casting, the highly directionally aligned discotic $HBC - C_{12}$ OFETs yielded hole mobilities of up to $10^{-2} cm^2 V^{-1} s^{-1}$, then the SWTDI devices were just inferior by one order of magnitude, even though no directional order has been induced.

5.3.2 Melt Processed SWTDI OFETs

Since apparently the domain size contributes to the enhanced transistor performance, devising a method for obtaining even larger crystalline areas is appropriate with the aim to optimize device performance. There are several possible ways to obtain extended crystalline regions. In the light of solution processing, zone-casting or dip-coating for example might generate directionally aligned layers with the high probability of forming large ordered domains. However, the disadvantage of those techniques is that most often time consuming optimization is needed to reach the desired film morphology. Another more simple route is the so called melt processing which function in the following way: The SWTDI can be turned into an isotropic or melt phase at 280°C as revealed by differential scanning calorimetry (DSC) [24]. In this isotropic phase, the material is melt, with the molecules being unbound into any film structure. By slowly cooling down this melt, the molecules rearrange themselves into a solid layer, in this way forming ordered crystalline films. This is an easy method for achieving large crystalline layers as compared to the more complicated vaccuum sublimation or the above mentioned solution techniques.

Based on this phenomenon, melt processed SWTDI OFETs were fabricated in the following steps: Bottom gate, bottom contact transistor substrates were used where the gate consisted of highly p-type doped silicon wafers covered by a 300

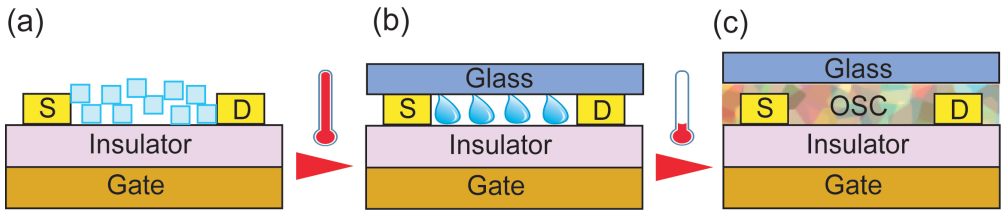

Figure 5.16: a.) Deposition of SWTDI on bottom gate, bottom contact transistor substrates. b.) Heating the substrate till the SWTDI molecules reached their isotropic (melt) phase. A glass plate was placed on top of the melt to prevent dewetting. c.) Slow cooling yielded crystallization of the melt.

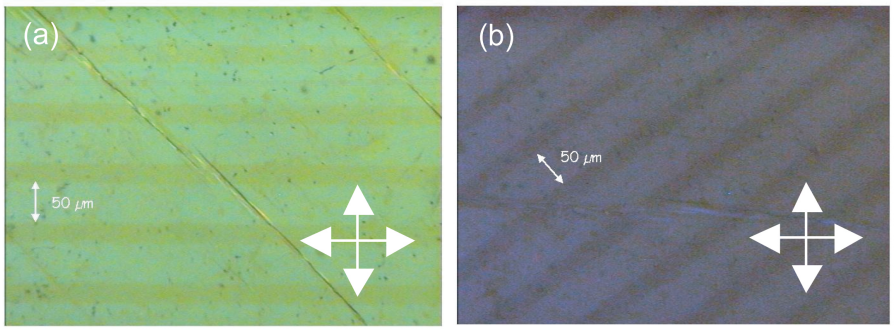

Figure 5.17: a.) POM of melt SWTDI film on transistor substrates. b.) Optical anisotropy of the same film.

nm thick SiO_2 layer acting as the insulator. Lithographically defined gold source and drain contacts with a width of 5 mm (channel width) and separated by a distance of 10 μm (channel length, see chapter 8.2) were evaporated (40 nm thick on 2 nm chrome as adhesive layer). The SiO_2 dielectric was functionalized with HMDS in order to prevent charge trapping at the organic semiconductor/dielectric interface. A small amount of SWTDI was put on these transistor substrates (Figure 5.16a). Then these samples were heated to 280°C in order to reach the isotropic phase of the SWTDI molecules. At his temperature, the SWTDI melted and hence became liquid. In order to obtain a thin film, a glass plate was deposited on the melt (Figure 5.16b). The weight of the glass plate pressed the melt into a broad, homogeneous thin film and furthermore prevented the formation of drops (dewetting) instead of a film. This sandwiched melt layer was then slowly cooled down to room temperature at a rate of 0.5°C per minute (Figure 5.16c) using a computer controlled cooling stage. The resulting crystalline film investigated by

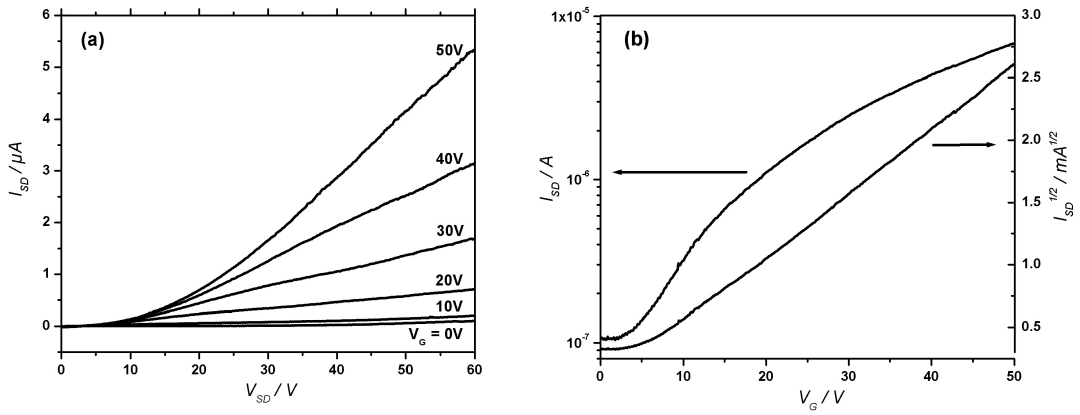

Figure 5.18: a.) Output curves for various gate biases V_G and b.) transfer characteristics at $V_{SD} = 50$V of melt SWTDI OFETs.

POM is illustrated in Figure 5.17a. As is evident from the image, very large crystals were formed that extended over several millimeters. Those crystals exhibited optical anisotropy as depicted in Figure 5.17b, suggesting a directionally ordered structure. Compared to the drop-cast film (Figure 5.13), the melt-processed structure was highly homogeneous and did not consist of cone-shaped domains of various sizes. Also, the melt-processed layer completely covered the transistor channels without the presence of any visible grain boundaries. Thus, charge carrier trapping should be minimized, yielding increased charge carrier mobilities.

Transistor measurements based on such large domain crystalline film resulted in typical device characteristics shown in Figure 5.18. The saturated electron mobility as extracted from the transfer curve (Figure 5.18b) was $\mu_{sat} = 6 \times 10^{-4} cm^2 V^{-1} s^{-1}$.

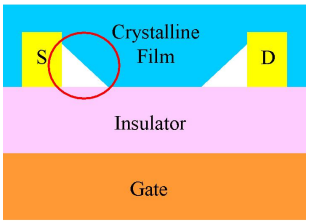

Figure 5.19: Rigid crystal structure leading to limited contact area with source and drain electrodes as highlighted by the red circle.

This value is suprising since it is comparable to the mobility reached by the drop-cast film which contained smaller crystal domains. In addition, X-ray studies of this melt-processed SWTDI layer illustrated molecular packing akin to the drop-cast films. Therefore, based on the larger scale crystalline morphology, the electron mobility of this film fabricated from the melt should be much higher. In addition, the threshold voltage of this melt-processed device was $V_T = 5V$, half the value as for the drop-cast transistors. This is an indication for a decrease of trapping sites within the melt film most probably originating from the larger crystalline domains and hence the elimination of grain boundaries. Therefore, the electron mobility is expected to exceed this observed value. However, as it is evident from the output curves (Figure 5.18a), a non-linear increase in current I_{SD} at low source-drain voltages V_{SD} together with the lack of current saturation was observed. These two factors generally indicate severe contact resistance prevailing in the device. Most probably this contact resistance between the source and drain electrodes and the organic semiconductor crystal was responsible for the low mobility [27]-[29]. Such contact resistance was already observed in the drop-cast transistors revealed by the non-linear increase of I_{SD} at low source-drain voltages V_{SD} (Figure 5.14a). Nevertheless, despite this non-linear I_{SD} rise, saturation was still achieved in those devices. In the melt-processed case this saturation was missing, alluding to more severe contact resistance and thus lower electron mobility even though larger crystal domains were present. It is reasonable to assume that the more extended the crystals are, the more rigid is the film and hence contact with the source and drain metals which are 40 nm higher than the insulator surface on which the film should be lying is limited (Figure 5.19). It is possible that while the SWTDI in the melt have sufficient contact with the electrodes since the film is liquid at this stage, during the crystallization process at which the material forms a solid film, the molecules move away from the electrodes, resulting in areas with poor organic semiconductor/metal contact (red circle in Figure 5.19).

Contact resistance limited charge carrier mobility in polycrystalline films is well known and studied in detail for pentacene bottom contact OFETs [30]-[32]. However, solution processed single crystalline domain OFETs are still rarely reported, even though such systems are interesting due to their minimized grain boundaries compared to polycrystalline films. Some single domain materials have been reported without any significant inhibition in contact resistance, alluding to the possibility that not all solution processed monodomain transistors always suffer from contact problems. Recently, solution deposited single domain OFETs made out of fluorinated 5,11-bis(triethylsilylethynyl) anthradithiophene (diF-TESADT, Figure 5.20a) have been reported. The single crystalline grains were fabricated by spin coating diF-TESADT chlorobenzene solution on bottom contact OFET substrates where the source and drain electrodes were functionalized with pentafluorobenzene thiol (PFBT, Figure 5.20b). With the help of scanning Kelvin probe microscopy (SKPM) the main charge transport barrier was pinpointed to a large injection barrier between the source contact and the organic semiconductor layer. Trapping within the bulk at the interface or due to defects within the crystal domain was secondary [33]. Hereby, the single domains which span over channel lengths of 5 μm were induced by the contact modification with PFBT. The same group has shown that crystal growth started from the PFBT modified contacts and extended over the whole transistor channel owing to sulfur-fluorine interaction between the sulfur atom in the thiophene units of diF-TESADT and the fluorine in PFBT. For channel lengths of 5 μm, single domains can be obtained whereas for larger channels, crystal formation initiated from both source and drain contacts with the crystals meeting somewhere within the channel, in this way forming a grain boundary as illustrated in Figure 5.20c. These long channel devices showed inferior charge carrier mobility than the single grain devices due to the presence of this grain boundary acting as a trapping site [34]. For even larger channels, grains nucleated within the channel as well, generating polycrystalline films. In the same

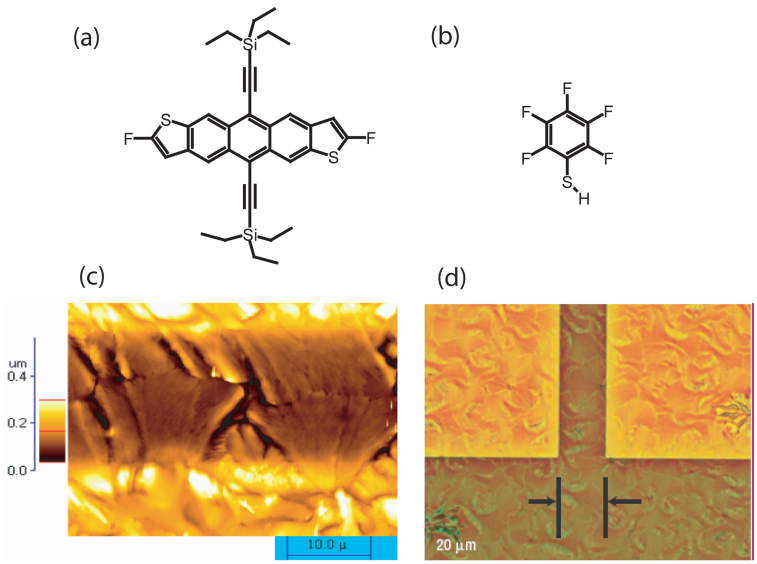

Figure 5.20: a.) Chemical structure of diF-TESADT and b.) of PFBT. c.) AFM image in tapping mode of diF-TESADT grains grown from the PFBT functionalized gold electrodes into the transistor channel. d.) POM of diF-TESADT film on untreated gold contacts [34].

work, untreated gold electrodes lead to formation of smaller grains on both the gold and within the channel, with little or no propagation of grains from the metal into the channel (Figure 5.20d). The resulting mobility was one order of magnitude lower than for the functionalized contacts. In the same sense, for the melt-processed SWTDI, no such thiol treatment of the gold electrodes was undertaken, making crystal growth from the electrodes unlikely as well. Therefore, peeling off of the SWTDI crystal domains from those electrodes seems to be a realistic scenario.

Melt processed OFETs as described in this section have not been reported until very recently by Konishi and coworkers [35]. In this work, 9,10-bis-(4,4′-alkyloxystyryl)anthracene with $C_{18}H_{37}$ alkyl chains (BSA18, Figure 5.21a) was melted and sandwiched between two glass plates similar to the procedure employed for SWTDI. Then, the melt was cooled down very slowly at a rate of 0.01°C per minute, resulting in films with crystalline domain sizes of several milimeters. One glass plate was then ripped off in order to contact the layer with source and drain electrodes with channel lengths of 50 μm. The top gate transistors were finished by

evaporating an inorganic insulator parylene-C on top of the crystalline layer followed by evaportion of the gate electrode. The transistor configuration is highlighted in the inset of Figure 5.21b. Output characteristics of these melt-processed OFETs are depicted in the same figure from which the presence of contact resistance is evident due to the non-linear rise of I_{SD} at low V_{SD}. In fact, source drain potentials of higher than -20V had to be applied in order to get a current flowing at all. This bias is quite high and a clear indication for heavy contact problems. The saturated hole mobilities in these devices were $10^{-4} cm^2 V^{-1} s^{-1}$. This mobility is in the same range as the melt-processed monodomain SWTDI OFETs. Even though monodomains are expected to contain minimal grain boundaries as in the case of small crystalline domain or polycrystalline films, the charge carrier mobility is low. The observed severe contact resistance in BSA18 might be a factor limiting transistor performance. On the other hand, the device configuration used with source drain electrodes evaporated on top of the crystalline film should provide sufficient contact and hence circumvent contact resistance. However, the authors did not report possible destruction of the crystalline film due to the rip-off of the glass plate before contact evaporation. This process might have caused cracking in the monodomain crystals, causing severe grain boundaries that is expressed in a non-linear increase of I_{SD} in the output curves as well. Another possible aspect that triggers low mobility is molecular packing. For melt-processed SWTDI films, the one-dimensional columnar stacking of the SWTDI molecules was pinpointed to generate the inferior transistor performance. However, in the BSA18 case, no such columnar arrangement was present. Instead, the melt-processed films exhibited layered structures with the BSA18 molecules standing with their alkyl chains on the surface with a tilt angle of 54°. Such an arrangement should enable three- dimensional charge transport and hence higher mobilities as in the columnar structure of SWTDI. Unfortunately, the authors did not provide any explanation for the low performance.

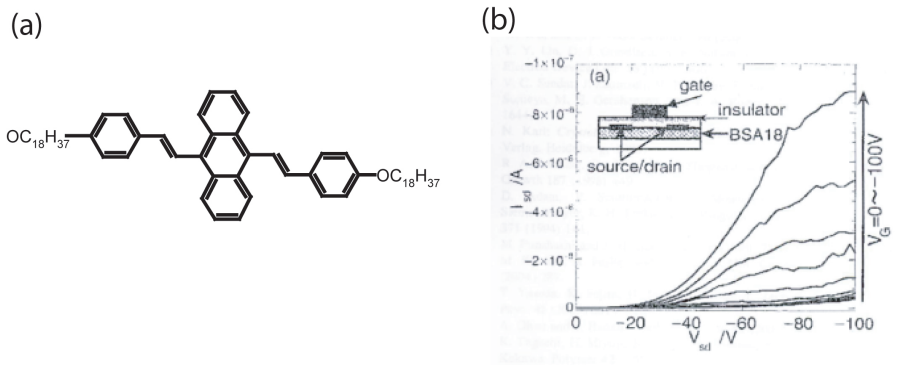

Figure 5.21: ***a.) Chemical structure of BSA18 and b.) output curves of melt-processed BSA18 OFETs [35].***

In order to circumvent the contact problem in SWTDI OFETs, the bottom gate, top contact device configuration was employed in which the source and drain electrodes were deposited on top of the organic semiconductor layer. This was achieved by first melt-processing the SWTDI molecules following the same procedure as described before in Figure 5.16, but on simple HMDS treated SiO_2 surface without source and drain electrodes. Once the film was formed, the glass plate that was used to sandwich the melt layer in order to prevent dewetting was taken off so that source and drain metals can be deposited on top of the film. Both gold and calcium electrodes were evaporated to finish the top contact devices. Calcium was used since it has a low work function, allowing better electron injection into the LUMO energy level of SWTDI. However, no transistor performance was observed in both top contact cases even though minimal contact resistance should be present with this device configuration. This absence of current flow is attributed to the possible destruction of the cystalline film during the peeling off process of the glass plate since parts of the film was also stuck on the glass plate, leading to cracking of the delicate crystals.

With the aim to avoid this destruction of the crystalline film caused by the ripping off of the glas plate but at the same time to keep the top contact structure in order to prevent contact resistance, the source and drain top contacts were first deposited on the glass plate via photolithography (see chapter 8.2 for more details).

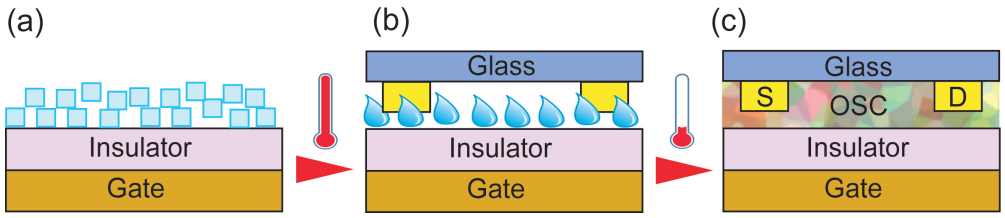

Figure 5.22: a.) Deposition of SWTDI on bottom gate transistor substrates. b.) Heating the substrate till the SWTDI molecules reached their isotropic (melt) phase. Then, a glass plate with predifined source and drain electrodes was placed on the melt film to achieve a top-contact configuration without crystal destruction. c.) Slow cooling yielded crystallization of the melt.

Then, these glass plates were placed on top of the melt layer such that the electrodes were in touch with the film (Figure 5.22b). In this way, a sandwiched top contact device was fabricated after cooling down the melt at the same rate as before (0.5°C per minute) (Figure 5.22c). These transistors yielded behavior highlighted in Figure 5.23 from which an electron mobility of $\mu_{sat} = 1.4 \times 10^{-4} cm^2 V^{-1} s^{-1}$ was extracted. This performance was lower than both the drop-cast and the bottom contact melt cases which was unexpected since contact resistance should have been minimized and crystal destruction avoided for this sandwiched top contact structure. However, as the output curves in Figure 5.23a suggest, contact resistance still prevailed as indicated by the again non-linear increase in I_{SD} and the absence of saturation. This behavior can be explained with the same arguements used for drop-cast, polycrystalline SWPDI top contact OFETs. There, the top electrodes should have minimized contact resistance. However, suprisingly no transistor performance was observed which we attributed to the hindered intercolumnar charge transport where the carriers have to pass twice through the film thickness in order to establish the current I_{SD} flowing between source and drain. The same reasoning holds true in this SWTDI case, with the difference that top-contact showed transistor behavior. This is caused by the highly homogenous melt film that was not polycrystalline as for SWPDI but rather almost single crystalline, effectively limiting grain boundaries and hence trapping sites. Still, contact resistance was observed, caused by the slower charge hopping of intercolumnar charge transport across the entire thick melt

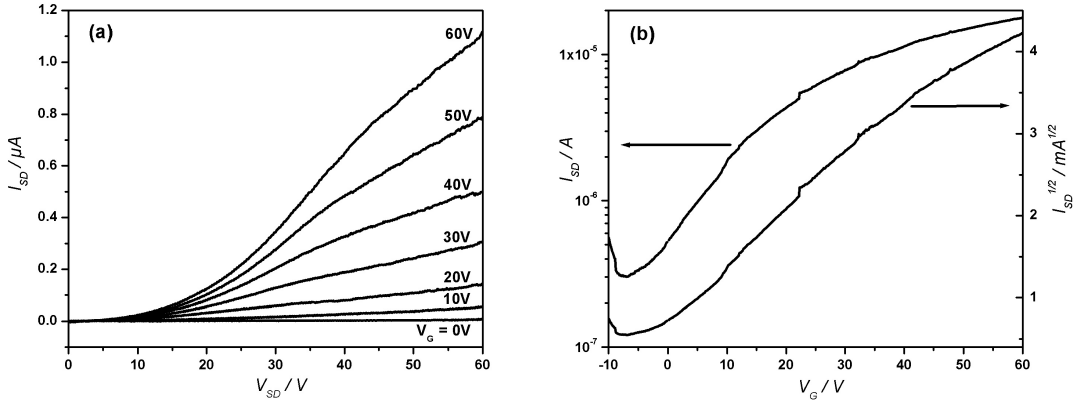

Figure 5.23: a.) Output curves for various gate biases V_G and b.) transfer characteristics at $V_{SD} = 60$V of melt SWTDI top-contact OFETs.

processed film from source to the insulator and back to the drain.

5.4 Summary

Electron transporting OFETs based on discotic rylene dyes SWPDI and SWTDI were successfully fabricated. Those compounds revealed the challenge in designing solution processable organic semiconductors. Theoretically, long aromatic cores like perylene and terrylene are expected to exhibit strong $\pi - \pi$ interaction and therefore good electronic orbital overlap for efficient charge carrier transport. However, bulky alkyl substituents have to be introduced to these cores in order to render them soluble. As a result, even though crystalline packing was still present, one-dimensional columnar structure was induced, leading to low charge carrier mobility. Further enhancement of crystalline domains via melt processing did not show improvement in mobility. This phenomenon was attributed to the combination of contact resistance and one-dimensional charge transport in helical columnar structures. Nevertheless, motivated by the tremendous success of insoluble, vacuum evaporated PDI derivatives OFETs, rylene dyes are still attractive candidates for electron transporting semiconductors. The main challenge is just to render them soluble in order to be able to apply easy and cheap processing methods for the fabrication of n-type transistors.

Our approach of utilizing swallow tailed alkyl chains resulted in low charge carrier mobilities mainly due to the columnar packing of these swallow tailed rylene dyes. Hence, as a next step, substitution of the perylene and terrylene tetracarboxdiimide cores with other solubilizing groups that do not trigger columnar arrangement will be surely of great interest in achieving high performance n-type OFETs, particularly for the more extended TDI which has been shown in this chapter to exhibit a more pronounced supramolecular ordering by the generation of larger crystalline domains. If linear alkyl chain substituted PDI-C13 has already shown electron mobilities of 2.1 $cm^2V^{-1}s^{-1}$, then linear alkyl chain substituted TDI's, whether vacuum sublimed or solution processed, hold great promise in even surpassing this PDI performance.

Bibliography

[1] Z. Bao, *Adv. Mater.* **2000**, *12*, 227.

[2] E. J. Meijer, D. M. de Leeuw, S. Setayesh, E. van Veenendaal, B.-H. Huisman, P. W. M. Blom, J. C. Hummelen, U. Scherf, T. M. Klapwijk, *Nat. Mater.* **2003**, *2*, 678.

[3] N. Koch, A. Kahn, J. Ghijsen, J.-J. Pireaux, J. Schwartz, *Appl. Phys. Lett.* **2003**, *82*, 1532102.

[4] H. Ishii, K. Sugiyama, E. Ito, K. Seki, *Adv. Mater.* **1999**, *11*, 605.

[5] C. R. Newman, C. D. Frisbie, D. A. da Silva Filho, J.-L. Brdas, P. C. Ewbank, K. R. Mann, *Chem. Mater.* **2004**, *16*, 4436.

[6] L. L. Chua, J. Zaumseil, J.-F. Chang, E. C.-W. Ou, P. K.-H. Ho, H. Sirringhaus, R. H. Friend *Nature* **2005**, *434*, 194.

[7] B. A. Jones, A. Facchetti, M. R. Wasielewski, T. J. Marks, *J. Am. Chem. Soc.* **2007**, *129*, 15259.

[8] A. Facchetti, M.-H. Yoon, C. L. Stern, H. E. Katz, T. J. Marks, *Angew. Chem. Int. Ed.* **2003**, *42*, 3900.

[9] Z. Bao, A. J. Lovinger, J. Brown, *J. Am. Chem. Soc.* **1998**, *120*, 207.

[10] B. A. Jones, M. J. Ahrens, M.-H. Yoon, A. Facchetti, T. J. Marks, M. R. Wasielewski, *Angew. Chem.* **2004**, *116*, 6523.

[11] H. E. Katz, A. J. Lovinger, J. Johnson, C. Kloc, T. Siegrist, W. Li, Y.-Y. Lin, A. Dodabalapur, *Nature* **2000**, *404*, 478.

[12] S. Tatemichi, M. Ichikawa, T. Koyama, Y. Taniguchi, *Appl. Phys. Lett.* **2006**, *89*, 112108.

[13] B. Yoo, T. Jung, D. Basu, A. Dodabalapur, B. A. Jones, A. Facchetti, M. R.Wasielewski, T. J. Marks, *Appl. Phys. Lett.* **2006**, *88*, 082104.

[14] M.-M. Ling, P. Erk, M. Gomez, M. Koenemann, J. Locklin, Z. Bao, *Adv. Mater.* **2007**, *19*, 1123.

[15] R. T. Weitz, K. Amsharov, U. Zschieschang, E. B. Villas, D. K. Goswami, M. Burghard, H. Dosch, M. Jansen, K. Kern, H. Klauk, *J. Am. Chem. Soc.* **2008**, *130*, 4637.

[16] D. Knipp, R. A. Street, A. Völkel, J. Ho, *J. Appl. Phys.* **2003**, *93*, 347.

[17] G. Horowitz, M. E. Hajlaoui, *Synth. Met.* **2001**, *122*, 185.

[18] J. H. Schön, B. Batlogg, *J. Appl. Phys.* **2001**, *89*, 336.

[19] G. Horowitz, M. E. Hajlaoui, R. Hajlaoui, *J. Appl. Phys.* **2000**, *87*, 4456.

[20] G. R. Dholakia, M. Meyyappan, A. Facchetti, T. J. Marks, *Nano Lett.* **2006**, *6*, 2447.

[21] L. Bürgi, T. J. Richards, R. H. Friend, H. Sirringhaus, *J. Appl. Phys.* **2003**, *94*, 6129.

[22] S. K. Lee, Y. Zu, A. Herrmann, Y. Geerts, K. Müllen, A. J. Bard, *J. Am. Chem. Soc.* **1999**, *121*, 3513.

[23] G. Horowitz, F. Garnier, A. Yassar, R. Hajlaoui, F. Kouki, *Adv. Mater.* **1996**, *8*, 52.

[24] F. Nolde, W. Pisula, S. Müller, C. Kohl, K. Müllen, *Chem. Mater.* **2006**, *18*, 3715.

[25] D. J. Gundlach, L. Zhou, J. A. Nichols, T. N. Jackson, P. V. Necliudov, M. S. Shur, *J. Appl. Phys.* **2006**, *100*, 024509.

[26] P. V. Pesavento, K. P. Puntambekar, C. D. Frisbie, J. C. McKeen, P. P. Ruden, *J. Appl. Phys.* **2006**, *99*, 094504.

[27] L. Bürgi, H. Sirringhaus, R. H. Friend *Appl. Phys. Lett.* **2002**, *80*, 2913.

[28] R. A. Street, A. Salleo, *Appl. Phys. Lett.* **2002**, *81*, 2887.

[29] H. Klauk, G. Schmid, W. Radlik, W. Weber, L. Zhou, C. D. Sheraw, J. A. Nichols, T. N. Jackson, *Solid-State Elec.* **2003**, *47*, 297.

[30] T. Maeda, H. Kato, H. Kawakami, *Appl. Phys. Lett.* **2006**, *89*, 123508.

[31] P. V. Necliudov, M. S. Shur, D. J. Gundlach, T. N. Jackson, *Solid-State Elec.* **2003**, *47*, 259.

[32] W.-K. Kim, J.-L. Lee, *Appl. Phys. Lett.* **2006**, *88*, 262102.

[33] L. C. Teague, B. H. Hamadani, O. D. Jurchescu, S. Subramanian, J. E. Anthony, T. N. Jackson, C. A. Richter, D. J. Gundlach, J. G. Kushmerick, *Adv. Mater.* **2008**, *20*, 1.

[34] D. J. Gundlach, J. E. Royer, S. K. Park, S. Subramanian, O. D. Jurchescu, B. H. Hamadani, A. J. Moad, R. J. Kline, L. C. Teague, O. Kirillov, C. A. Richter, J. G. Kushmerick, L. J. Richter, S. R. Parkin, T. N. Jackson, J. E. Anthony, *Nat. Mater.* **2008**, *7*, 216.

[35] M. Konishi, K. Fujita, T. Tsutsui, *Jpn. J. Appl. Phys.* **2008**, *47*, 4732.

Chapter 6

Ambipolar Discotic Rylene Dye OFETs

6.1 Introduction

Ambipolar organic field-effect transistors (FETs) are of special interest due to their application for instance as light emitting field-effect transistors (LFETs) [1]. LFETs are particularly interesting for applications in displays where in conventional silicon technology each pixel consists of a transistor that switches a light emitting unit to generate an image on the screen. An LFET can both switch and emit light in one device, rendering them attractive for new generation displays. This light emission is possible due to the radiative recombination taking place in the transistor channel when both electrons and holes meet each other which happens since in an ambipolar transistor both charge carrier types can be injected into and transported through the channel. The intensity and position of recombination and hence light emission can be controlled by the applied V_G and V_{SD} biases. Aside from this potential application, ambipolar OFETs are appealing for the study of fundamental charge transport mechanisms in organic semiconductors. This point will be discussed in more detail during the cause of this chapter in which we illustrate how morphology

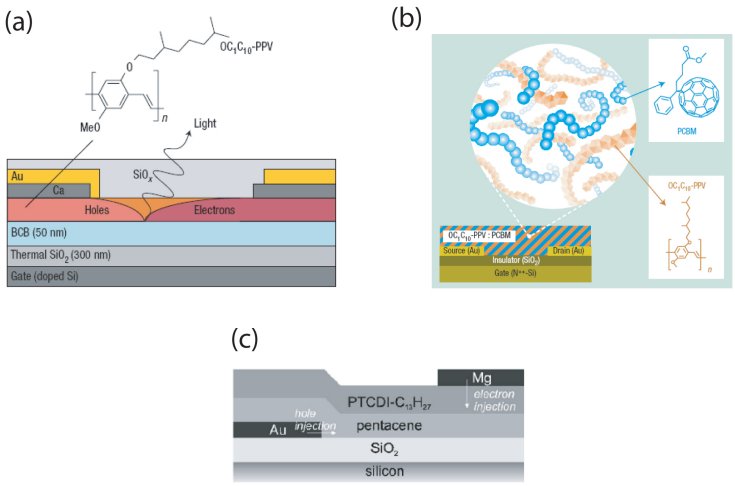

Figure 6.1: a.) Top-contact, light emitting ambipolar transistor using both calcium and gold electrodes for electron and hole injection respectively [2]. b.) Bottom contact ambipolar OFET consisting of a blend of electron transporting PCBM and hole transporting OC_1C_{10}-PPV polymer [6]. c.) Heterostructure ambipolar transistor consisting of stacked vacuum sublimed layers of p-type pentacene and n-type PDI-C13 [7].

again influences the operation mode of OFETs.

So far in this work OFETs have been described that either only carry holes or electrons. In inorganic semiconductors like silicon, both charge carriers should flow inherently in the material. Only doping of the semiconductor induces an excess of electrons or holes, making the material either electron conductive (n-type) or hole conductive (p-type). Likely, organic semiconductors should tranport intrinsically both charge carriers as well [3][6]. A small number of organic materials have shown to exhibit ambipolar behavior. It is commonly believed that organic semiconductors are generally both hole and electron conductors, and their mostly unipolar behavior is caused mainly by a too high charge injection barrier resulting from a drastic mismatch of the HOMO and LUMO energy levels with the source and drain electrodes' workfunction [4][5].

This latter hurdle in realizing ambipolar transistors can be overcome by the introduction of two different electrodes each facilitating electron and hole injection. Exactly this idea has been followed by using one hole and one electron injecting electrode as the source and drain contacts respectively, in this way enabling the

injection of both charge carriers into the polymer OC_1C_{10}-PPV (Figure 6.1a) [2] which is a well known material for solution processed organic light emitting diodes. As a result, light emitting ambipolar transistors were realized. However, fabrication of such devices with non identical source and drain contacts is an experimental challenge because of the requirement for the relative offset of the different metals during the electrode evaporation process. Another more convenient method would be to use a combination of donor and acceptor materials, either by employing a heterostructure (Figure 6.1c) [7]-[9] or by blending (Figure 6.1b) [10]. Transistor fabrication is easier in terms of the possibility of using just one type of electrode, since the proper choice of the donor and acceptor species allows the lowering of charge injection barrier by the suitable match up of the energy levels with the electrode's work function. The employment of a bilayer is most straightforward for achieving ambipolar performance. A thin film of a compound which is well known to exhibit good n-type transport is simply deposited on top of another material that notoriously shows high p-type action or vice versa (Figure 6.1c). However, charge transport in this kind of heterostructure critically depends on the interface between the two layers at which charges flow. Thus, bilayer deposition is straightforward only when vacuum deposited. Solution processed heterostructures face the obstacle of being partly or even completely dissolved if non orthogonal solvents are used for the successive deposition of the films [11]. Blended interpenetrating networks on the other hand introduce in general poor molecular order, resulting in low charge carrier mobilities [6]. The most attractive ambipolar transistors in terms of fabrication and performance should consist of a single layer that can be simply solution processed from a low bandgap material which allows electron and hole injection from one single type of electrode. Charge injection is realized for low bandgap materials if source and drain electrodes are employed whose workfunction is situated within the bandgap. In this way, the injection barriers can be lowered by the appplication of gate and source/drain biases V_G and V_{SD} as described in the previous chapter 4.2.

6.2 Ambipolar Swallow-tailed Quaterrylene-tetracarboxdiimide OFETs

It has been shown for rylene dyes that by extending the aromatic core by additional naphtalene units, the LUMO energy levels remain essentially unchanged but the HOMO energy levels decrease [17]. That is, the bandgap of PDI is larger than TDI which is in turn again larger than QDI. Hence, there is a possibility that both electrons and holes can be injected into QDI layers, thus enabling the fabrication of ambipolar OFETs. This result provides a tool for tailoring low bandgap n-type organic semiconductors like the SWQDI (Figure 6.2a). In addition, the introduction of swallow-tailed alkyl chains (Figure 6.2a) provides high solubility to this material (SWQDI was synthesized by Fabian Nolde and Dr. Zhihong Liu at the Max-Planck Institute for Polymer Research in Mainz). These combined advantages of bandgap modification and excellent solubility make this dye a promising candidate for solution processed, single compound ambipolar field-effect transistors. However, the introduction of these swallow-tails also promotes self-assembly into discotic columnar superstructures [18] which has been shown in the case of SWPDI and SWTDI to inhibit charge carrier transport. Nevertheless, improved device performance in the more extended core of SWTDI in comparison to the shorter SWPDI was observed due to the larger crystalline domains. Therefore, the even more elongated SWQDI core might evoke further enhanced intermolecular $\pi - \pi$ interaction, yielding larger crystalline domains and thus possibly higher charge carrier mobilities.

In this aspect, bottom gold contact, bottom gate field-effect transistors were fabricated by drop-casting a 10mg ml^{-1} SWQDI 1,2-dichlorobenzene solution on HMDS treated SiO_2 substrates. FET performances after solvent evaporation and

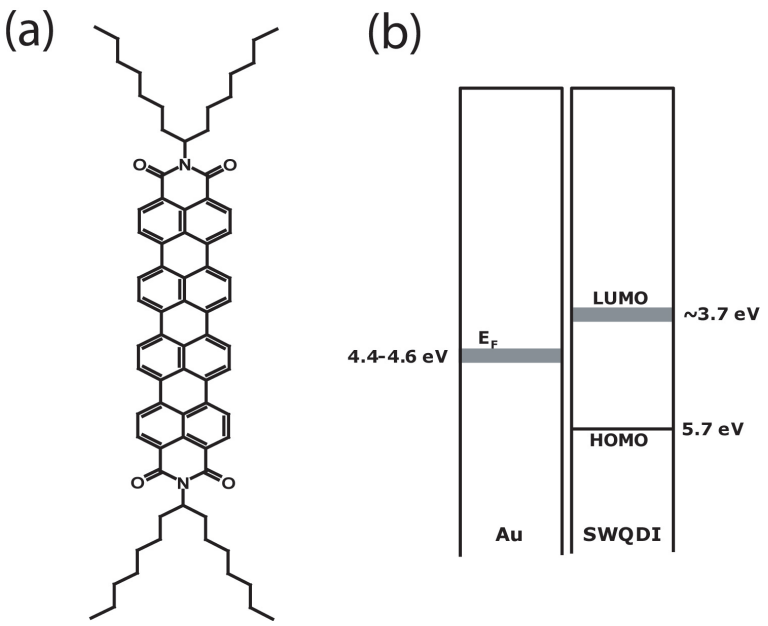

Figure 6.2: a.) Chemical structure and b.) HOMO LUMO energy levels of SWQDI.

film formation are depicted in Figure 6.3. The output curves biased both in the electron (right half of Figure 6.3a for positive V_G and V_{SD}) and hole regimes (left half of Figure 6.3a for negative V_G and V_{SD}) showed an increase in source and drain current I_{SD} at low gate voltages (Figure 6.3a). This behavior cannot be observed in unipolar devices (OFETs that transport either electrons or holes but not both).

Apparently, ambipolar transistors operate differently than unipolar ones. As mentioned before, in unipolar transistors only one type of charge carrier can flow

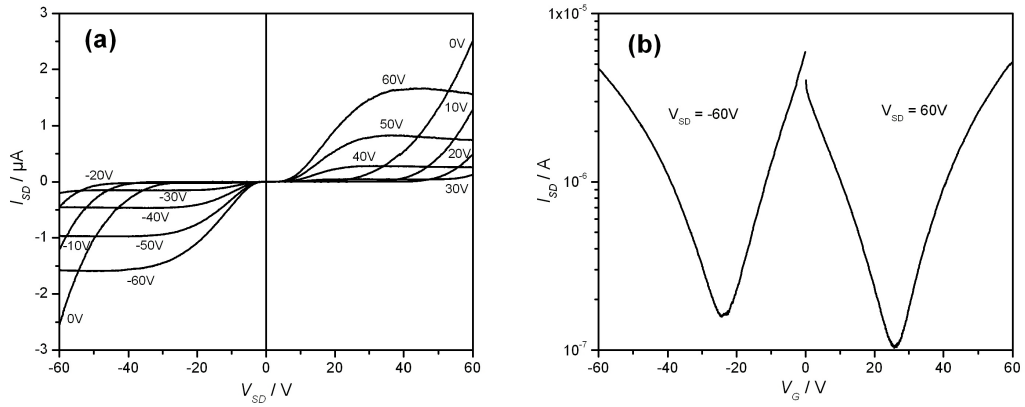

Figure 6.3: a.) Output and b.) transfer characteristics of ambipolar SWQDI OFETs.

(Figure 6.4a) whereas in ambipolar ones, both types can contribute to the current at the same time (Figure 6.4b) [12]. This does not mean that this state is always present in the device but rather depends on how the transistor is biased. At certain applied V_G and V_{SD}, ambipolar transistors can turn into unipolar ones. This takes place when $|V_G| \geq |V_{SD}|$. In this case, more and more majority carriers (for negative voltage biases, they consist of holes and the electrons are the minority carriers, whereas for positive biases, electrons are present in majority and holes in minority) are being accumulated by the increasing gate voltage, leading those majority charges to take over the current flow. This is the typical unipolar behavior and saturation was observed in the output curves (characteristics for V_G from 40V to 60V and from -30V to -60V in Figure 6.3a). For $|V_G| < |V_{SD}|$ on the other hand, a unipolar transistor would be in saturation and a depletion layer will form at the drain electrode. In an ambipolar device however the depletion layer is replaced by the injection of the minority carriers. In this way, both carrier types are present in the semiconductor layer at the same time since both carriers can be injected from the source and drain electrodes due to the favorable energy level alignment. As a consequence, an electron and a hole channel form, similar to a diode or a pn-junction. That is why with increasing V_{SD}, the current increases in the output curves as is also typical for diodes. This ambipolar regime ($|V_G| < |V_{SD}|$) was reached in the SWQDI OFETs at V_G from 0V to 30V in the electron and from 0V to -20V in the hole regime (Figure 6.3a).

Similar to the output curves, an ambipolar regime is expressed in the transfer curves as well. As is evident from the transfer characteristics of SWQDI (Figure 6.3b), at some applied non zero V_{SD}, the current I_{SD} does not simply increase with increasing gate bias V_G as is typical for unipolar operation. Instead, V-shaped curves are observed for which at low gate biases, I_{SD} drops with stronger V_G to a minimum. From this point, the current rises again with larger V_G. For instance, taking the left curve (the hole regime since negative V_G and V_{SD} are applied) of

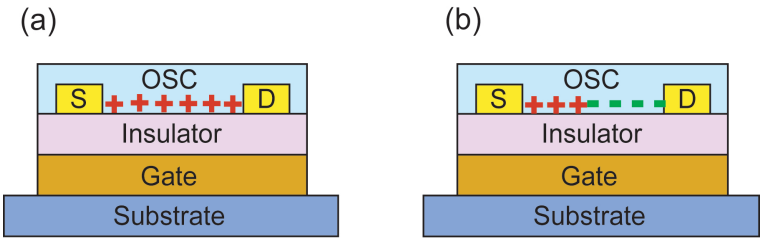

Figure 6.4: a.) Unipolar p-type operation and b.) ambipolar OFET operation with both holes (red) and electrons (green) accumulated in the transistor channel.

(Figure 6.3b), starting from zero gate bias, the current drops to a minimum with ongoing V_G. This branch of the transfer curve depicts the ambipolar regime and is generated by the minority carriers, in this case by electrons. As V_G grows, more majority carriers (here holes) are being accumulated, causing an increase in current again. This is the typical unipolar regime as already discussed for the output curves. The saturated electron and hole mobility extracted from the transfer curves (Figure 6.3b) were $\mu^e_{sat} = 1.5{\times}10^{-3} cm^2V^{-1}s^{-1}$ and $\mu^h_{sat} = 1.0{\times}10^{-3} cm^2V^{-1}s^{-1}$, respectively. Both mobilities were similar and comparable, suggesting sufficient injection from the gold electrodes of both types of charge carriers and a good transport for both of them through the SWQDI layer as well. Overall, these SWQDI transistors exhibited clean ambipolar device performance.

There are only a few single component ambipolar transistors reported so far. Four of them are illustrated in Figure 6.5. Hereby, oligothiophene/fullerene dyad (16T-2C60) and bis(4-di-methylaminodithiobenzyl)nickel (Nickel Dithiolene) whose chemical structures are illustrated in Figures 6.5a and b respectively have been applied from solution in bottom gold contact OFETs, the same device configuration as in the case of SWQDI. For 16T-2C60, ambipolar transistor action was observed with a hole mobility of $\mu^h_{sat} = 1.1{\times}10^{-5} cm^2V^{-1}s^{-1}$ and an electron mobility of $\mu^e_{sat} = 4.3{\times}10^{-5} cm^2V^{-1}s^{-1}$ [13], around two orders of magnitude lower than for the SWQDI devices. Ambipolar OFETs based on nickel dithiolene on the other hand exhibited higher hole and electron mobilities both in the order of $10^{-4} cm^2V^{-1}s^{-1}$

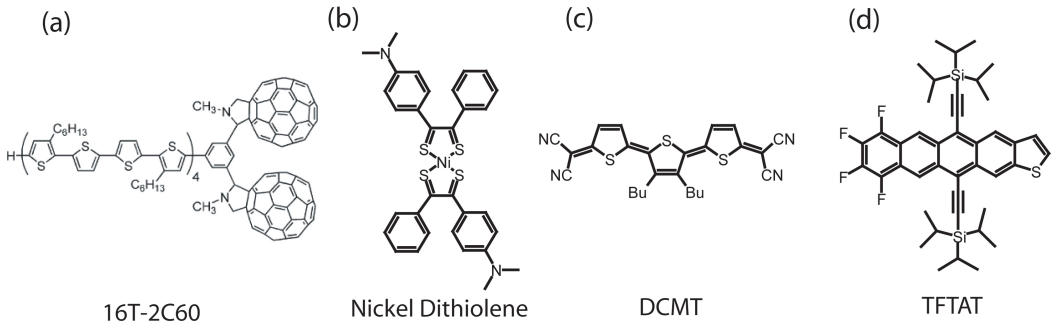

Figure 6.5: a.) b.) Solution processed and c.) d.) vacuum sublimed organic semiconductors applied in single layer ambipolar OFETs.

[16], about one order of magnitude inferior to the SWQDI case. Therefore, for solution processed, bottom gold contact ambipolar transistors, the rylene dye SWQDI shows the highest device performance up to date.

Vacuum sublimed single layer ambipolar OFETs have also been demonstrated for example for 3′,4′-dibutyl-5,5″-bis(dicyanomethylene)-5,5″-dihydro-2,2′:5′,2″-terthiophene (DCMT, Figure 6.5c) whose films resulted in both hole and electron mobilities less than $10^{-4} cm^2 V^{-1} s^{-1}$ [14]. Again, the SWQDI OFETs yield more pronounced performance. The best ambipolar transistor up to date consists of vacuum sublimed single layer 7,8,9,10-tetrafluoro-5,12-bis(TIPSethynyl)tetraceno[2,3-*b*]thiophene (TFTAT, Figure 6.5d) with electron and hole mobilities up to $0.37 cm^2 V^{-1} s^{-1}$ and $0.065 cm^2 V^{-1} s^{-1}$ respectively [15]. All four compounds depicted in Figure 6.5 were chemically engineered to become low bandgap semiconductors in order to allow efficient hole and electron injection into the HOMO and LUMO levels respectively from gold electrodes. For instance, TFTAT contains electron withdrawing fluoro groups on the tetraceno[2,3-*b*]thiophene donor, yielding a low bandgap of 1.82 eV.

However, when thermally annealing the SWQDI film at 100°C for 1 hour, hole transport vanished and only electron transport could be observed. This is evident from the lack of the ambipolar regime expressed by the drastic increase of I_{SD} at low gate voltages in the output curves (Figure 6.6a). Furthermore, the transfer

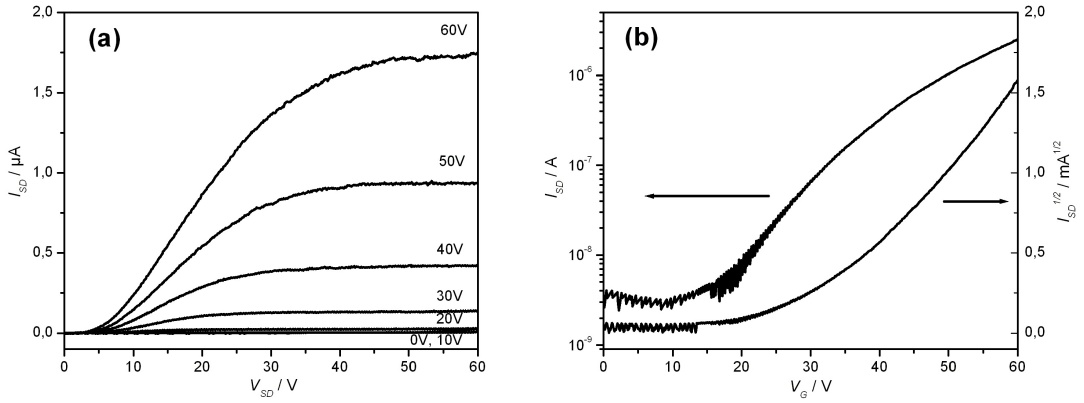

Figure 6.6: a.) Output and b.) transfer characteristics of annealed SWQDI OFETs.

characteristic showed no V-shape (Figure 6.6b) as is typical for the ambipolar state [19] and revealed a ten times lower electron mobility of $\mu^e_{sat} = 2{\times}10^{-4} cm^2 V^{-1} s^{-1}$. Up to now, this is the first time ever that such a thermally induced extinction of hole transport in ambipolar field-effect transistors has been demonstrated.

As was presented in the case of the amorphous CDT-BTZ donor acceptor copolymer, thermal annealing has the effect of extracting the residual solvent traces encapsulated within the organic film after solvent evaporation. Thus, it is possible that the not completely dried film in some way promoted ambipolar behavior and a dried film after annealing resulted in a loss of hole transport. In order to examine this aspect, the same SWQDI OFET was kept in nitrogen atmosphere for two months. This is a long enough period of time in which the solvent traces must have completely evaporated, leaving behind a dried film. This drying method without thermal influence ensures that no other thermally activated effects like change in molecular packing or phase transitions mask the true solvent induced device performance. Figure 6.7 highlights the transistor performance after two months of drying. As is evident from these curves, typical ambipolar behavior was still being observed after such a long storage time. The extracted electron and hole mobilities were μ^e_{sat} $= 5 \times 10^{-4} cm^2 V^{-1} s^{-1}$ and $\mu^h_{sat} = 5.3 \times 10^{-4} cm^2 V^{-1} s^{-1}$ respectively. From these results it was concluded that solvent traces within the film have no effect on the

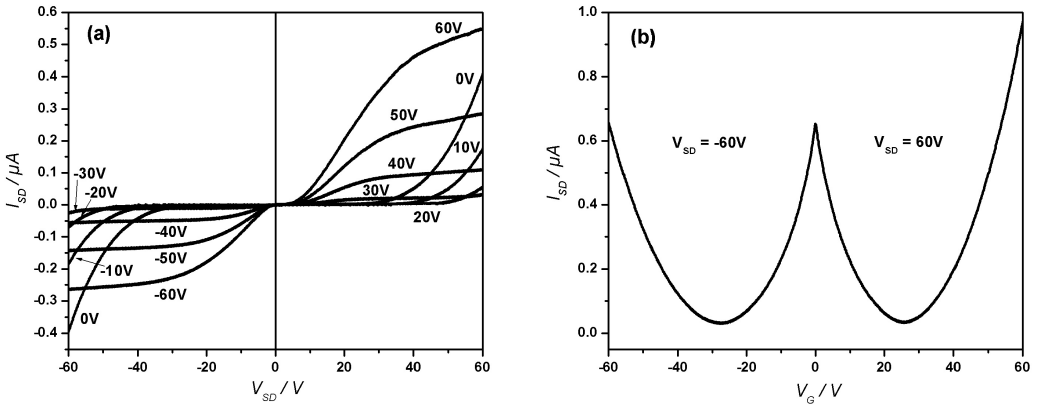

Figure 6.7: a.) Output curves for various gate biases V_G and b.) transfer characteristics at $V_{SD} = \pm 60V$ of SWQDI OFETs dried in nitrogen atmosphere for two months.

ambipolar or unipolar behavior of these SWQDI OFETs. The slight decrease of the mobilities by a factor of two as compared to the fresh new sample can be caused by air and moisture traces that has accumulated during this long time as well as light exposure caused by the regularly turning on and off of the light in the glove box by different users. As a further evidence, freshly drop-cast SWQDI OFETs were dried in vacuum at a pressure of 9×10^{-7} mbar for 12 hours. No loss of ambipolar operation could be detected, stressing that 1,2-dichlorobenzene traces within the SWQDI layer have no influence on ambipolar or unipolar transistor behavior.

6.2.1 The Role of Charge Injection

A possible explanation for the absence of hole transport might be a change of the material's electronic structure, i.e. band formation as well as a shift of the HOMO level after thermal treatment with the consequence of building up an injection barrier for holes. Typically, in a perfectly ordered crystal, the HOMO energy level can be thought of as bandlike. This band is made out of the consecutive HOMO level splitting from one single molecule towards a highly arranged assembly of molecules. That is, the periodic packing of the molecules generate the energy band. In organic polycrystalline films however the molecular order is generally not as high as in a

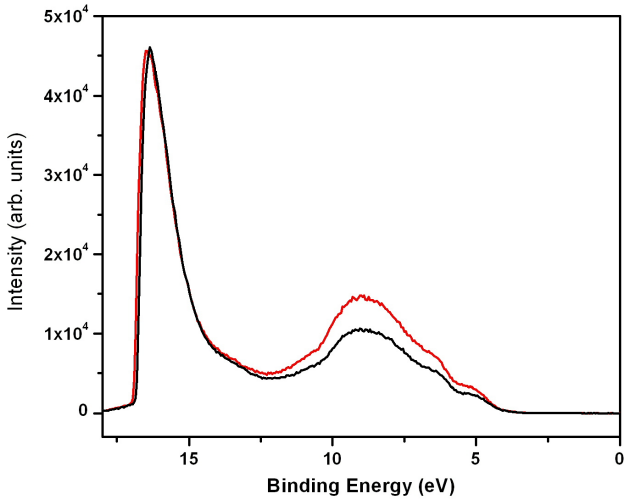

Figure 6.8: UPS spectra of drop-cast SWQDI film before (black curve) and after (red curve) annealing.

perfect crystal. The consequence is the division of the energy band into several more narrow discrete bands. In such a case, the HOMO energy level of the film changes. Conversely, an improved molecular arrangement can also lead to energy band broadening with the effect of shifting the HOMO. For some organic semiconductor layers, the molecular packing can be improved by thermal annealing. Thus, it is possible that annealing of the SWQDI film triggered a change in morphology and hence altered the HOMO level, leading to a more distinct hole injection barrier. Detailed ultraviolet photoemission spectroscopy (UPS) studies of drop-cast SWQDI films on gold were carried out by Dr. Wojciech Osikowicz in Sweden to verify these possibilities. UPS is a tool for probing the binding energy of electrons within a solid state film. Roughly speeking, the principle lying behind this method is the following: The sample, in our case the drop-cast SWQDI layer, is exposed to ultraviolet radiation. Those photons are energetic enough to release the electrons in the film. Those liberated unbound electrons travel with a certain kinetic energy away from the film. A detector measures their kinetic energies from which the electron binding energy within the layer can be deduced. In this way, a UPS spectrum was recorded as shown in Figure 6.8.

Obviously, no evidence for annealing related modifications of the SWQDI electronic structure was found. The UPS spectra prior to and after annealing in N_2 atmosphere were essentially identical. Specifically, the hole injection barrier, defined as the energy difference between the semiconductor's HOMO and Au Fermi level at zero binding energy, remained unchanged, along with the interface energetics which follows vacuum level alignment (Schottky-Mott limit), i.e. no organic/gold interfacial dipole was observed. This can be readily appreciated from the following considerations. The ionization potential of 5.7 eV was directly estimated from the HOMO onset of UPS spectra, whereas the electron affinity of approximately 3.7 eV was derived based on the SWQDI optical band gap and the estimated exciton binding energy of 0.6 eV [20]. The work function of air-handled Au at 4.4-4.6 eV [21] falls therefore close to the middle of the SWQDI band gap (Figure 6.2b). Thus, for passivated interfaces, no spontaneous charge transfer across the interface took place and the vacuum level alignment regime correctly describes interface energetics [22][23]. Hence, barrier heights for charge injection can be estimated as 0.7-0.9 eV for electrons and 1.1-1.3 eV for holes irrespective of applied post treatment. The UPS results clearly show that annealing does not change the electronic structure of SWQDI nor hole injection barriers at the SWQDI/Au interface, and therefore can be safely excluded as the cause for quenching of hole transport in annealed FETs.

6.2.2 The Role of Interface Charge Trapping

Since the transistor channel directly forms at the organic semiconductor/insulator interface, trapping sites on the dielectric surface can inhibit charge transport, in this way limiting OFET performance. It has been demonstrated that organic polymers that usually show hole transport only can be turned to exhibit solely electron transport with the application of a specific crosslinked polymer dielectric divinyltetramethyldisiloxane-bis(benzocyclobutene) (BCB) (Figure 6.12b) [3]. This

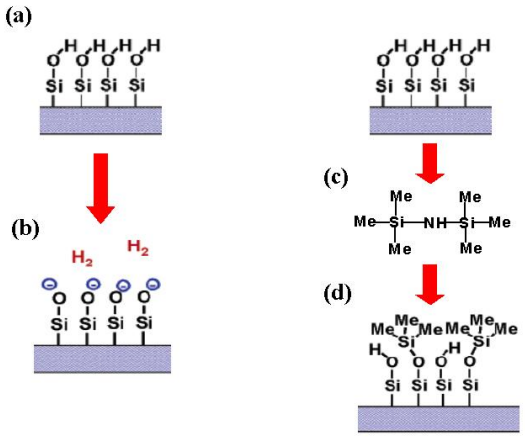

Figure 6.9: a.)Polar OH groups on SiO_2 surface. b.) Electron trapping on these OH groups. c.) Self-assembled monolayer HMDS. d.) Trimethylsilyl monolayer on SiO_2 surface after application of HMDS.

is possible since in general all organic semicondcutors are both hole and electron transporters but the SiO_2 contains polar OH terminated groups which trap electrons, rendering them completely immobile and hence causing the often observed hole transport only (Figure 6.9a,b). The BCB dielectric however effectively eliminates those polar groups, enabling electron behavior in certain organic semiconductors with calcium electrodes as good electron injecting source and drain contacts. In some organic semiconductors even ambipolar operation was observed using the same BCB layer. In this aspect, it is hence also possible that the holes in the SWQDI film after annealing got completely trapped at the semiconductor dielectric interface due to some unknown thermally induced change in the nature of the dielectric surface. However, this point can be safely excluded since the SiO_2 was treated with HMDS (Figure 6.9c) which is well known to enhance hole transport but not to specifically immobilize this type of charge carrier (Figure 6.9d)[24][25]. Also, HMDS is covalently bound to the SiO_2 surface, making it very unlikely that the methyl groups on this surface get broken by treatment at 100°C for 1h.

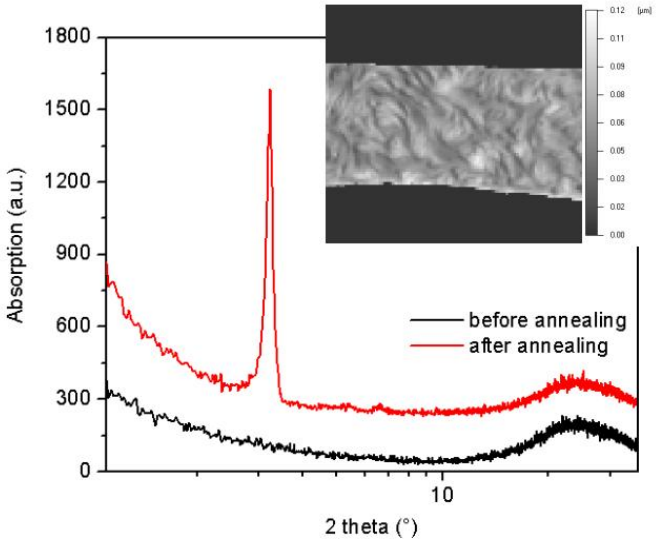

Figure 6.10: XRD of drop-cast SWQDI film before (black curve) and after (red curve) annealing. Inset: NanoFocus image of the same SWQDI film.

6.2.3 The Role of Molecular Packing

Another possible reason for the switching from ambipolar to unipolar characteristics is a thermally induced change in film morphology and connected to this an increase of trapping sites responsible for the extinction of hole conduction and the observed reduction of electron mobility. Therefore, structural analysis of drop-cast SWQDI films was performed by X-ray diffraction (XRD), leading to the surprising result that no macroscopic order in as cast films could be detected, as revealed by the lack of any diffraction peaks. However, after thermally annealing the same layers at 100°C for 1 hour, the supramolecular order improved, as can be deduced from the appearance of the intensive and sharp diffraction peak (Figure 6.10), indicating an edge-on orientation of the disc-shaped molecules with randomly in-plane arranged columnar structures.

Based on these results, apparently disorder favored the occurrence of both electron and hole current, whereas better ordering suppressed hole transport. Even though ambipolarity in disordered systems has been reported before [12], this is the first time that a discotic material without macroscopic alignment displayed an

ambipolar state, with relatively high electron and hole mobilites for solution processed and non-annealed organic semiconductors apart from fullerene derivatives [26]. Generally, in discotic columnar structures, charge transport takes place along the column axis, providing one-dimensional pathways only and hence making efficient charge transfer very prone to structural defects within the columns. On the other hand, charge carrier transport in a discotic, disordered, or even amorphous layer, as schematically presented in Figure 6.11a, does not suffer from such dimensional confinement, resulting in the occurrence of ambipolar behavior since no type of charge carrier flow is favored. This equivalence of both electron and hole transport is mirrored by the similar mobilities for both n- and p-type regimes. Such disordered ambipolar systems are attractive since they lend themselves particularly well to cheap, easy, fast, and large area commercial OFETs printing processes where molecular alignment is in most cases difficult to control.

To account for the loss of hole transport caused by the improved ordering after annealing, the Nanofocus technique has been applied to study the change in morphology on the film surface (inset Figure 6.10). However, no topographic variation could be recorded prior to and after annealing. This is expected due to the fact that the annealing procedure was performed below the liquid crystalline phase transition. Thus, the enhanced arrangement must have occurred not on the film surface but at the semiconductor/dielectric interface and the bulk itself, since the change in X-ray diffraction measurements mirrors the ordering within the entire film.

It is assumed that heating the devices triggered the formation of ordered columnar structures, leading to local well-organized domains within the SWQDI layer, as schematically illustrated in Figure 6.11b. The emergence of such a polycrystalline-like structure went hand in hand with the formation of local macroscopic domain boundaries. The dramatic decrease of hole mobility is attributed to charge carrier trapping at those boundaries [27]-[32]. This lowering of hole transport might be further reinforced by the appearance of one-dimensional columns, which are consid-

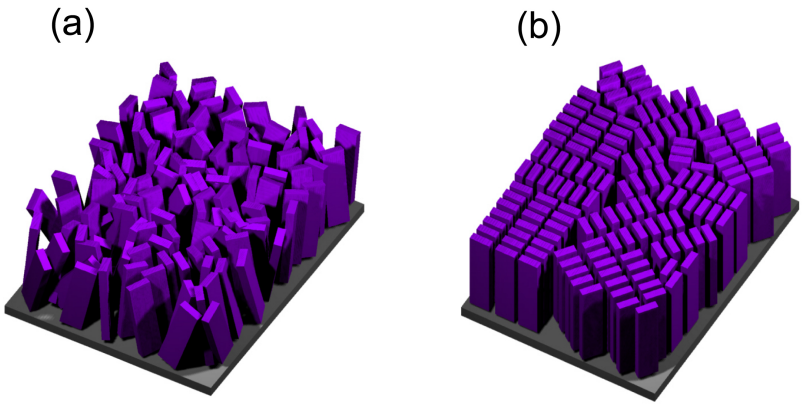

Figure 6.11: a.) Schematic representation of disordered and b.) annealed SWQDI film containing domains with columnar arrangements separated by grain boundaries.

ered to be particularly sensitive to structural defects, ultimately causing the loss of p-type behavior. These limiting factors are expected to equally affect electron current. However, since SWQDI has a strong affinity for electrons, the latter were able to diffuse through the macro- and microscopic defects within the columns, resulting in the observed ten times decrease of electron mobility but not in the entire absence of n-type performance. In fact, theoretical calculations and temperature dependent measurements on OFETs based on amorphous organic semiconductor layers have elucidated that some disordered molecular systems can pose shallow traps for charge carriers, in this way enabling efficient charge transport via thermally activated hopping out of those shallow traps [33]-[35]. This point is a further possible explanation for the presence of ambipolar behavior in the disordered SWQDI system but not in the more ordered case where confined columnar one-dimensional charge transport paired with deep grain boundary traps triggered the loss of the minority hole carriers.

No such phenomenon has been reported so far in discotic systems. In fact, this SWQDI is the first discotic exhibiting ambipolar transport. However, a similar morphology dependent transistor operation mode was observed by Singh and coworkers. In their case, the active device layer consisted of a blend of three organic semiconductors, namely methanofullerene [6,6]-phenyl C_{61}-butyric acid methyl ester (PCBM)

and two polymers poly[2-methoxy-5-(3,7-dimethyloctyloxy)]-1,4-phenylenevinylene (MDMO-PPV) and poly-(9,9-dioctylfluorenyl-2,7-diyl) end capped with N,N-bis(4-methylphenyl)-4-aniline (PF) as illustrated in Figure 6.12a. Hereby, three different polymer dielectrics, polyvinyl alcohol (PVA), poly(4-vinyl phenol) (PVP), and divinyltetramethyldisiloxane-bis(benzocyclobutane) (BCB, Figure 6.12b) were utilized in a bottom gate, top-contact OFET configuration using gold as source and drain electrodes. The blend was spin-coated on each of these dielectrics to fabricate the transistors. Interestingly, electron transport only was measured in the devices containing PVA as the insulator, whereas for PVP and BCB, ambipolar behavior was present [10]. A hole injection barrier from the gold electrodes into the blend was excluded as a possible reason for the absence of ambipolar action in PVA based devices due to the fact that for the other PVP and BCB ambipolar transistors, gold was also used as injecting contacts. Another obvious explanation is charge trapping at the different insulators used. For BCB, it is known that electron transport can be enhanced due to the absence of polar groups at the BCB interface, in this way minimizing electron trapping and hence elimination of n-type behavior [3]. On the other hand, both PVA and PVP contain polar OH groups which effectively trap charge carriers. The authors made no indication on the possibility of interface trapping. Instead, they observed phase separation in films on PVA, whereas no such phenomenon occurred on PVP and BCB. On PVA, the blend formed nanocrystalline films with domain sizes of about 200 nm on average. In these layers, grain boundaries were evident as AFM images clearly illustrated. However, on PVP and BCB, no phase separated domains occurred, resulting in a more amorphous like film morphology [10]. Similar to the SWQDI case, such amorphous layers also yield ambipolar behavior which is explained by the simultaneous electron transport through the n-type PCBM and hole transport via the two polymers MDMO-PPV and PF. Nevertheless, the authors did not take into account grain boundaries as possible origin for the absence of hole transfer in the crystalline phase separated blend layer

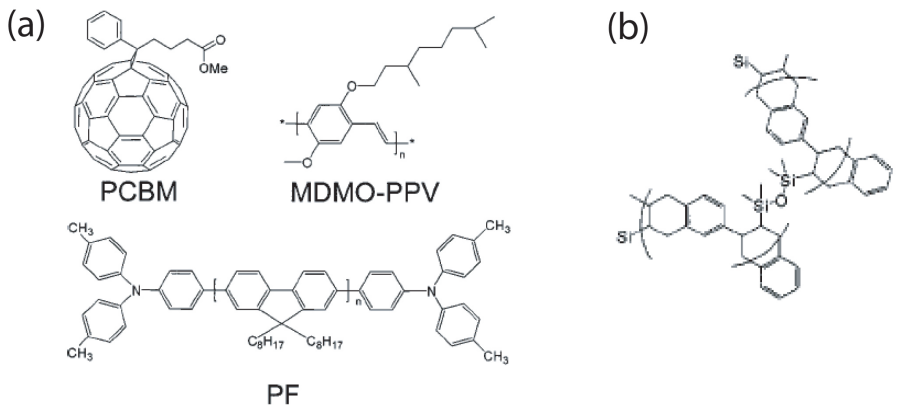

Figure 6.12: a.) Chemical structures of PCBM, MDMO-PPV, and PF. b.) Chemical structure of corsslinkable polymer dielectric BCB.

on PVA. Still, their work is further evidence for the significance of morphology on charge carrier transport, even though their results are not as clear as the SWQDI system. For instance, why the crystalline phase separated blend on PVA gave only electron behavior even though p-type polymers possibly exhibiting hole transport were present as well in the blend could not be explained by the authors. Also, intrinsic charge transport phenomena in relation to film morphology is best illustrated in single component systems like SWQDI and not in blends where the contribution of each compound cannot be clearly and unanominously deduced.

As an additional proof for this morphology generated ambi- to unipolar behavior, disorder in the SWQDI film was re-established by vapor annealing the previously heated transistors that exhibited electron transport only. The vapor of the solvent in which the compound was dissolved has been shown to alter film morphology of the material, i.e. enhancement of the crystalline domains [36]. Vapor annealing was accomplished by placing the sample in a petri dish filled with 1,2-dichlorobenzene reservoir. Closing the petri dish and heating the solution to 150°C caused the SWQDI film to turn into a liquid after about 20 seconds in the solvent atmosphere. Then, the petri dish was opened to let the drop evaporate again, in this way forming a new SWQDI film. This procedure is akin to drop-casting without adding new solvent drops to the solid film in order to

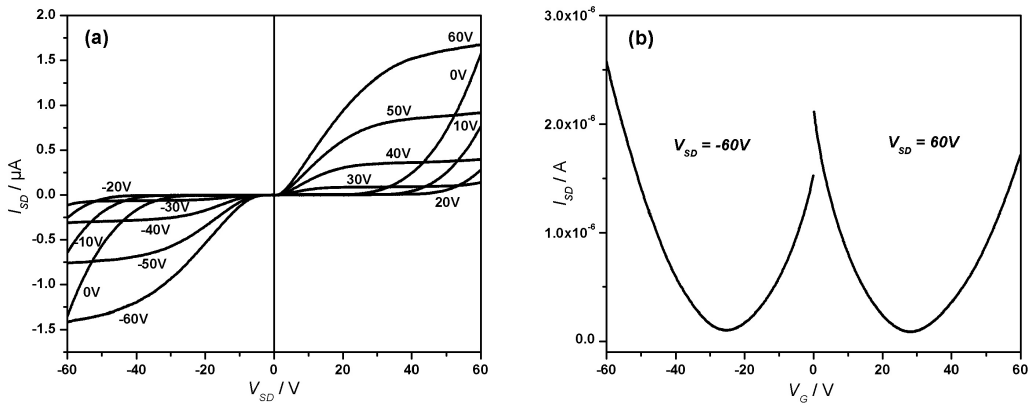

Figure 6.13: a.) Output and b.) transfer characteristics of vapor annealed SWQDI OFETs.

liquify it again. Interestingly, the transistors could be switched back from unipolar n-type to ambipolar behavior (Figure 6.13) by vapour annealing the thermally treated SWQDI layer to its liquid phase, followed by film formation after solvent evaporation. In this way, structural disorder was again induced, leading to electron and hole mobilities of $\mu^e_{sat} = 4{\times}10^{-4} cm^2 V^{-1} s^{-1}$ and $\mu^h_{sat} = 6{\times}10^{-4} cm^2 V^{-1} s^{-1}$, respectively. This decrease of charge carrier mobility compared to the initial values was most probably caused by degradation of the SWQDI film after several repetitive FET measurements and annealing steps.

Since ambipolar behavior of this discotic dye system is strongly dependent on film morphology, additional experiments concerning this point were conducted. As a way to influence molecular order, various solvents with different boiling points were used since solvents with low boiling points promote fast film formation due to quick evaporation. Thus, the molecules are not given a lot of time to self-assemble, probably leading to disordered films. On the other hand, high boiling point solvents evaporate slower, allowing enough time for self-assembly and thus higher order [37]. This point can of course not be applied to all organic materials but is particularly relevant for molecules that have a strong tendency to pack into crystalline structures. With this in mind, a high boiling point solvent, namely 1,2,4-trichlorobenzene

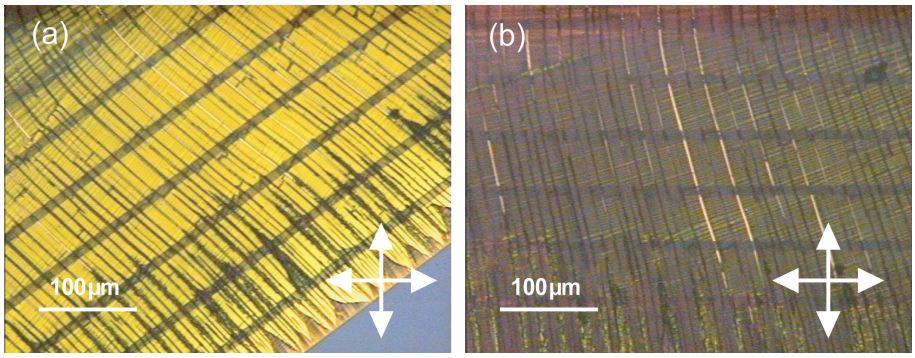

Figure 6.14: a.) POM of drop-cast SWQDI film from 1,2,4-trichlorobenzene and b.) optical anisotropy of the same film indicating directional molecular alignment.

(boiling point at 212°C compared to 180°C for 1,2-dichlorobenzene) was used to dissolve 10 mg ml^{-1} SWQDI and drop-cast on HMDS modified bottom gate, bottom contact transistor substrates in nitrogen atmosphere.

The resulting film is illustrated by the POM image in Figure 6.14, showing a crystalline film with directional order as deduced from the optical anisotropy (Figure 6.14b). The molecules form crystalline stripes that are directed along the evaporation direction of the drop. These crystal stripes were several hundreds of micrometers long and were found at the edges of the drop where nucleation sites appeared from which crystallization started to grow into the center of the drop. In the center of the drop, those stripes dissappeared and only crystals with sizes of $10 - 20\mu$m were found. However, transistors were only measured in the region of the directionally ordered crystalline stripes.

OFET measurements of this film immediately after its formation resulted in no transistor performance. However, after thermally annealing the device at 100°C for 2h only electron transport could be observed with a low saturated electron mobility of $\mu^e_{sat} = 8{\times}10^{-5} cm^2 V^{-1} s^{-1}$. In order to investigate how film morphology could have possibly triggered this behavior, XRD was conducted on this film as depicted in Figure 6.16. Both POM and XRD were unchanged before and after the thermal annealing step. In the XRD, two peaks are evident, suggesting some structural order. Since this structural order does not seem to be affected by thermal treatment,

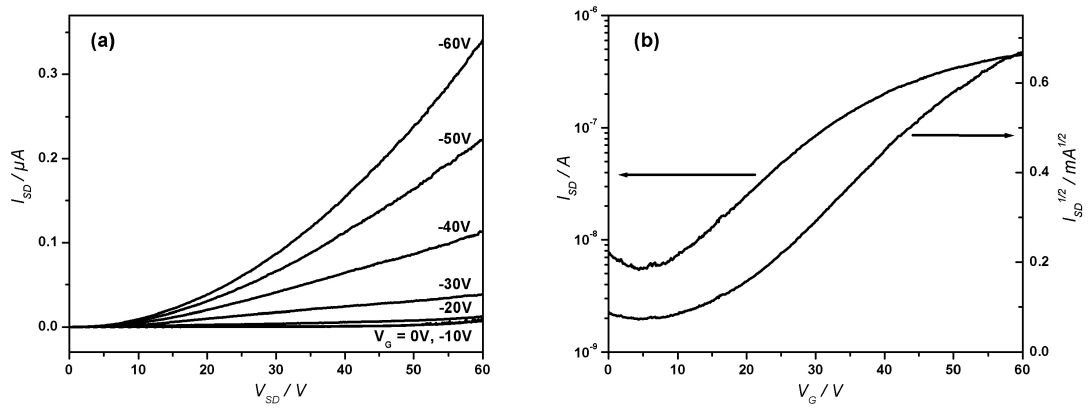

Figure 6.15: a.) Output and b.) transfer characteristics of annealed drop-cast SWQDI OFETs from 1,2,4-trichlorobenzene.

it is reasonable to assume that some solvent traces must have been present in the as prepared film, leading to significant trapping sites and hence no transistor performance even though both POM and XRD highlight an ordered organic layer. In fact, this assumption makes sence since 1,2,4-trichlorobenzene has a high boiling point and therefore solvent traces need more time to be completely extracted from the film. Annealing the film at 100°C for 2h promotes the drying process, consequently leading to the extinction of those solvent trapping sites and ultimately to transistor behavior. The measured low electron mobility can be attributed to the increased order of the film. Again, the SWQDI forms one-dimensional columns. Based on the better packing revealed from both POM and XRD, this one dimensional charge transport confinement is even more pronounced than in the previously described 1,2-dichlorobenzene case where no such distinct molecular order could be found. This aspect leads to a higher sensitivity to structural defects within a single colunm and hence to lower charge carrier mobility. In addition, an increased macromolecular arrangement into crystalline films also implies deeper domain boundaries which exhibit energetically deeper charge carrier traps, leading to a deterioration of electron mobility as well. This higher crystalline system is further evidence for the morphology controlled operation of the SWQDI transistors.

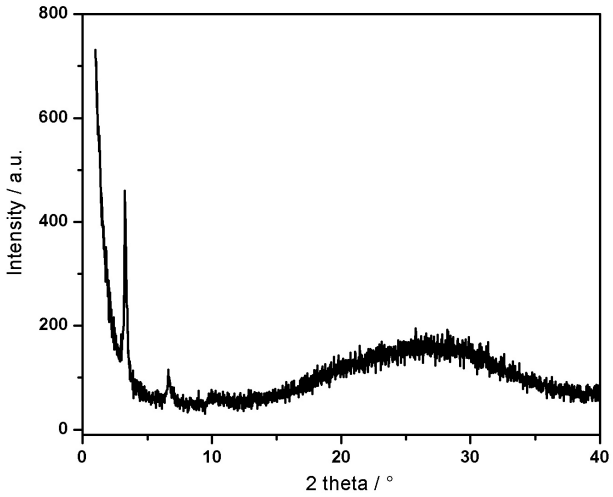

Figure 6.16: XRD of drop-cast SWQDI film from 1,2,4-trichlorobenzene.

Stricter one-dimensional confinement of the charge carriers and deeper trapping sites at the domain boundaries are not the only factors coming along with a higher degree of crystallinity that limit charge transport. As is evident from the non linear increase of the source drain current I_{SD} and the lack of saturation in the output curves as mirrored in Figure 6.15, there is a high contact resistance present. Based on the fact that electron transport was obtained after annealing, the mismatch of the LUMO of SWQDI and the workfunction of the gold source and drain contacts cannot be the reason for this contact resistance since obviously electrons can be injected from the gold metals into the LUMO. Instead, the peeling off of the rigid crystalline film from the electrodes is more realistically taking place, leading to charge injection into the SWQDI layer only from a small area of the gold electrodes, in this way increasing the contact resistance.

The extremely slow evaporation of the 1,2,4-trichlorobenzene drop lead to the formation of ordered film. In order to investigate the other extreme, chloroform was used. This solvent has a low boiling point and hence evaporation is fast, giving the SWQDI molecules not enough time to highly pack. Therefore, 10 mg ml^{-1} SWQDI chloroform solution was drop-cast on HMDS treated bottom gate, bottom contact

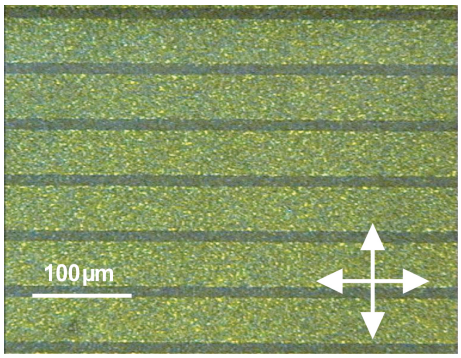

Figure 6.17: POM of drop-cast SWQDI film from chloroform.

transistor substrates as conducted for the other two aforementioned cases with 1,2-dichlorobenzene and 1,2,4-trichlorobenzene. The film obtained is highlighted by POM (Figure 6.17) showing no large directionally ordered layer since no optical anisotropy was present. Very small dot like spots were rather observed. This film morphology was independent of thermal treatment. Measurements of those chloroform fabricated transistors exhibited no device performance at all both before and after thermal annealing.

To study the reasons for this lack of transistor behavior, XRD of the chloroform fabricated thin film was carried out with the aim to understand how molecular order influences the absence of current flowing in the devices. The XRD depicted in Figure 6.18 illustrates one small peak, suggesting that the film is not amorphous but at the same time also lacks high order. It is believed that the small dot like domains contain partially ordered molecules and thus the film is expected to exhibit charge transport to an extend that a current should be existing in the transistors. However, as is evident from the POM image (Figure 6.17), those domains were rather small, leading to a higher number of domain boundaries which act as trapping sites. Even though some ordering was revealed by the XRD, exactly those numerous domain boundaries were again most probably responsible for severe charge trapping and ultimately for the loss of any transistor action.

SWQDI is an excellent example for the importance of molecular packing and film morphology on OFET behavior. This rylene dye was initially chosen for achiev-

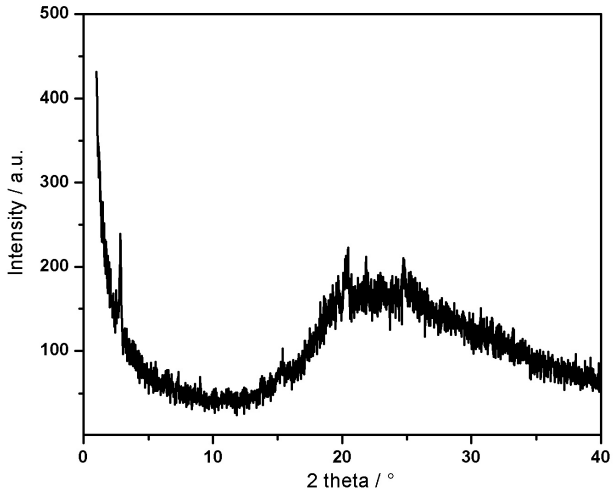

Figure 6.18: XRD of drop-cast SWQDI film from chloroform. No change after annealing was observed.

ing ambipolar transistors based on the low bandgap, in this way possibly enable injection of both holes and electrons into the organic semiconductor layer. However, as the results in this chapter reveal, the increase of the HOMO energy level in SWQDI compared to SWPDI and SWTDI was not the reason for the absence of ambipolar transistor action in the latter two dyes. It might be possible that those two compounds also exhibit ambipolarity if a highly disordered film akin to the one in SWQDI can be generated. Attemps to realize amorphous films of SWPDI and SWTDI failed after drop-casting and spin-coating those compounds from various organic solvents with different boiling points. Even though 2D-WAXS of extruded fibers of all three rylene dyes showed columnar self-assembly in the bulk, only SWQDI forms disordered thin films when solution cast, whereas the other two dyes kept their columnar structure in thin films. In addition, the tendency of SWQDI molecules to self-assemble into supramolecular order is lower than in the case of SWPDI and SWTDI as the amorphous SWQDI film from 1,2-dichlorobenzene shows. Also, a high boiling solvent 1,2,4-trichlorobenzene is needed in order to generate a macroscopically arranged film, revealing that the SWQDI molecules need more time to form macroscopically ordered structures. For SWPDI and SWTDI on

the other hand, large crystalline domains can easily be achieved with lower boiling solvents. Based on the observation in the previous chapter that a more extended rylene dye core triggers better intermolecular $\pi - \pi$ interaction and hence enhanced supramolecular arrangement, SWQDI negates this trend. No comparable morphology was present for drop-cast SWQDI from toluene on the same HMDS treated SiO_2 surface. The resulting film has a structure comparable to that obtained for chloroform processed layers (Figure 6.17). Therefore, these three swallow-tailed rylene dyes vividly emphasize the complexity in fabricating organic OFETs and how molecular order and film morphology sensitively dictate device behavior.

6.3 Summary

In conclusion, we have demonstrated solution processable ambipolar organic field-effect transistors based on a discotic dye. Such single component devices allow the study of the influence of supramolecular ordering on OFET charge transport properties. These transistors exhibited ambipolarity even without any structural order. Surprisingly, hole conduction was lost after thermal treatment. This absence of p-type behavior could not be explained by the increase of hole injection barrier or by interface trapping, both factors being believed to be solely responsible for the lack of ambipolar operation. It was rather observed that the change in morphology most probably lead to such a phenomenon. These findings suggest that besides charge injection barriers and interface trapping, structural composition, i.e. microscopic domain boundaries together with local defects in one-dimensional columnar systems, also trigger the loss of ambipolarity due to lowering of the minority charge carrier mobility. It is again stressed that this discotic dye SWQDI is the first system so far that highlights in such a direct and clear way the importance of molecular packing for the existance of the type of charge carrier transport (either electron or hole transport or both at the same time) present in an organic field-effect transistor. Furthermore, our experiments with various solvents inducing different film

morphologies elucidated how delicately charge transport in this SWQDI system was dependent on these morphologies. Counterintuitively, well packed crystalline films do not neccessarily lead to efficient charge transport and to high charge carrier mobility, at least not in this one-dimensional columnar system. On the other hand, highly disordered amorphous layers do not automatically imply poor charge transport due to insufficient overlap of neighboring molecular orbitals. Instead, in this case, shallow traps combined with two dimensional charge transport pathways seem to enable both the flow of electrons and holes. This result should help focusing on molecular packing and film morphology in the general investigation of ambipolar OFETs. Besides the problem of charge carrier injection, the trapping of electrons at the insulator surface has been shown by the pioneering work of Sirringhaus to prevent ambipolar behavior [3]. As easy as electrons can be totally trapped even though electron injection into the organic semiconductor was guaranteed, likewise, it can be expected that holes can also be entirely captured by grain boundaries or defect sites within the active layer itself. Therefore, in order to completely characterize ambipolar systems, at least three factors should be taken into consideration: Charge carrier injection, interface trapping, and finally charge carrier capture by grain boundaries or defects within the organic semicondutor layer. Nevertheless, the physics behind ambipolar transistors is still not completely understood. One good example for this aspect are OFETs based on DCMT (Figure 6.5c). For this material, it was found that only electron transport took place when vacuum deposited at substrate temperatures below 136°C, whereas films generated at higher temperatures exhibited ambipolar transistor action for the same source and drain electrodes and insulator surface treatment. The authors made no reference to injection barrier change. However, no contact resistance was observed for both n-type and ambipolar devices, highlighting the invariance of injection barriers that might have favored hole injection. Furthermore, the same interface, namely untreated SiO_2 renders a sudden promotion of hole transport improbable, excluding the role

of interface charge trapping. The authors conceded that the underlying morphology change that might have possibly lead to the observed emergence of ambipolar transport is not clear [14]. In this special case, something else, maybe yet not fully proven factor than morphology might influence the type of charge carrier being transported, making ambipolar transistors particularly interesting for fundamental research in charge transport phenomena in OFETs.

Based on this still incomplete picture of organic field effect transistors, there is no general recipe for fabricating ambipolar devices. Some puzzle pieces are still missing for a complete picture of ambipolar devices, making them particularly exciting for further investigations.

Bibliography

[1] M. Muccini, *Nat. Mater.* **2006**, *5*, 606.

[2] J. Zaumseil, R. H. Friend, H. Sirringhaus, *Nat. Mater.* **2005**, *5*, 69.

[3] L. L. Chua, J. Zaumseil, J.-F. Chang, E. C.-W. Ou, P. K.-H. Ho, H. Sirringhaus, R. H. Friend *Nature* **2005**, *434*, 194.

[4] E. C. P. Smits, S. Setayesh, T. D. Anthopoulos, M. Buechel, W. Nijssen, R. Coehoorn, P. W. M. Blom, B. De Boer, D. M. de Leeuw, *Adv. Mater.* **2007**, *19*, 734.

[5] M. Chikamatsu, T. Mikami, J. Chisaka, Y. Yoshida, R. Azumi, K. Yase, A. Shimizu, T. Kubo, Y. Morita, K. Nakasuji, *Appl. Phys. Lett.* **2007**, *91*, 043506.

[6] E. J. Meijer, D. M. de Leeuw, S. Setayesh, E. van Veenendaal, B.-H. Huisman, P. W. M. Blom, J. C. Hummelen, U. Scherf, T. M. Klapwijk, *Nat. Mater.* **2003**, *2*, 678.

[7] G. Paasch, Th. Lindner, C. Rost-Bietsch, S. Karg, W. Riess, S. Scheinert, *J. Appl. Phys.* **2005**, *98*, 084505.

[8] E. Kuwahara, Y. Kubozono, T. Hosokawa, T. Nagano, K. Masunari, A. Fujiwara, *Appl. Phys. Lett.* **2004**, *85*, 4765.

[9] C. Rost, S. Karg, W. Riess, M. A. Loi, M. Murgia, M. Muccini, *Appl. Phys. Lett.* **2004**, *85*, 1613.

[10] T. B. Singh, S. Günes, N. Marjanovic, N. S. Sariciftci, *J. Appl. Phys.* **2005**, *97*, 114508.

[11] J. Cornil, J.-L. Bredas, J. Zaumseil, H. Sirringhaus, *Adv. Mater.* **2007**, *19*, 1791.

[12] E. C. P. Smits, T. D. Anthopoulos, S. Setayesh, E. van Veenendaal, R. Coehoorn, P. W. M. Blom, B. de Boer, D. M. de Leeuw, *Phys. Rev. B* **2006**, *73*, 205316.

[13] Y. Kunugi, K. Takimiya, N. Negishi, T. Otsubo, Y. Aso, *J. Mater. Chem.* **2004**, *14*, 2840.

[14] R. J. Chesterfield, C. R. Newman, T. M. Pappenfus, P. C. Ewbank, M. H. Haukaas, K. R. Mann, L. L. Miller, C. D. Frisbie, *Adv. Mater.* **2003**, *15*, 1278.

[15] M. L. Tang, A. D. Reichardt, N. Miyaki, R. M. Stoltenberg, Z. Bao, *J. Am. Chem. Soc.* **2008**, *130*, 6064.

[16] T. D. Anthopoulos, S. Setayesh, E. Smits, M. Cölle, E. Cantatore, B. de Boer, P. W. M. Blom, D. M. de Leeuw, *Adv. Mater.* **2006**, *18*, 1900.

[17] S. K. Lee, Y. Zu, A. Herrmann, Y. Geerts, K. Müllen, A. J. Bard, *J. Am. Chem. Soc.* **1999**, *121*, 3513.

[18] F. Nolde, W. Pisula, S. Mller, C. Kohl, K. Müllen, *Chem. Mater.* **2006**, *18*, 3715.

[19] J. Zaumseil, H. Sirringhaus, *Chem. Rev.* **2007**, *107*, 1296.

[20] M. Knupfer, *Appl. Phys. A* **2003**, *77*, 623.

[21] W. Osikowicz, M. P. de Jong, S. Braun, C. Tengstedt, M. Fahlman, W. R. Salaneck, *Appl. Phys. Lett.* **2006**, *88*, 193504.

[22] C. Tengstedt, W. Osikowicz, W. R. Salaneck, I. D. Parker, C.-H. Hsu, M. Fahlman, *Appl. Phys. Lett.* **2006**, *88*, 053502.

[23] S. Braun, W. Osikowicz, Y. Wang, W. R. Salaneck, *Org. Electron.* **2007**, *8*, 14.

[24] H. Sirringhaus, N. Tessler, R. H. Friend, *Synt. Met.* **1999**, *102*, 857.

[25] M.-H. Yoon, C. Kim, A. Facchetti, T. J. Marks, *J. Am. Chem. Soc.* **2006**, *128*, 12851.

[26] T. D. Anthopoulos, C. Tanase, S. Setayesh, E. J. Meijer, J. C. Hummelen, P. W. M. Blom, D. M. de Leeuw, *Adv. Mater.* **2004**, *16*, 2174.

[27] G. Horowitz, *Adv. Funct. Mater.* **2003**, *13*, 53.

[28] T. W. Kelley, C. D. Frisbie, *J. Phys. Chem. B* **2001**, *105*, 4538.

[29] G. Horowitz, *Adv. Funct. Mater.* **2003**, *13*, 53.

[30] A. Di Carlo, F. Piacenza, A. Bolognesi, B. Stadlober, H. Maresch, *Appl. Phys. Lett.* **2005**, *86*, 263501.

[31] F. Cicoira, C. Santato, F. Dinelli, M. Murgia, M. A. Loi, F. Biscarini, R. Zamboni, P. Heremans, M. Muccini, *Adv. Funct. Mater.* **2005**, *15*, 375.

[32] S. Verlaak, V. Arkhipov, P. Heremans, *Appl. Phys. Lett.* **2003**, *82*, 745.

[33] H. Sirringhaus, *Adv. Mater.* **2005**, *17*, 2411.

[34] M. C. J. M. Vissenberg, M. Matters, *Phys. Rev. B* **1998**, *57*, 12964.

[35] D. S. Chung, D. H. Lee, C. Yang, K. Hong, C. E. Park, J. W. Park, S.-K. Kwon, *Appl. Phys. Lett.* **2008**, *93*, 033303.

[36] K. C. Dickey, J. E. Anthony, Y.-L. Loo, *Adv. Mater.* **2006**, *18*, 1721.

[37] J.-F. Chang, B. Sun, D. W. Breiby, M. M. Nielsen, T. I. Sölling, M. Giles, I. McCulloch, H. Sirringhaus, *Chem. Mater.* **2004**, *16*, 4772.

Chapter 7

Conclusion and Outlook

In conclusion, p-type, n-type, and ambipolar organic field-effect transistors have been demonstrated in this work. Hereby, the influence of film morphology on the performance of solution processed OFETs has been illuminated. In particular, highly macroscopically disordered structures do not necessarily imply low charge carrier mobility, and well ordered films do not automatically lead to excellent device behavior as is generally believed and numerously reported in literature. Of course, only one system was presented in this work and exist so far as a support for the claim that hole mobilities surpassing 0.1 $cm^2V^{-1}s^{-1}$ can be reached without any long range order but with close $\pi-$stacking distance. More such organic materials have to be found in the future to underscore the claim. Hereby, different routes can be taken in order to obtain compounds that pack with tight $\pi-$stacking, for example by changing the strength of the donor and acceptor in a donor-acceptor system or by varying the alkyl substituents that provide solubility but on the other hand demand high steric hindrance, in this way enlarging $\pi-$stacking distance. Also, in the case of polymers, molecular weight might play a crucial role as well when coming to alterations of film morphology as demonstrated in chapter 4. Unfortunately, there is no universal formula for the correct prediction of such strong $\pi-$stacking materials, so one has to learn more or less by trial and error. However,

the positive OFET results illustrated in this work should encourage an approach towards this direction.

Surely, film morphology is one of numerous factors that influence OFET behavior, among them endgroups of the insulator surface, contact resistance, charge carrier injection barriers and so on, emphasizing the complexity and challenge in fabricating high performance OFETs. However, it is shown in this thesis that film morphology itself has a tremendous impact on transistor operation, especially in the case of discotic SWQDI rylene dye. For this organic semiconductor, it was for the first time demonstrated that not only charge injection barriers and charge carrier trapping at the insulator surface prevent ambipolarity but also supramolecular arrangement. In short, the aim to design new organic semiconductors for high performance OFETs is unavoidably linked with an understanding of the interplay between molecular order and device operation. I hope that the findings of this work has contributed partly to a deeper insight into the influence of film morphology on solution processed organic field-effect transistors.

Nevertheless, there is still a long way to go in the field of organic electronics in general. For OFETs, tremendous progress has been made till now in terms of transistor performance, mostly owing to the clever design of new organic semiconductors. However, the high charge carrier mobilities like the donor-acceptor CDT-BTZ copolymer presented in this work have been fabricated on SiO_2, on which basically all transistor configurations can be accomplished (bottom contact, top contact, or top gate as illustrated in Figure 3.6). The next challenge will be to test and optimize OFETs processed on plastic foils in order to bring plastic electronics further to reality. Here, however, the top gate architecture should be employed since the plastic substrate contains no gate electrode as in the case of a highly doped silicon wafer covered by an insulating SiO_2 layer. In addition, the top dielectric sandwiching the organic semiconductor layer between the substrate guarantees encapsulation preferable for OFET operation in ambient conditions

required for everyday use. For this top gate structure, solution processable dielectrics are needed. Thus, another future challenge is the design of novel dielectric materials that can be solution processed. The effect of the dielectric on transistor peformance is tremendous and cannot be neglected. The reasons are manifold. Especially portable electronic devices like cell phone displays require operation at low voltages, typically up to 15V or less. One route to enhancing low voltage operation is the ease of polarisability of the dielectric in response to the applied gate bias. This leads to high capacitance of the dielectric, in this way promoting charge carrier density at the insulator semiconductor interface. The heightened charge carrier density helps in turning on the transistors at low operating voltages [1]-[4]. Newest trends in realizing high capacitance dielectrics are ion gels [5] or polyelectrolytes [6][7] where operation voltages at a couple of volts have been realized for organic semiconductors for which several tens of volts are needed for functioning on conventional SiO_2 layers. These insulator classes are interesting since they fulfill solubility for easy processing and high dielectric strength which is essential for preventing leakage currents from the semiconductor through the insulator due to possible breakdown at high gate fields. In combination with the high mobility CDT-BTZ copolymer presented in this work, plastic OFETs are close to be realized by fast printing. This is motivated by the fact that spin-coating which is very similar to rapid printing processes resulted in excellent transistor performance.

Bibliography

[1] A. Facchetti, M.-H. Yoon, T. J. Marks, *Adv. Mater.* **2005**, *17*, 1705.

[2] M. Halik, H. Klauk, U. Zschieschang, G. Schmid, W. Radlik, W. Weber, *Adv. Mater.* **2002**, *14*, 1717.

[3] C. D. Dimitrakopoulos, S. Purushothaman, J. Kymissis, A. Callegari, J. M. Shaw, *Science* **1999**, *283*, 822.

[4] M.-H. Yoon, H. Yan, A. Facchetti, T. J. Marks, *J. Am. Chem. Soc.* **2005**, *127*, 10388.

[5] J. H. Cho, J. Lee, Y. Xia, B. Kim, Y. He, M. J. Renn, T. P. Lodge, C. D. Frisbie, *Nat. Mater.* **2008**, *7*, 900.

[6] A. S. Dhoot, J. D. Yuen, M. Heeney, I. McCulloch, D. Moses, A. J. Heeger, *PNAS* **2006**, *103*, 32.

[7] L. Herlogsson, Y.-Y Noh, N. Zhao, X. Crispin, H. Sirringhaus, M. Berggren, *Adv. Mater.* **2008**, in press.

Chapter 8

Experimental Details

8.1 Transistor Probe Station

For OFET measurement, a home-built probe station was used (Figure 8.1). The whole setup is situated in a glove box filled with nitrogen in order to perform the transistor studies in an oxygen and water free inert atmosphere. This aspect is important particularly for organic semiconductors that potentially degrade in air. Due to space limitations in the glove box, commercial transistor probe stations were not bought. Instead, a small home built system was set up. It consists of the following components: A microscope tube (red arrow in Figure 8.1) that is mounted on millimeter manipulators (orange arrow in Figure 8.1) in order to move the microscope. This movement is necessary to be able to observe the whole transistor substrate. Arbitrary areas of the sample can be contacted in this way for OFET measurements. The microscope allows the observation of the source and drain electrodes that are generally only a couple of tens of micrometers large. The electrodes (source, drain, gate) are contacted by movable probe heads PH100 (yellow arrow in Figure 8.1) purchased from Süss MicroTech Test Systems GmbH. Those probe heads can be manipulated in the x, y, and z directions and contain electrically shielded probe arms (red arrow in Figure 8.2) with tungsten tips (yellow arrow Figure 8.2).

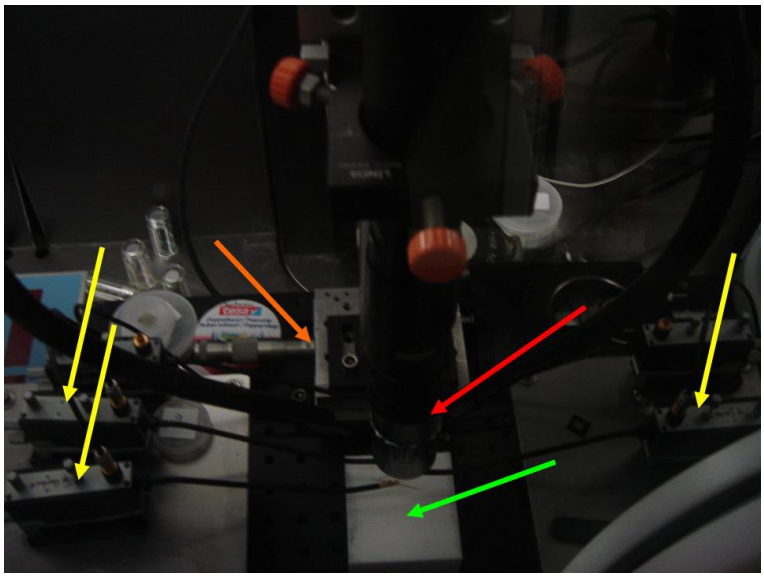

Figure 8.1: Image of transistor probe station.

Those tungsten tips have a diameter of 20 μm and are purchased also from Süss MicroTech Test Systems GmbH. Figure 8.2 illustrates the contacting of a transistor sample (blue arrow in Figure 8.2). Contacts with the source, drain, and gate electrodes are established with the tungsten tips. Each probe head is used for one of the three electrodes source, drain, and gate. In addition, arbritary and unwanted movements of the tips on the transistors are avoided by magnetic bases situated on the bottom of the probe heads. The probes are connected to a Keithley SCS 4200 which is a semicondcutor characterization system. It contains a software enabling the sweep of the transistor current I_{SD} in dependence of V_G and V_{SD}.

8.2 Bottom Contact OFET Preparation

Highly doped silicon wafers covered with 150 nm or 300 nm thick thermally grown SiO_2 purchased from Silicon Quest International were used as bottom gate, bottom contacts transistors. First, the wafers were cleaned by sonication in acetone for 5 minutes, followed by rinsing in isopropanol and drying with nitrogen. The substrates were then dried on a hotplate at 110°C for at least 5 minutes. From here on, the photolithographic process starts that enables the patterning of source and drain

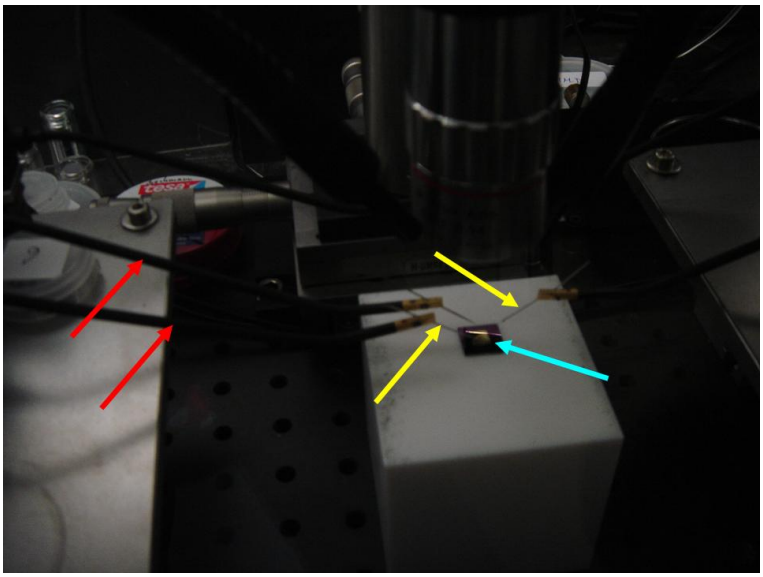

Figure 8.2: Probes contacting the devices.

electrode structures in micrometer dimensions (Figure 8.3).

Negative photoresist AZ nLOF 2070 diluted 1:0.40, 2 μm grade from Micro-Chemicals GmbH was spin-coated at 4000 rotations per minute (rpm) for 30 seconds on the dried wafers (Figure 8.3a). The lithographic process was performed in the clean room in order to avoid contamination of the samples by dust particles. Subsequently, the spin-coated film was dried on a hotplate at 110°C for 1 to 2 minutes to remove residual solvents in the photoresist film. Using a maskaligner, these samples were then pressed against a negative mask contaning the desired electrode structures. The negative masks consists of quartz on which the structures that are supposed to be fabricated are made out of a thin chrome layer. The assembly of mask and substrate is exposed to ultraviolet (UV) light for 2 seconds (Figure 8.3b). Afterwards, the samples are again heated on a hotplate at 110°C for 1 minute. In this process, only the parts of the photoresist that were exposed to UV get crosslinked. The other areas not touched by UV (the chrome parts of the mask) are removed after immersing the samples in the developer solution AZ 726 MIF puchased from MicroChemicals GmbH for 60 seconds, followed by rinsing in deionized water to remove residual developer traces (Figure 8.3c). The samples are then dried with nitrogen. After this step, the source and drain electrodes are evaporated in vacuum

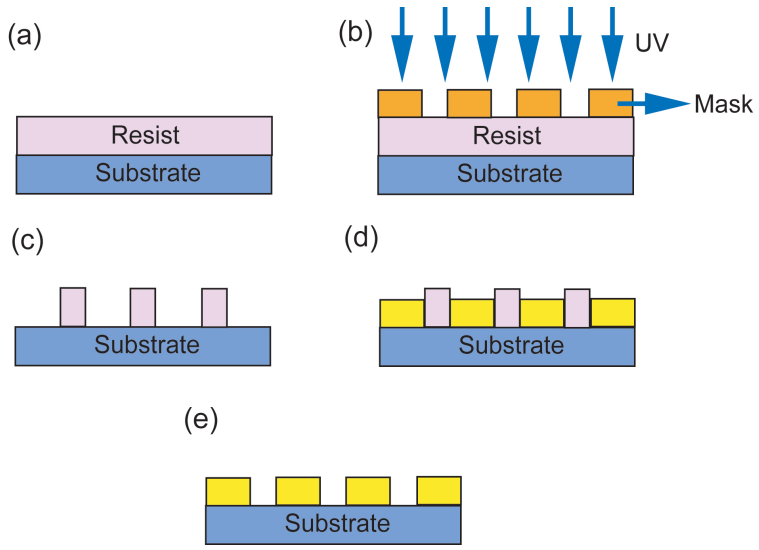

Figure 8.3: Schematic illustration of the photolithographic process using negative mask and photoresist: a.) Spin-coated negative photoresist on the substrate. b.) Ultraviolet (UV) exposure of the photoresist through a mask that defines the desired microstructures. c.) Parts of the photoresist that are treated with UV are crosslinked via thermal treatment and cannot be removed when immersed in the developer. The other parts blocked from UV by the mask are removed by the developer. d.) Evaporation of metal on the patterned samples. e.) Removing the remaining photoresist (*Lift off*) by sonication in NMP and acetone.

onto these samples, resulting in metal contacts separated by pieces of photoresist (Figure 8.3d). Finally, the remaining photoresist is washed away by sonication in N-Methyl-2-pyrrolidon (NMP) for 5 minutes. This latter process is called *Lift-off*, leaving behind the desired structured microcontacts (Figure 8.3e). In order to clean the samples from NMP, they are first rinsed with acetone and afterwards sonicated in acetone for another 5 minutes. Rinsing the samples in isopropanol and drying with nitrogen finish the patterned bottom contact FET substrates.

8.3 Self-assembled Monolayers

In this section, the functionalization procedures of SiO_2 surfaces with self-assembled monolayers (SAM) are described. In this Ph.D. work, mainly two SAMs were utilized: HMDS and PTES. Prior to SAM deposition, all substrates are cleaned in the same way as follows: First, the substrates are sonicated in acetone for 5 min-

utes, then rinsed in isopropanol and dried with nitrogen. Then, they are cleaned in plasma consisting of 90 percent argon and 10 percent oxygen for 5 to 10 minutes to remove any organic traces on the SiO_2 surface.

8.3.1 Functionalization with HMDS

1,1,1,3,3,3-Hexamethyldisilazane (HMDS) in electronic grade was purchased from Alfa Aesar. About one mL of HMDS was put on a small petri dish. Another petri dish was used to place the cleaned substrates. Both petri dishes were then positioned in a glass container with a sealable cap that does not permit outflow of gas. This glass container was sealed and placed in an oven at 120°C for 3 hours. In this last step, the container will be filled with HMDS vapor in which the HMDS molecules adsorb on the SiO_2 surface, in this way forming methyl endcapped interfaces. After these 3 hours, the samples are taken out from the container and cleaned by sonication in acetone for 5 minutes followed by rinsing in isopropanol and drying with nitrogen.

8.3.2 Functionalization with PTES

Phenyltriethoxysilane (PTES) was purchased from Merck. A glass container was filled with 20 ml of tetrahydrofuran (THF) followed by 20 μl of PTES. Then, three drops of HCl was added to this mixture. The cleaned substrates were then left in this solution for 2 hours. After this period of time, the samples were taken out, rinsed with toluene and dried with nitrogen. Then, they were put in an oven at a temperature of 120°C for 2 hours. Following this heat treatment, the samples are sonicated for 5 minutes in toluene. The toluene on the substrates was removed by rinsing with acetone with sucessive sonication for 5 minutes in the same solvent. As the final step, the samples were rinsed in isopropanol and dried with nitrogen.

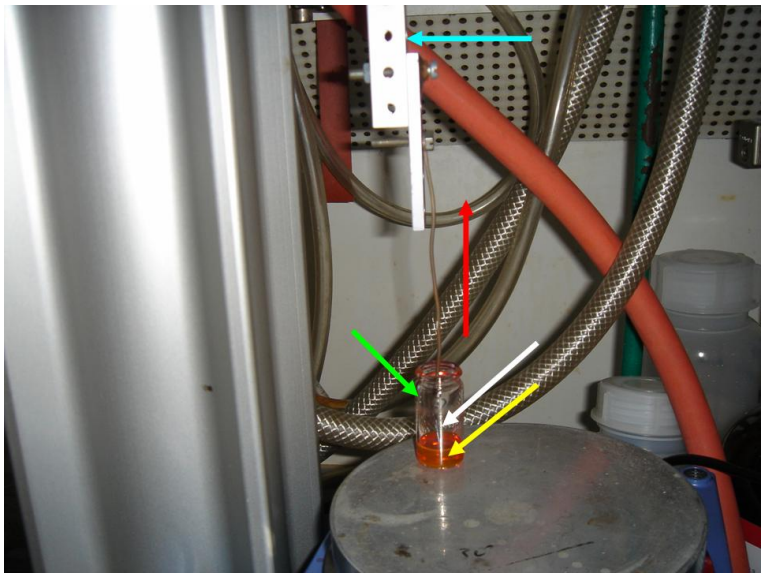

Figure 8.4: Dip-coating setup.

8.4 Dip-coating

The dip-coating setup is illustrated in Figure 8.4. It consists of an electronically controllable engine (blue arrow in Figure 8.4) to which the substrate (white arrow) is attached. A cylindrical glass container with a diameter of 13mm and a height of 39mm (green arrow) was filled up with the organic semiconductor solution (yellow arrow) to a height of about 13mm. The transistor substrates with a size of typically 1cm by 1cm were completely immersed in this solution and taken out at a specific rate that can be controlled by the engine. This whole process was performed in ambient conditions at room temperature (typically at about 23°C). That is, both the solution and the substrates were at this temperature.

Publication List

- M. Zhang, H. N. Tsao, W. Pisula, C. Yang, A. K. Mishra, K. Müllen **Field-Effect Transistors Based on a Benzothiadiazole-Cyclopentadithiophene Copolymer**, *J. Am. Chem. Soc.*, **129**, 3472 (2007).

- D. Wu, L. Zhi, G. J. Bodwell, G. Cui, N. Tsao, K. Müllen **Self-Assembly of Positively Charged Discotic PAHs: From Nanofibers to Nanotubes**, *Angew. Chem. Int. Ed.*, **46**, 5417 (2007).

- X. Wang, L. Zhi, N. Tsao, Z. Tomovic, J. Li, K. Müllen **Transparent Carbon Films as Electrodes in Organic Solar Cells**, *Angew. Chem. Int. Ed.*, **47**, 2990 (2008).

- P. Gao, D. Beckmann, H. N. Tsao, X. Feng, V. Enkelmann, W. Pisula, K. Müllen **Benzo[1,2-b:4,5-b]bis[b]benzothiophene as solution processible organic semiconductor for field-effect transistors**, *Chem. Commun.*, 1548 (2008).

- H. N. Tsao, H. J. Räder, W. Pisula, A. Rouhanipour, K. Müllen **Novel organic semiconductors and processing techniques for organic field-effect transistors**, *phys. stat. sol. (a)*, **205**, 421 (2008).

- H. N. Tsao, W. Pisula, Z. Liu, W. Osikowicz, W. R. Salaneck, K. Müllen **From Ambi- to Unipolar Behavior in discotic dye field-effect transistors**, *Adv. Mater.*, **20**, 2715 (2008).

- H. N. Tsao, D. Cho, J. W. Andreasen, A. Rouhanipour, D. W. Breiby, W. Pisula, K. Müllen **The Influence of Morphology on High Performance Polymer Field-Effect Transistors.**, *Adv. Mater.*, accepted (2008).

- P. Gao, D. Beckmann, H. N. Tsao, X. Feng, V. Enkelmann, M. Baumgarten, W. Pisula, K. Müllen **Dithieno[2,3-d:2,3-d]benzo[1,2-b:4,5-b]dithiophene (DTBDT) - as Semiconductor for High Performance, Solution-Processed Organic Field-Effect Transistors.**, *Adv. Mater.*, accepted (2008).